Tréhu, A.M., Bohrmann, G., Rack, F.R., Torres, M.E., et al., 2003
Proceedings of the Ocean Drilling Program, Initial Reports Volume 204

8. Site 1249[1]

Shipboard Scientific Party[2]

INTRODUCTION

Site 1249 (proposed Site HR4b) was drilled in ~775 m of water on the summit of southern Hydrate Ridge (see Fig. F1, p. 51, in the "Leg 204 Summary" chapter). This area is characterized by massive gas hydrate deposits at the seafloor (Suess et al., 2001). Vigorous streams of bubbles are known to emanate from the seafloor, as documented by submersible observations and high-frequency echo sounding surveys, which have repeatedly imaged "bubble plumes" in the water column (Tréhu and Bangs, 2001; Heeschen et al., 2003). These observations are interpreted to indicate that some of the methane rising through the sediment column is trapped as hydrate near the seafloor and that some escapes into the water column (Suess et al., 2001).

The seafloor in this area is anomalously reflective (Johnson et al., in press), and the seafloor reflectivity is spatially correlated with subsurface seismic reflectivity that extends to ~30 meters below seafloor (mbsf) (see Fig. F7, p. 57, in the "Leg 204 Summary" chapter). These geophysical observations have been interpreted to indicate the spatial extent of lenses of massive hydrate intercalated with sediment (Tréhu et al., 2002). Seismic data also indicate that the bottom-simulating reflector (BSR) at this site is at ~115 mbsf. However, coring was only permitted to 90 mbsf because of the possibility of trapped gas beneath the BSR at this structural high.

The primary objective at Site 1249 was to determine the distribution and concentration of gas hydrate with depth at the southern summit of Hydrate Ridge and to investigate processes that allow methane gas bubbles to coexist with gas hydrate and pore water within the hydrate stability field. A second objective was to test whether the pattern of chaotic reflectivity accurately predicts the spatial extent of massive hydrate lenses.

[1]Examples of how to reference the whole or part of this volume.
[2]Shipboard Scientific Party addresses.

Ms 204IR-108

Twelve holes were drilled at Site 1249 (Fig. F1). Logging-while-drilling (LWD) measurements were made during drilling in Hole 1249A. Hole 1249B was drilled using the new resistivity-at-the-bit (RAB)-8 LWD and coring system, which permits simultaneous acquisition of core and logging data. The 90-m sediment sequence was then sampled with the advanced piston corer (APC) in Holes 1249C–1249F, with core recoveries of <30% in the uppermost 20 mbsf and increased core recovery (up to 70%) deeper in the holes. Six holes (Holes 1249G–1249L) were cored with the APC or extended core barrel (XCB) for a special shore-based "geriatrics" study, in which several means of preserving gas hydrates for future study will be compared. During this effort, 244 m of gas hydrate–bearing sediments were cored with 35% core recovery. The samples were either stored in liquid nitrogen or steel pressure vessels, which were repressurized using methane gas and water.

F1. Bathymetric map, p. 36.

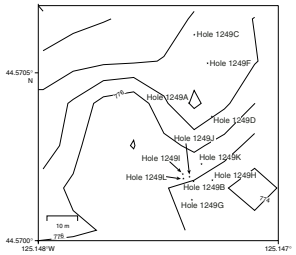

OPERATIONS

Twelve holes were drilled at this site (Table T1), under good weather conditions. Wind speed was 0–8 kt, gusting to 12 kt; seas were 0–4 ft; swell was 4–7 ft; and the prevailing sea-surface current was from the north at ~0.5 kt. LWD data were collected from Hole 1249A on 21 July 2002. We returned to this site on 24–26 July for LWD operations in Hole 1249B using the new RAB-8 coring system and to core Hole 1249C to 89.5 mbsf with the APC. We returned to this site again on 4–6 August to core Holes 1249D–1249F. Near the end of the leg, we occupied this site one last time on 27–29 August to core Holes 1249G–1249L with the APC/XCB for a shore-based hydrate geriatrics study. During this last visit, wind speed had increased to 14–19 kt, gusting to 23 kt; seas were 6–7 ft; and swell was 8–10 ft.

T1. Coring summary, p. 76.

All pressure coring systems available were used at Site 1249. The ODP pressure core sampler (PCS) was deployed a total of six times, and the Fugro Pressure Corer (FPC) and HYACINTH Hydrate Autoclave Coring Equipment (HYACE) Rotary Corer (HRC) were each deployed three times at this site. Eleven in situ temperature runs were made at this site: nine using the APC temperature (APCT) tool and two using the Davis-Villinger Temperature-Pressure Probe (DVTPP). Pressure data were measured using the DVTPP.

The *Mauna Loa* came alongside on 25 July and was secured on the starboard side at 0605 hr to transfer freight and personnel to the *Joides Resolution*. Personnel included HYACINTH FPC engineers Floris Tuynder and Roeland Baas, logging scientist Gilles Guérin, Dallas Morning News journalist Alexandra Witze, paleontologist Mahito Watanabe, and HRC engineer Felix Weise. A linear X-ray scanner (LXS) from Lawrence Berkley National Laboratory (Freifeld et al., in press, 2002) was installed in the core laboratory, and training of personnel was conducted. In addition, the TAMU logistics coordinator, a LXS scientist, and a LXS student technician/programmer came on board for the day. Off-going personnel included logging scientists Nathan Bangs and David Goldberg, LWD engineers Stefan Mrozewski and Khaled Moudjeber, and geophysisist Marteen Vanneste. LWD tools were loaded, and the *Mauna Loa* departed for Coos Bay, Oregon, at 1715 hr.

On 6 August, a helicopter arrived on deck at 1227 hr with passengers Bill Gwilliam from Department of Energy (DOE)/National Energy Tech-

nology Laboratory (NETL), Dean Ferrell, electrical technician from the Ocean Drilling Program (ODP)/Texas A&M University (TAMU), and Transocean 3rd engineer Yorn Verschoor. The helicopter departed at 1243 hr carrying passengers Alexandra Witze, a journalist from the Dallas Morning News, and John Beck, ODP/TAMU photographer.

The final rendevous of the leg took place on 27 August, when the *Mauna Loa* tied up along port side at 0650 hr. We loaded crates for packing the off-going Vertical Seismic Imager (VSI)/Schlumberger equipment, DOE pressure vessels/sample dewars, liquid nitrogen dewars, and equipment for the German film crew (CONTEXT-TV). Schlumberger downhole tools/pallets and off-going samples were off-loaded. Passengers joining the *JOIDES Resolution* included Jan Hartmann and Stephan Braun from German CONTEXT-TV and Randy Showstack, *Eos* journalist. The *Mauna Loa* released at 0900 hr to transfer personnel and equipment to and from the *Ewing*. The *Mauna Loa* returned alongside the *JOIDES Resolution* at 1100 hr and off-loaded the remaining Schlumberger VSI surface equipment. Passengers departing the *JOIDES Resolution* included Alexei Milkov, sedimentologist, and Herbert Leyton, Schlumberger VSP engineer. The *Mauna Loa* departed at 1130 hr.

Hole 1249A was spudded at 0900 hr on 21 July to conduct LWD measurements using the same tools as were used at the other sites during this leg. Drilling proceeded at reduced rates of penetration (ROPs) of 15 m/hr and 15 strokes per minute (spm) circulation to moderate formation washout at shallow depths below seafloor. No real-time measurement-while-drilling (MWD) or nuclear magnetic resonance (NMR) data were recorded over this interval. The ROP was increased to 25 m/hr from a bit depth of 30 mbsf to a total depth (TD) of 90 mbsf, and real-time MWD and NMR data were recorded (see **"Downhole Tools and Pressure Coring,"** p. 20). The LWD tools were pulled to ~60 m above the seafloor at 1600 hr on 21 July. Total bit run took ~7 hr.

Hole 1249B was drilled using the new LWD RAB-8 and coring system, which permits simultaneous acquisition of core and logging data. LWD operations began with initialization of the RAB-8 at 1315 hr on 24 July. Although exercised fully in Houston, Texas, the inner mandrel in the RAB-8 BHA was too high to make up with the $6^5/_8$-in pin above. The inner diameter of the pin was ground down, and the motor-driven core barrel (MDCB) was tested until it passed through. Hole 1249B was finally spudded at 2000 hr. Drilling proceeded ahead to 30 mbsf, and coring operations began with sequential 4.5- and 9-m cores recovered through hydrate-bearing clays to a TD of 74.9 mbsf. Bit rotation varied from 15 to 45 rpm, increasing with depth, and the average ROP using this system was ~8 m/hr. The RAB-8 was recovered at the rig floor at 1200 hr on 25 July, and the data recorded in computer memory were downloaded. Total testing time was ~22 hr.

The recorded RAB data from Hole 1249B are of good quality over the drilled interval and correlate well with the log curves in Hole 1249A (see **"Downhole Logging,"** p. 29). The eight rotary cores recovered from Hole 1249B had an average of 32.9% recovery. These test cores were normally processed and archived and will be correlated to the RAB logs over the same depth interval. RAB-8 images and logs are of high quality but require additional depth correction to account for the coring process (see **"Downhole Logging,"** p. 29). With harder formations and faster rotary coring, both core recovery and log data quality are expected to improve using the RAB-8 coring system.

This successful test marks the first ever logging-while-coring experiment, a new technology that allows for precise core-log depth calibra-

tion and core orientation within a single borehole and without a pipe trip. It represents an outstanding example of a successful cooperative effort between Lamont-Doherty Earth Observatory (LDEO) and TAMU to develop and validate the logging-while-coring concept.

Holes 1249C–1249F recovered a 90-m sediment sequence with the APC (Table T1). Core recoveries were <30% in the uppermost 20 mbsf and increased to 70% deeper in the holes. All pressure coring devices were used to sample this sediment sequence in an effort to capture massive hydrate samples under pressure and to compare the capabilities of each of these tools in sampling gas hydrates (see Table T2, p. 72, in the "Leg 204 Summary" chapter). The PCS was deployed six times in these holes, but only three cores were recovered under pressure. Two deployments of the FPC at 8 mbsf did not recover core at in situ pressures. A deployment of the HRC at 8 mbsf in Hole 1249F resulted in successful recovery of core under full pressure, which was rapidly cooled in the ice bath to maintain stability, successfully sheared, and transferred into the HYACINTH logging chamber. It was subsequently logged repeatedly in the Geotek Vertical Multi Sensor Core Logger (V-MSCL) while being degassed over the following 2 days (see "Downhole Tools and Pressure Coring," p. 20).

Temperature measurements were collected during six runs of the APCT tool (one in Hole 1249C and five in Hole 1249F) and two runs of the DVTPP (one in each of Holes 1249C and 1249F). Whirl-Paks and perfluorocarbon tracer (PFT) were used for microbiology cores in Holes 1249D–1249F (see Table T3, p. 73, in the "Leg 204 Summary" chapter), and the Drill String Acceleration (DSA) tool was run in Holes 1249C (once) and 1249F (twice).

Holes 1249G–1249L were APC/XCB cored for a special shore-based geriatrics experiment in which several means of preserving gas hydrates for future study will be compared. Of the 40 steel pressure vessels that were taken on board, 34 were repressurized with core samples. The total quantity of core preserved in pressure vessels is ~50 m of sediment. The pressure being maintained in each of these vessels is nominally 550–600 psi at 4°–6°C. The remaining ~35 m of core recovered was placed into labeled cloth bags and is preserved in liquid nitrogen cryofreezers. Both the pressure vessels and the cryofreezers were stored in a refrigerated container van aft of the drill floor on the core tech shop roof. We conducted systematic periodic monitoring of the ambient air inside the container van by taking samples and running them through the shipboard gas chromatograph. We also monitored the gas pressures in each of the pressure vessels, the levels of the liquid nitrogen in the cryofreezers, and the temperature in the containers.

Two pressure vessels originally filled and repressurized with sediment containing significant quantities of hydrogen sulfide were taken out of service because of the risk of steel metal fatigue as a result of contact with hydrogen sulfide. In addition, two pressure vessels failed to maintain pressure because of leaks in valve or gauge connections; some of the hardware from these vessels was used to replace faulty gauges on other pressure vessels. Two additional pressure vessels were not used because of the termination of coring. These are available for future studies and for use as "standards" to make gamma ray attentuation (GRA) density measurements.

The Transocean drillers, core technicians, and rig crew did a superb job of handing the cores recovered on deck and transferring them to the ODP Marine Laboratory Technicians and ODP Shipboard Curator for processing on the catwalk. All the personnel involved were ex-

tremely fast, efficient, and professional in their handling of these hydrated cores in a way to maximize core preservation and ensure core quality. The safe handling of the pressure vessels, their repressurization, and the resulting preservation of the cores contained inside was successfully carried out in a short space of time immediately following the arrival of a large amount of equipment transported to the *JOIDES Resolution* by supply boat.

In addition to the APC/XCB cores for the geriatrics study, there were three deployments of pressure coring devices in these holes (Table T17). The HRC deployment at 13.5 mbsf in Hole 1249G successfully recovered a 75-cm core with massive hydrate layers at full pressure and transferred this material into a HYACINTH storage chamber (see "Downhole Logging," p. 29). It was subsequently frozen in He under pressure and successfully transferred into liquid nitrogen for preservation. It is probably the most pristine sample of natural gas hydrate ever recovered and preserved.

The FPC was also deployed at 13.5 mbsf in Hole 1249G and recovered 75 cm of core at full pressure. A good GRA density log was obtained from the core in the storage chamber showing massive hydrate layers (see "Downhole Logging," p. 29). This core was designated as a "reference core" and companion to the APC and XCB cores that were taken and repressurized under methane. It was kept in the refrigerator ready for transportation to Texas A&M University for further study.

The HRC was deployed again, deeper in the sediments in Hole 1249L (37.5 mbsf), in an attempt to recover pristine material under pressure from a region where the hydrate is more disseminated. Some pressure was lost during disassembly, but it was rapidly repressurized to in situ pressures before being transferred to the logging chamber.

Temperature measurements were collected with one APCT tool run in each of Holes 1249G, 1249I, and 1249L (Table T15).

LITHOSTRATIGRAPHY

Eleven holes (Holes 1249B–1249L) were cored at Site 1249. Table T2 records the depth of penetration and core recovery in each hole drilled. All of the recovered sediments from Holes 1249G–1249L were placed directly into either pressure vessels or liquid nitrogen to be preserved for future studies. Thus, these cores were not, therefore, described or logged according to standard ODP procedures.

Site 1249 is located near the crest of southern Hydrate Ridge in close proximity to Sites 1248 and 1250 (see Figs. F1, p. 51, and F7, p. 57, both in the "Leg 204 Summary" chapter). We were able to distinguish two separate lithostratigraphic units (Units I and II) above Horizon Y at Sites 1245, 1247, and 1250 but were unable to do so at Site 1249 because of poor recovery (~56%). However, because of the proximity of the sites at the ridge crest, we call our first lithostratigraphic unit at this site Unit I-II, for better correlation with the other sites and do not distinguish between a clay-dominated Unit I and a turbidite-dominated Unit II. The lithostratigraphic sequence recovered at Site 1249 was divided into two lithostratigraphic units (Units I-II and III) based on variations in sedimentary structure and grain size as well as changes in the biogenic and lithogenic components (Fig. F2).

Calcium carbonate content (expressed as weight percent $CaCO_3$) and mineralogy from X-ray diffraction (XRD) were also used to delineate the lithostratigraphic unit boundaries of Site 1249. Additionally, we

T2. Core recoveries, p. 81.

F2. Lithostratigraphic summary, p. 37.

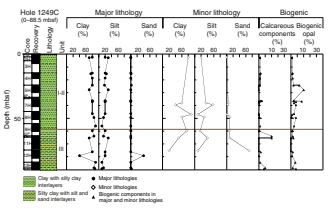

compare and correlate our results with the three-dimensional (3-D) seismic data, downhole LWD data, and physical property measurements (magnetic susceptibility [MS] and GRA density) to better define the entire stratigraphic sequence (Fig. F2). Correlation of the lithostratigraphic units defined here with the other Leg 204 sites is summarized in Figure F10, p. 60, in the "Leg 204 Summary" chapter.

Lithostratigraphic Units

Lithostratigraphic Unit I-II

Intervals: Sections 204-1249B-1H-1 through 8H-1; 204-1249C-1H-1 through 9H-4; Section 204-1249D-1H-1 through Core 3H; Cores 204-1249E-1H through 3H; and Sections 204-1249F-1H-1 through 10H-2
Depths: Hole 1249B: 29.90–57.62 mbsf; Hole 1249C: 0.00–59.30 mbsf; Hole 1249D: 0.00–18.50 mbsf; Hole 1249E: 0.00–11.00 mbsf; and Hole 1249F: 0.00–51.52 mbsf.
Age: early Pleistocene–Holocene

Lithostratigraphic Unit I-II is composed of clay and silty clay with a varying biogenic component that ranges from nannofossil- to diatom-bearing and diatom-rich clay. The sediments of lithostratigraphic Unit I-II tend to be dark greenish gray (5GY 4/1), although very dark gray (N3) sediments are also found in zones containing sulfide precipitates. These precipitates are absent from the top 15 mbsf in every hole cored and tend to increase with depth in the hole (Fig. F3). The homogeneous nature of the recovered sediments, combined with the poor recovery (~56%) of lithostratigraphic Unit I-II (Table T2), made correlation between holes difficult. However, the location of the lower boundary of lithostratigraphic Unit I-II, which was placed above the first occurrence (FO) of fining-upward silty to sandy interlayers in lithostratigraphic Unit III, agrees to within 8 m in all the holes cored and ranges in depth from 51.5 mbsf in Hole 1249F to 59.3 mbsf in Hole 1249C.

F3. Mottled texture and sulfide precipitates, p. 38.

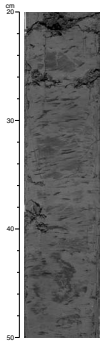

The primary texture of the mineralogic components of lithostratigraphic Unit I-II ranges from clay to silty clay. On average, ~70% of the total components are clay and ~30% are silt. The silt fraction of the sediment decreases slightly with depth from ~37% to 20% at the lithostratigraphic Unit I-II/III boundary in Hole 1249F. This trend, however, is not observed in either Holes 1249B or 1249C, the only other holes in which the lithostratigraphic boundary was recovered. Sand grains can be found in smear slide samples taken from both Holes 1249C and 1249F, though sand does not exceed 5% of the total components of lithostratigraphic Unit I-II in any hole.

Biogenic components typically compose 5%–15% of the sediments in lithostratigraphic Unit I-II. Calcareous nannofossils compose 2%–5% of the major lithology and tend to be more abundant in the top 30 mbsf than below. Siliceous microfossils, primarily diatoms, compose 2%–15% of the sedimentary components in both the major and minor lithologies of the lithostratigraphic unit. An increase in the siliceous microfossil content occurs at 24 mbsf in Hole 1249C and continues to 37 mbsf.

Perhaps the most distinguishing feature of lithostratigraphic Unit I-II is the ubiquitous presence of mousselike and soupy textures. Core 204-1249F-9H was the only core recovered from lithostratigraphic Unit I-II that did not contain either texture. The disruption of the original sedi-

mentary fabric is presumed to have resulted from the dissociation of gas hydrate. This hypothesis is supported by the abundant gas hydrate specimens sampled at this site, the multiple cold anomalies observed with the infrared (IR) camera (see "Physical Properties," p. 17), chloride anomalies in the geochemical data (see "Chloride Concentration and the Presence of Gas Hydrate," p. 11, in "Interstitial Water Geochemistry") and, most especially, by the resistivity log data (see "Gas Hydrate," p. 32, in "Interpretation of LWD Logs" in "Downhole Logging").

Lithostratigraphic Unit III

Intervals: Sections 204-1249B-8H-1 through 9H-CC; 204-1249C-9H-4 through 14P-1; and Cores 204-1249F-10H-2 through 16H-CC
Depths: Hole 1249B: 57.62–74.90 mbsf; Hole 1249C: 59.33–89.50; and Hole 1249F: 51.52–90.00 mbsf
Age: ~middle Pleistocene

The major lithology of lithostratigraphic Unit III is diatom-bearing to diatom-rich clay and silty clay with nannofossil-bearing to nannofossil-rich zones. Clay and silty clay are punctuated by minor lithologies of silt, silty sand, and sand (1 mm to 10 cm thick), which compose the bases of the turbidite sequences. The majority of the lithostratigraphic unit is dark greenish gray (5GY 4/1) but varies to very dark gray (N3) in the presence of sulfide. The upper boundary of lithostratigraphic Unit III with Unit I-II is defined by (1) the presence of visible turbidites in the core, (2) an increase in grain size (major lithology sand fraction), (3) a slight increase in calcareous components, and (4) a slight decrease in biogenic opal (Fig. F2). The boundary between these lithostratigraphic units is also coincident with seismic Horizon Y (see Fig. F7, p. 57, in the "Leg 204 Summary" chapter). Although Horizon Y appears conformable at Site 1249, seismic correlation between sites suggests it may be a regional unconformity, supporting a unit contact at its interface (see Figs. F5, p. 55, and F7, p. 57, both in the "Leg 204 Summary" chapter). Recovery of lithostratigraphic Unit III was much improved in Holes 1249C (99.1%) and 1249F (94%) compared to the recovery of lithostratigraphic Unit I-II in the same holes, 66.0% and 66.6%, respectively (Table T2).

Grain size of both the major and minor mineral components and the biogenic components of lithostratigraphic Unit III was determined by smear slide analyses (Fig. F2). The character of individual turbidites varied from thin (1–2 mm) layers to closely spaced (1–2 cm) silts and sands (Fig. F4A) to thicker (2–3 cm) single graded beds (Fig. F4B). Sulfide mottles and dark gray (N3) zones are common throughout the unit. Abundant iron sulfide nodules were observed near the bottom of Holes 1249C (Section 204-1249C-16H-2) and 1249F (Sections 204-124FC-15H-5, 15H-6, and 15H-7). Moderate to rare bioturbation is also common throughout the unit and is best preserved beneath the bases of the turbidites.

Although Holes 1249C and 1249F reached similar TDs, Hole 1249F recovered a sedimentary sequence that contained soft-sediment deformation features and clay clasts (1–2 cm in diameter) (intervals 204-1249F-16H-4, 10–65 cm, and 16H-5, 0–56 cm). We interpret this matrix-supported clay-clast deposit as a debris flow (similar to those seen at other sites). An abundance of (authigenic) carbonate-rich clay was seen as a lens in Sample 204-1249F-16H-1, 18–20 cm, and glass-rich silty clay (30% glass) was observed as a lens or thin clast in both Samples 16H-3,

F4. Inclined silt layers, p. 39.

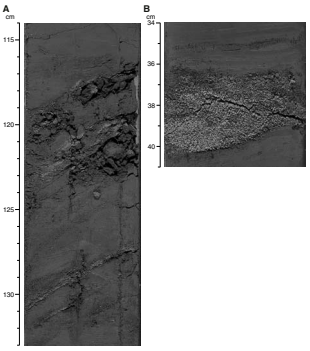

148–149 cm, and 16H-4, 2–5 cm. In addition, glauconite is present as a concentrated lens (~25% glauconite) in interval 204-1249F-16H-4, 33–50 cm.

Sedimentary Evidence of Gas Hydrate

A total of 57 gas hydrate samples were taken at Site 1249 between 0 and 75 mbsf. Six samples were taken from Hole 1249B, 28 samples from Hole 1249C, 5 samples from Hole 1249D, 5 samples from Hole 1249E, and 13 samples from Hole 1249F. Soupy and mousselike textured sediments related to the in situ presence and subsequent dissociation of gas hydrates were observed in all holes cored at Site 1249 (Fig. F5). These textures were mainly observed in lithostratigraphic Unit I-II (Fig. F6). Please note that Figure F5 does not necessarily show the overall distribution of gas hydrate because bad recovery and extensive whole-round sampling prior to core description limited our ability to completely report all of the hydrate-related sediment disruption occurrences in the stratigraphy.

Based on observations of dissociating gas hydrate, we presume the soupy textures result from the dissociation of massive gas hydrate and mousselike textures result from the dissociation of disseminated gas hydrates. Soupy textures are present in the upper <25 cm of the first section of Cores 204-1249B-2A through 5A, 8A, and 9A. In the first core sections of Cores 204-1249C-1H and 7H, soupy textures are present from 0 to 95 cm as well as from 0 to 75 cm in the first section of Cores 204-1249F-1H and 5H. Some of these textures present within the first 10 cm of a core might be caused by coring disturbance. Mousselike textures are observed in much higher abundance than soupy textures (Fig. F5). They are present throughout the sections and are not limited to the upper 25 cm of a section (Figs. F6, F7). The longest interval of sediment exhibiting mousselike textures is 1.95 m long and is present in Sections 204-1249F-3H-1 through 3H-2 (Fig. F5).

In Hole 1249F, we were able to obtain a whole-round core sample (Sample 204-1249F-8H-2, 117–127 cm) that displayed a thin gas hydrate vein (at the top of the interval; Fig. F8A) in order to examine the relationship between the location of gas hydrate in a core and the resulting response of the sediment fabric during dissociation. The sample was immediately placed in liquid nitrogen after it was removed from the core on the catwalk and was later transferred to the –80°C freezer for several days. The whole-round sample was then split along multiple perpendicular planes inside a walk-in –4°C freezer. Photographs were taken, and notes were made on textural and structural relationships.

An initial split of the whole-round sample perpendicular to the axis of the core revealed that the hydrate vein, far from being tabular, was nonhomogeneous in both its breadth and width within the sample (Fig. F8B). The vein was thicker at depth in the sample than it was as seen on the face exposed on the catwalk (Fig. F8B). Additionally, the first cut made in the freezer revealed several thinner subparallel veins that were closely associated with sulfide precipitates (yellow arrow in Fig. F8B). In order to determine the 3-D characteristics of the hydrate vein, a second split was made parallel to the first (perpendicular to the axis of the core), through the lower half of the sample. The primary vein was seen to span almost the entire width of the sample, and a second smaller vein crosscutting the first at ~20° became visible. This split also revealed nodular hydrate around the main vein. Black sulfide precipitates were visible adjacent to the gas hydrate vein parallel to the

F5. Soupy and mousselike sediments, lithostratigraphic Units I-II and III, p. 40.

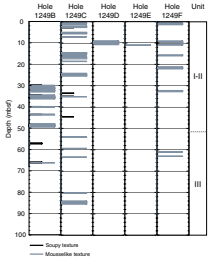

F6. Disrupted sediments, p. 41.

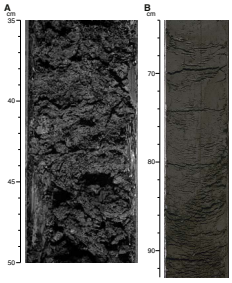

F7. Mousselike textured sediments, p. 42.

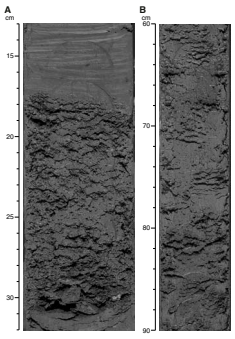

F8. Whole round before and after splitting, p. 43.

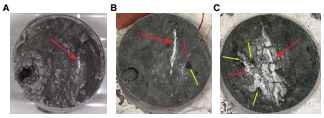

core axis (yellow arrows in Fig. F8C). A third cut was made parallel to the main gas hydrate vein along the core axis (Fig. F9) and revealed that the vein spanned the width of the core and appeared nodular at the base of the sample. Closely spaced vertical cracks or cleavage planes were also visible with ~1-mm spacing (red lines in Fig. F10). Though these features appear to be original, we cannot rule out their formation upon core recovery and refreezing in liquid nitrogen. Figure F10 also shows that the gas hydrate vein was not preserved along the outside edges of the core, possibly as a result of friction and/or dissociation during the sampling process. Finally, we allowed the hydrate to dissociate completely and observed the formation of the mousselike textures characteristic of hydrate-bearing sediments (Fig. F11).

Once the gas hydrates had completely dissociated in the whole-round sample, we took smear slides from the soupy and mousselike textured regions of the sample in order to examine the potential differences in grain size in the sediments that hosted the hydrate. These slides, along with slides taken from sediment unaffected by gas hydrate indicate that the soupy textured sample (Sample 204-1249F-8H-2, 123 cm) is a silty clay with a marginally higher percentage of coarser grains (2% sand and 40% silt), whereas the mousselike textured sample (Sample 8H-2, 119 cm) and the hydrate-unaffected sample (Sample 8H-2, 122 cm) are both silty clay (1% sand and 24% silt). The percentage of microfossils is highest in the soupy and mousselike textured samples, with ~22% of biogenic opal vs. 11% in the unaffected sample and 6% calcareous biogenic components vs. 4%, respectively.

Environment of Deposition

The lithostratigraphy at Site 1249 is very similar to that at Site 1248 (see **"Lithostratigraphy,"** p. 2, in the "Site 1248" chapter). Lithostratigraphic Units I-II and III have the same sedimentological characteristics, and seismic Horizon Y can be identified at each site (see Fig. F7, p. 57, in the "Leg 204 Summary" chapter). Lithostratigraphic Unit III is characterized by the presence of fining-upward turbidite sequences with silt, silty sand, and sand layers at their bases. The presence of these turbidites coincides with an increase in sedimentation rate toward the base of the hole (see **"Summary,"** p. 10, in "Biostratigraphy"). The lowest part recovered of lithostratigraphic Unit III at Site 1249 is marked by a matrix-supported conglomerate with clay clasts. These clasts are interpreted to be a debris flow deposit and would also be consistent with higher sedimentation rates. The debris flow deposit is thinner at this site and is present slightly higher in the section than at Site 1248, which was expected from the 3-D seismic data (see Fig. F7, p. 57, in the "Leg 204 Summary" chapter).

In lithostratigraphic Unit I-II, coarse-grained layers are lacking, suggesting that deposition is dominated by hemipelagic clay accumulation. The sedimentation rates (see **"Summary,"** p. 10, in "Biostratigraphy") range from 2 to 9 cm/k.y. for lithostratigraphic Unit I-II and decrease toward the base of the unit.

BIOSTRATIGRAPHY

Site 1249 was drilled near the top of the southern summit of Hydrate Ridge. Twelve holes were drilled, and eleven were cored. Hole 1249C was cored to 90.0 mbsf, with 67% core recovery of a Pleistocene–

F9. Split gas hydrate vein, p. 44.

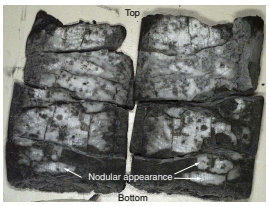

F10. Cleavage planes, p. 45.

F11. Sediment after dissociation of hydrate, p. 46.

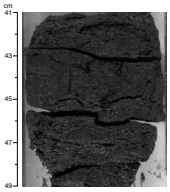

Holocene sedimentary sequence. Biostratigraphy at Site 1249 was based on the examination of diatoms and calcareous nannofossils from all core catcher samples in Hole 1249C.

Diatoms

Hole 1249C yielded common and moderately preserved diatoms, except for Samples 204-1249C-3H-CC and 13H-CC, where diatoms are few and poorly preserved. Diatom assemblages from Hole 1249C are dominated by such species as *Stephanopyxis dimorpha, Stephanopyxis* spp., *Neodenticula seminae,* and *Thalassionema nitzschioides*. Warm-water species, such as *Fragilariopsis doliolus* and *Thalassiosira oestrupii,* are sporadically present.

The interval between Samples 204-1249C-1H-CC (1.60 mbsf) and 3H-CC (7.18 mbsf) contains *N. seminae* but does not contain *Proboscia curvirostris*. These samples were assigned to North Pacific Diatom Zone (NPD) 12 (*N. seminae* Zone). The last occurrence (LO) of *P. curvirostris* was placed between Samples 204-1249C-3H-CC (7.18 mbsf) and 4H-CC (18.82 mbsf). *P. curvirostris* is present continuously down to the bottom of Hole 1249C, indicating that the age of the bottom is younger than 1.6 Ma.

Calcareous Nannofossils

Rare to common calcareous nannofossils were observed in almost every core catcher sample from Hole 1249C, except for Sample 204-1249C-8H-CC, where calcareous nannofossils are absent.

Common to rare *Emiliania huxleyi* is continuously present in the top interval of 1.42–18.82 mbsf, and this interval was assigned to Zone NN21. Sample 204-1249C-5H-CC contains neither *E. huxleyi* or *Pseudoemiliania lacunosa* and was assigned to Zone NN20. The LO of *P. lacunosa* in Sample 204-1249C-7H-CC (40.64 mbsf) marks the NN19b/NN20 zonal boundary for the stratigraphic level. Various small *Gephyrocapsa* species are common in Sample 204-1249C-7H-CC (40.64 mbsf) but are absent in the next sample below (Sample 204-1249C-8H-CC), which is barren of calcareous nannofossils. As a result, the small *Gephyrocapsa* spp. Acme Zone was not recognized in Hole 1249C. Sample 204-1249C-9H-CC (59.97 mbsf) and samples below it contain rare *Calcidiscus macintyrei*. The LO of *C. macintyrei* (1.59 Ma) was placed at 59.97 mbsf. *Gephyrocapsa lumina* is common in sediments from near the bottom of Hole 1249C (Sample 204-1249C-17H-CC [148.47 mbsf]), assigning the sample to the lower part of early Pleistocene Zone NN19, with an age of younger than 1.67 Ma.

Summary

Based on analysis of diatoms and calcareous nannofossils from the Pleistocene–Holocene sedimentary sequence in Hole 1249C, one diatom and three nannofossil events were recognized (Table T3; Fig. F12). The age of the bottom sediment of Hole 1249C was estimated to be younger than 1.6 Ma, based on the diatom assemblage, or to be younger than 1.67 Ma, based on the nannofossil assemblage. Therefore, the age of the sediment sequence in Hole 1249C is early Pleistocene–Holocene.

We estimated the linear sedimentation rates for Site 1249 using the identified events (Fig. F12). The sedimentation rates are estimated to be

T3. Bioevents, p. 82.

F12. Age-depth plot, p. 47.

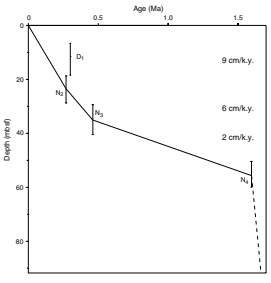

9 cm/k.y. for the interval from the top of Hole 1249C to 25 mbsf, 6 cm/k.y. for the interval from 25 to 35 mbsf, and 2 cm/k.y. for the interval from 35 to 55 mbsf.

INTERSTITIAL WATER GEOCHEMISTRY

The main objectives of the interstitial water (IW) program at this site were to measure geochemical proxies for the presence and abundance of gas hydrate, which had been previously observed in near-surface sediments at this location (Suess et al., 2001) and resulted in poor recovery in the upper 40 mbsf. Twelve holes were drilled at this site, and we collected a total of 49 whole rounds for pore water analyses. Seven samples were taken from Hole 1249B, which was drilled with the new RAB-8 instrument (see "Operations," p. 29, in "Logging While Drilling" in "Downhole Logging"). These data were collected to compare the quality of samples recovered using this tool with that of the conventional ODP coring devices. Hole 1249C was cored in its entirety with the APC and sampled for IWs at a resolution of approximately two samples per core, for a total of 20 samples spanning the entire depth of the borehole. In Holes 1249D and 1249E, pressure coring devices were deployed to recover gas hydrate from the upper 30 mbsf, where core recovery was generally poor. We collected two samples from Hole 1249D and one sample from Hole 1249E, in an effort to better constrain the chloride distribution in these upper sediments. Hole 1249F was heavily sampled for microbiological studies. We collected nine samples from this hole in a coordinated program with the shipboard microbiologists. The IW geochemistry data are tabulated in Table T4 and are illustrated in Figure F13.

Site 1249 was cored to a TD of 90 mbsf (Holes 1249B and 1249F), thus the bulk of the IW data obtained at this site lies within the gas hydrate stability zone (GHSZ). The composition of IWs in this zone is influenced by gas hydrate geochemistry and by the effects of fluid advection. Fluid flow in this area has been shown to reach rates of 100–300 cm^2/yr (Torres et al., 2002; Tryon et al., 2002).

Chloride Concentration and the Presence of Gas Hydrate

The pore fluids recovered at Site 1249 show a pronounced enrichment in the dissolved chloride values, which in Hole 1249B reach a maximum value of 1008 mM at 6.96 mbsf (Sample 204-1249B-3H2, 41–51 cm). During gas hydrate formation, ions are excluded from the hydrate structure and will accumulate in the interstitial fluids. This process causes the pore water to become saltier. If the rate of hydrate formation is slower than that of ion diffusion and/or that of advective transport, the excluded ions will be removed from the zones of hydrate formation by advection or diffusion. When this is the case, gas hydrate dissociation during core recovery results in freshening of the pore fluids by addition of water formerly sequestered by gas hydrate (Hesse and Harrison, 1981) (see "Interstitial Water Geochemistry," p. 13, in the "Explanatory Notes" chapter). In these situations, negative chloride anomalies relative to in situ concentrations are proportional to the amount of gas hydrate. These negative anomalies, relative to background in situ values, have been observed at other sites drilled during Leg 204 (see "Interstitial Water Geochemistry," p. 13, in the "Site

T4. Dissolved species in pore waters, p. 83.

F13. Concentration profiles of various dissolved species, p. 48.

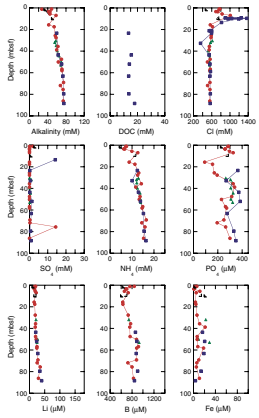

1244" chapter; **"Interstitial Water Geochemistry,"** p. 13, in the "Site 1245" chapter; **"Interstitial Water Geochemistry,"** p. 7, in the "Site 1246" chapter; and **"Interstitial Water Geochemistry,"** p. 9, in the "Site 1248" chapter).

However, at Site 1249, we infer that methane hydrate is forming at a faster rate than ions can be removed from the surrounding fluid, leading to the observed positive chloride anomalies (i.e., chloride values that are saltier than baseline values) (Fig. **F14**). Suess et al. (2001) reported such chloride enrichments in fluids recovered at 1.2 mbsf from the southern summit of Hydrate Ridge. The chloride anomalies observed by drilling at Site 1249 confirm the presence of a gas hydrate–generated brine at this location and extend the minimum depth of high chloride values to 10 mbsf.

The chloride anomalies observed in the whole-round IW samples reflect not only the in situ enrichment but include a freshening component resulting from gas hydrate decomposition during core retrieval and processing. In an effort to recover the most pristine sample that would reflect the in situ chloride concentration, we inspected and collected 10 samples from the working half of Cores 204-1249F-3H and 7H, as listed in Table **T5,** within 90 min of core retrieval. The dissociation of gas hydrate resulted in heterogeneous textures within the core. Some sediment retained its original structure ("dry appearance"), whereas nearby material had liquefied during gas hydrate dissociation leading to very unconsolidated sediment ("wet appearance"). Sediments with unconsolidated mousselike textures have been used by the sedimentologists to infer locations where gas hydrate was present in the core (see **"Lithostratigraphy,"** p. 5). An example of such a heterogeneous texture, induced by very localized dissociation of gas hydrate, is shown in Figure **F15.** Paired samples (~10 cm^3) were collected from both consolidated and mousselike sediments for pore water analyses of chloride content (shipboard) and isotopic characterization of the water (shore based). Companion samples were taken for measurement of moisture and density (MAD) (see **"Physical Properties,"** p. 22, in the "Explanatory Notes" chapter). The shipboard results of this experiment are listed in Table **T5.** In all cases, samples collected from the "wet-looking" sediment indeed have a significantly higher water content and a chloride concentration that was significantly lower than a nearby sample, which had retained its coherent structure. These differences are illustrated in Figure **F14B.** Pore fluids in the "dry-looking" samples had the highest chloride concentrations, with a maximum of 1368 mM (Sample 204-1249F-3H-1,76–78 cm [9.76 mbsf]).

The high chloride content in the pore fluid reveals that gas hydrate at Site 1249 is forming in a system where the rate of gas hydrate formation exceeds the rate at which excess salts can be removed by diffusion and/or advection. In a perfectly closed system, complete dissociation of gas hydrate during core recovery will, theoretically, result in a chloride concentration equivalent to that of the pore fluid before gas hydrate formation. The fact that whole-round core samples from the upper 40 mbsf show a wide range of chloride values reflects the heterogeneity of the gas hydrate distribution and sampling artifacts. The sampling artifacts are induced in part by the selective removal of gas hydrate samples from the core for a variety of studies on the composition (see **"Organic Geochemistry,"** p. 14) and distribution (see **"Lithostratigraphy,"** p. 5,) of these deposits.

F14. Chloride concentration profile, p. 50.

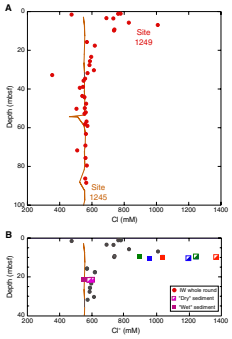

T5. Chloride and MAD on wet and dry samples, p. 84.

F15. Disturbed and undisturbed sediments, p. 51.

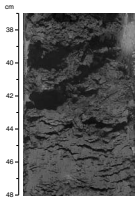

Carbon Cycling

Zero to near-zero concentrations of sulfate in the shallow subsurface (1.7 mM) (Section 204-1249C-1H-1 [1.10 mbsf]) identify Site 1249 as a locality where methane is delivered directly to the seafloor. Advection promotes the co-consumption of methane and bottom water sulfate by the microbially mediated process of anaerobic methane oxidation (AMO) (see **"Interstitial Water Geochemistry,"** p. 9, in the "Site 1248" chapter). This results in elevated pore water alkalinity as methane carbon is oxidized to form dissolved carbon dioxide (Table **T4;** Fig. **F13**).

Underwater vehicle surveys over the southern Hydrate Ridge summit revealed extensive bacterial mat coverage, clearly indicating communities that actively utilize methane. Indeed, dense aggregates of a structured Bacteria-Archaea consortium exist within *Beggiatoa* mats collected from active seeps on Hydrate Ridge (Boetius et al., 2000). This consortium apparently carries out the AMO at the sediment surface (e.g., Boetius et al., 2000; Reeburgh, 1976). Near-surface pore water samples (0–2 cm below seafloor) and benthic instrumentation deployed at these sites have documented fluxes of methane and H_2S out of the sediments on the summit of Hydrate Ridge. Sahling et al. (2002) calculated H_2S fluxes as high as 63 mM/m^2/day, and Torres et al. (2002) document methane fluxes of 10–100 mM/m^2/day out of mat-covered sites at this location.

Major and Minor Element Distributions

The presence of a brine in the upper 20 mbsf affects the concentration of all dissolved species. In the same way as Cl^- ions are excluded from the hydrate structure, so are other dissolved ions. This results in enrichments that are clearly noticeable in the Na^+, K^+, Ba^{2+}, Sr^{2+}, and Mg^{2+} distributions (Fig. **F12**). Superimposed on the enrichment resulting from brine formation is the effect of rapid advection of fluids that have been modified at depth and in near-surface sediments. For example, sulfate is so readily utilized by methane oxidizers that its concentration is below detection limits even within the brine. Sulfate in mat-covered sediments on Hydrate Ridge is consumed within the upper 5 cm below seafloor (Torres et al., 2002). The advection of calcium-depleted fluids, plus in situ consumption by carbonate formation, results in a profile showing very low calcium concentration within the entire depth sampled. Similar depletion in dissolved calcium was reported by Torres et al. (2002) in sediments covered by bacterial mats at the summit of southern Hydrate Ridge. At these sites calcium reaches the background levels of 2 mM at 2–5 cm below seafloor, consistent with advective transport at rates ranging from 50 to 100 cm/yr. The calcium and sulfate data obtained by drilling at Site 1249 is consistent with these observations.

Fluid advection and sulfate depletion also result in very large dissolved barium concentrations throughout the sediments. Even the shallowest sample analyzed (Sample 204-1249C-1H-1, 110–125 cm [1.10 mbsf]) has a concentration of 90 µM, which is three orders of magnitude higher than the barium content of the bottom water at this site (~9×10^{-2} µM) (M. Torres, unpubl. data). At locations where advective flow results in transport of sulfate-depleted barium-rich fluids to the seafloor, barium is released to the bottom water (Torres et al., 1996). At Hydrate Ridge, high barium fluxes have been measured with benthic instrumentation (M. Torres, unpubl. data; Tryon et al., 2002) that are consistent with the observations obtained by drilling at this site.

ORGANIC GEOCHEMISTRY

Site 1249 is located near the summit of Hydrate Ridge. The shipboard organic geochemistry program at Site 1249 consisted of analyses of hydrocarbon and nonhydrocarbon gases from headspace, voids, dissociated gas hydrates, and samples from the PCS degassing experiments. A description of the methods used for these analyses is summarized in "Organic Geochemistry," p. 16, in the "Explanatory Notes" chapter.

Hydrocarbon Gases

The levels of methane (C_1), ethane (C_2), ethylene ($C_{2=}$), and propane (C_3) in the cores were measured using the headspace technique. The results are reported in Table T6 and plotted as parts per million by volume (ppmv) of gas component vs. depth in Figure F16. Methane contents are very high near the seafloor, with as much as 31,000 ppmv at 0.6 mbsf. Headspace samples generally contain <100,000 ppmv of methane because of degassing during core retrieval. However, at Site 1249 several samples (Sections 204-1249B-2A-2, 204-1249C-3H-1, 3H-2, 4H-1, and 204-1249F-6X-1) contain extremely high amounts (220,000–560,000 ppmv) of methane. These large quantities of gas could only be caused by the presence of gas from dissociated hydrate in the headspace samples. The concentration of ethane is also very high in these samples, ranging from several hundred to 1426 ppmv. Ethylene is sporadically present at trace levels (0.4–0.7 ppmv). Propane is present in relatively high concentrations (tens of ppmv), even in the upper part of the analyzed section (Table T6; Fig. F16). Enrichment of ethane and propane at shallow depths probably reflects the presence of migrated thermogenic hydrocarbons. The high concentrations of methane in the sediments and the presence of gas hydrate at the seafloor are consistent with the observations of active venting of gas at this location.

The composition of gas samples from voids or expansion gaps in the core liner are listed in Table T7. The void gas (vacutainer [VAC]) samples are relatively pure methane, generally with minimal air contamination. Contents of methane in the voids are generally >900,000 ppmv (>90% by volume), unless diluted by air (Fig. F17). Ethane contents of core void gas samples decrease with depth from ~1,300–2,000 ppmv near the seafloor to 48 ppmv near the base of the cored sequence. Concentrations of propane in void gas samples are also relatively high, ranging from 5 to 79 ppmv. Iso- and normal butanes are present below 20 mbsf down to the base of the cored sequence, and their concentrations are also significant considering the shallow depth of the sediments (Table T7; Fig. F17).

These trends are evidence against a diffuse upward migration of thermogenic hydrocarbon gases through the cored section. Instead, the gas probably migrates along focused conduits to relatively permeable zones near the seafloor. The formation and decomposition of gas hydrate may also have some influence on the observed gas compositions.

Gas composition expressed as the C_1/C_2 ratio of headspace and void gas is plotted vs. depth in Figure F18. Several values of C_1/C_2 for headspace gas fall within the trend line of the void gas profile, probably because these samples contained gas hydrate. C_1/C_2 ratios for both headspace and void gas show a systematic decrease from the seafloor to 40 mbsf and then a gradual increase down to base of the cored section. The

T6. Methane, ethane, ethylene, and propane, p. 85.

F16. C_1, C_2, $C_{2=}$, and C_3 vs. depth, p. 52.

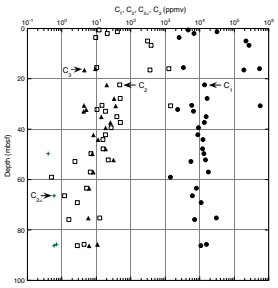

T7. Light hydrocarbon and nonhydrocarbon gases, p. 86.

F17. Light hydrocarbons vs. depth, p. 53.

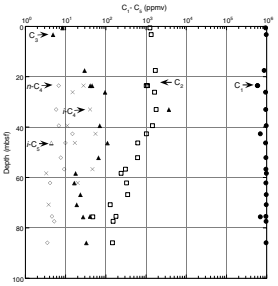

F18. C_1/C_2 ratio vs. depth, p. 54.

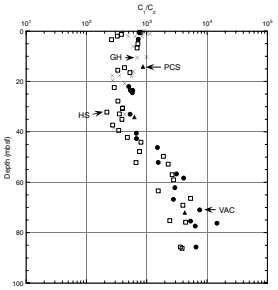

minimum in the C_1/C_2 trend at 30–40 mbsf suggests proximity to the permeable zone at this depth.

When C_1/C_2 ratios of the void gas are plotted vs. temperature (Fig. F19), the C_1/C_2 trend falls within the "anomalous" field from the seafloor down to 40–50 mbsf and shifts back to the normal range at greater depths.

F19. C_1/C_2 ratio vs. temperature, p. 55.

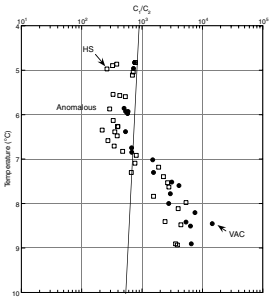

Gas Hydrate and Pressure Cores

Gas hydrates and gas hydrate–bearing sediments were recovered from cores on the catwalk. A total of 16 hydrate samples were decomposed in syringes, and the gas hydrate–bound gases were analyzed (Table T8). The concentration of methane varies from 169,544 to 983,641 ppmv as a result of air contamination during sampling. Four samples of gas hydrate–bound gas contain only methane and ethane, consistent with that gas being derived from Structure I gas hydrate. However, the other samples contain considerable amounts of propane and butanes, suggesting the possibility of Structure II gas hydrate. The C_1/C_2 ratio also reflects the enrichment of ethane in the gas hydrate–bound gas. Dissociated gas hydrate samples with relatively high C_1/C_2 ratios may reflect the influence of gas from surrounding sediments (Table T8; Fig. F18).

T8. Gas hydrate–bound gases, p. 87.

Three deployments of the PCS successfully retrieved full (1 m) cores from depths of 14.0–71.9 mbsf (Cores 204-1249C-6P and 204-1249F-4P and 14P). The composition of gas samples obtained during controlled PCS degassing experiments are listed in Table T9. All three PCS samples show pressure curves and gas contents that confirm the subsurface occurrence of methane hydrate (see "Downhole Tools and Pressure Coring," p. 20). Based on the volume-averaged composition, the C_1/C_2 ratios for gas from the PCS cores fall on the VAC/void gas trend (Fig. F19).

T9. PCS gas samples, p. 88.

MICROBIOLOGY

The primary focus of the microbiological studies at Site 1249 was the relationship of sedimentary microbial communities to methane hydrates. At the summit of Hydrate Ridge, the methane flux overwhelms the sulfate flux; sulfate was nonexistent in the upper sediments (see "Carbon Cycling," p. 13, in "Interstitial Water Geochemistry"), and methane hydrates were present in the "mudline" cores. Because methane was present up to the seafloor (see "Hydrocarbon Gases," p. 14, in "Organic Geochemistry") and the holes at Site 1249 were shallow, all sediment acquired at this site came from within the GHSZ and showed IR thermal anomalies indicative of hydrate presence (see "Infrared Scanner," p. 17, in "Physical Properties").

Microbiological Sampling

At Site 1249, the methane that was our focus was also our nemesis. Massive hydrates made for difficult coring, gas expansion caused poor recovery, and melting hydrates liquified surrounding sediment. All microbiological sampling took place in Hole 1249F, which was drilled to 90 mbsf. The upper 40 m contained significant quantities of massive hydrate and appeared very disturbed ("wet-looking" core and pieces of sediment liberally distributed along the length of the core liner), and

few sections were chosen for microbiological sampling. Cores deeper in Hole 1249F had better recovery and were sampled more often. Sampled intervals are listed in Table T10.

Microbiological samples (with the exception of those from Core 204-1249F-1H) did not show large IR temperature anomalies that might indicate massive hydrate. Smaller thermal anomalies that might indicate disseminated hydrates were present in microbiological core sections, but because postcruise processing will be required before the actual locations of these smaller anomalies are known, sampling was performed without consideration of these potential hydrates. Soupy or moussy sediments were noted and tentatively identified as hydrate influenced, and samples from the same section with different sediment textures were sampled for comparative microbiology studies.

Most gas hydrates were removed from the cores before microbiological sampling began, but the microbiologists had the opportunity to sample a core at the top of Hole 1249F that still contained massive hydrate (Core 204-1249F-1H). A 20-cm hydrate sample was taken from the top of Core 204-1249F-1H, and the remainder of the core (Sections 204-1249F-1H-1and 1H-2) was processed for microbiological investigations. The liner was slit (without splitting the core) so that the top of the liner could be removed. This was done in an attempt to minimize disturbance of the very gassy and soft material. Hydrates were present throughout the core. Two nearly circular "biscuits" of ~1-cm-thick massive hydrate were placed in liquid nitrogen, and thinner "biscuits" of hydrate with interlayered sediment were also observed. These circular layers indicate that the APC punched through near-horizontal horizons of hydrate. Millimeter-thick veins of hydrate cut through the sediment at all angles, from horizontal to subvertical. The structure of both the thick hydrate layers and thin hydrate veins was flaky and platy (like mica); the surrounding sediments looked and felt like aerated pure clay. This core was sampled with extreme caution. The outer layers were repeatedly lifted off the top of the sediment with a flame-sterilized spatula until the center of the core was exposed, and samples were removed with another sterile spatula. Sediments were not stiff enough to use syringe corers.

T10. Intervals sampled for microbiology, p. 90.

Core Quality Assessment

Contamination tests were run on cores from Hole 1249F (Table T11), but most of the results are inconclusive (see below). However, some measure of comfort can be gained from looking at the sulfate concentrations from this site (see "Carbon Cycling," p. 13, in "Interstitial Water Geochemistry"). IW samples are squeezed from sediments taken from the core interior, similar to microbiological samples. Zero sulfate values below the zone of sulfate depletion indicate that the drilling fluid (sulfate-rich surface seawater) has not penetrated the interior of the core. At Site 1249, even though gas hydrates are abundant and the potential for core disturbance is high, sulfate values do not show large intrusions of seawater.

T11. Core quality indicators, p. 91.

Perfluorocarbon Tracer

Only deeper cores were sampled for PFT at Site 1249 because of logistical difficulties. Raw data (grams of PFT per sample), uncorrected for sediment weight, are presented in Table T11. Average sample size was 5 g of sediment. Although samples from the inside of the core show a

hundredfold reduction in PFT as compared to outer layers, all concentrations are extremely low and probably reflect loss from sampling vials. Samples were not analyzed until much later in the cruise, and the perfluorocarbon is extremely volatile.

Fluorescent Microspheres

Results of microsphere counts for Site 1249 are shown in Table T11. Of the eight core sections sampled, three showed successful tracer deployment and five had no detectable spheres in subsamples taken for analysis. One of the three cores with successful microsphere deployment also had a significant number of spheres in the internal sample. Both the apparent failure of deployment and interior presence of spheres are likely to be related to the difficulties encountered in coring this site.

PHYSICAL PROPERTIES

At Site 1249, five individual holes were drilled, but only three were used for physical property analyses. Holes 1249B and 1249C had very poor core recovery and are combined with Hole 1249F to describe the physical property results. Hole 1249F had almost complete core recovery, and therefore, data gaps in Holes 1249B and 1249C were filled when the equivalent intervals were cored in Hole 1249F. Physical properties were acquired following the standard procedures (see "Physical Properties," p. 22, in the "Explanatory Notes" chapter). IR thermal imaging of all cores was done in Holes 1249B and 1249F, but only the top two cores of Hole 1249C were imaged to speed up the sampling of gas hydrates on the catwalk.

Infrared Scanner

IR imaging of cores recovered at Site 1249 enabled the on-catwalk identification of hydrate zones in each core, as described in "Physical Properties," p. 22 in the "Explanatory Notes" chapter. This information was used to facilitate hydrate sampling and preservation for most cores. The IR thermal anomalies are catalogued in Table T12, which includes an interpretation of the overall hydrate texture for each anomaly. Half of the hydrate detectable by IR imaging of Hole 1249F is present as nodular or massive textures (43% nodular and 8% massive). Apparently, disseminated hydrate accounts for 28% of the presence and vein structures for 21%. Core recovery is poor in Holes 1249B and 1249C above 40 mbsf. Core liners partially filled with hydrate fragments result in a nodular appearance even if the original material is massive or highly concentrated hydrate (Fig. F20A). For this reason, nodular and massive hydrate presence in the upper part of Hole 1249C is considered to be a single category. Textures differ systematically from the upper to the lower parts of the holes cored at this site, with massive and nodular textures dominating the upper part of Hole 1249F and all of Hole 1249C. Below ~47 mbsf in Hole 1249F, disseminated zones and veins or lenses become the dominant textures of hydrate. Figure F20B is a representative example of a steeply dipping relatively thick hydrate vein. In Hole 1249F, below 47 mbsf, five veins (23% of hydrate below 47 mbsf) appear to crosscut bedding, indicating that a significant amount of hydrate has been emplaced in fractures or faults.

T12. Gas hydrate, p. 92.

F20. IR images of hydrate, p. 56.

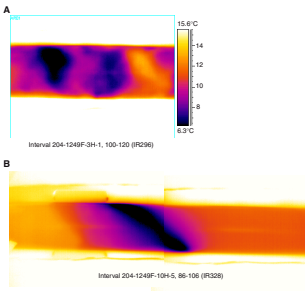

From this observation, we infer that stratigraphic control may be of less importance at Site 1249 than at other sites (e.g., Site 1245). Successive thermal images were used to produce downcore thermal profiles for each core recovered in Holes 1249B, 1249C, and 1249F (Fig. **F21**). Extensive cold anomalies are present in Holes 1249B and 1249F above 40–50 mbsf. The temperature anomalies created by hydrate have been extracted from the downcore temperature data and from direct examination of IR images for Hole 1249F. Figure **F22** shows the magnitude of the temperature anomalies as a function of depth for Hole 1249F plotted against pore water saturation (S_w) calculated from LWD (see **"Downhole Logging,"** p. 29). Results are consistent and show the decrease in IR anomalies at depths mirrored by the change in S_w. Poor recovery in the upper part of Hole 1249F makes precise assignment of IR anomaly depths impossible. This uncertainty explains the apparent presence of IR anomalies in zones of no core recovery in Figures **F21** and **F22.** The assignment of depth to intervals of unfilled core liners is somewhat arbitrary; however, depth assignment of IR anomalies are in their appropriate stratigraphic sequence, and actual depths are certainly within 9.5 m (length of cored interval) of their estimated in situ depth.

Sediment Density from Multisensor Track and Moisture and Density

The sediment density trend, which combines data from all of the available holes cored at this site, shows a normal compaction-related downhole increase (Fig. **F23**). Sediment density is ~1.55 g/cm³ at the seafloor and increases to ~1.65 g/cm³ at a depth of ~90 mbsf (Table **T13**). Porosity decreases downhole with increasing depth, from values of ~65% at the seafloor to 50% at 90 mbsf. The GRA density record is highly scattered because of gas cracking and is offset by 0.2 g/cm³ to the LWD and MAD data. The LWD data indicate an increase in sediment density at a depth of ~55 mbsf that is associated with seismic Horizon Y (Fig. **F24**); however, neither the MAD nor the GRA data show a similar trend across this interval.

The grain density does not show any downhole trend. The average grain density is 2.70 g/cm³. The anomalously low grain densities and bulk densities and associated high porosities at ~10 mbsf (e.g., in Sections 204-1249F-3H-1 and 3H-2) correspond to an interval where gas hydrate is present. The presence of gas hydrate in these core sections was inferred from the strong IR anomalies (Fig. **F23**) and mousselike textures, as described in the core descriptions (see **"Lithostratigraphy,"** p. 5). As a result of the highly disrupted nature of the sediments and the high water content of the samples associated with dissociated hydrate, these samples are not representative of the general trend.

Magnetic Susceptibility

MS shows an irregular downhole trend with several MS peaks. These peaks correspond to individual turbidite layers or to intervals with abundant sulfides (see **"Lithostratigraphy,"** p. 5). One example of a sulfide-related MS anomaly can be seen in Core 204-1249F-15H, at a depth of 78–86 mbsf. Another MS anomaly in Core 204-1249C-9H, at a depth of 55 mbsf, is correlated with seismic Horizon Y. Horizon Y is characterized by abundant turbidite sequences with sandy layers (see **"Lithostratigraphy,"** p. 5), which may be the cause of these MS peaks.

F21. IR temperature profiles, p. 57.

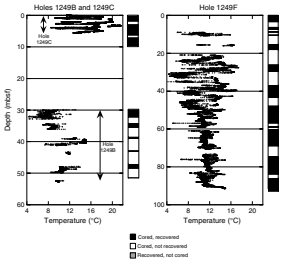

F22. IR temperature anomalies compared to S_w from LWD, p. 58.

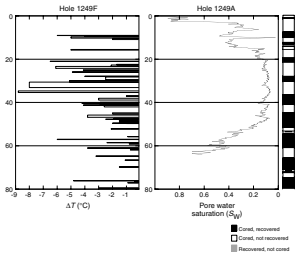

F23. Overview of physical properties, p. 59.

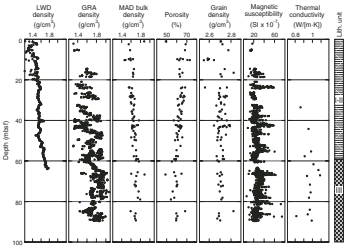

T13. MAD properties, p. 93.

F24. Comparison of physical properties with 3-D seismic data, p. 60.

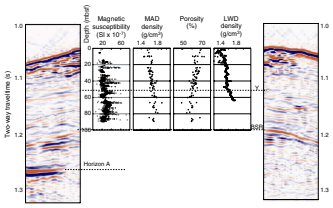

Compressional Wave Velocity from Multisensor Track and Hamilton Frame

No velocity measurements were carried out at this site because of poor core recovery and extensive gas-expansion cracks.

Thermal Conductivity

As a result of poor core recovery and overall poor core quality (abundant gas expansion cracks), only a few thermal conductivity measurements were made in Hole 1249C (Table T14). A more detailed profile was acquired in Hole 1249F.

T14. Thermal conductivity, p. 94.

Shear Strength

No shear strength measurements were carried out at this site because of poor core recovery and/or abundant gas expansion cracks.

Special Hydrate Dissociation Experiment

At this site, we conducted a second hydrate dissociation experiment similar to that performed on a core section from Site 1248. Section 204-1249F-9H-3 was used for this experiment, and it contained two different types of gas hydrate. Disseminated hydrate was inferred from IR thermal imaging throughout intervals 204-1249F-9H-3, 0–40 cm, and 95–130 cm (Fig F25). Within interval 204-1249F-9H-3, 80–95 cm, hydrate was present in a vein-type structure. The experiment was conducted over a period of ~3 hr. During this time, the section was scanned six times with the X-ray line scanner and was measured five times with the MST (Non Contact Resistivity system, GRA, and MS). After the experiment was finished, the section was split open lengthwise and discrete samples were taken every 10 cm. The section was finally imaged and analyzed to examine structural controls on gas hydrate occurrence. The temperature increased from an initial average value of 10° to 21°C, which is the average ambient room temperature, over the duration of the experiment.

F25. Hydrate dissociation experiment, p. 61.

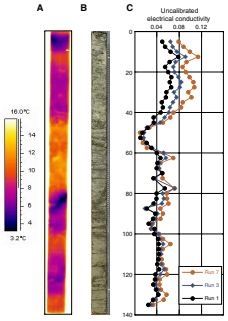

The electrical conductivity showed a significant change in the upper 40 cm during the 3-hr experiment (Fig. F25). GRA and MS did not change during that time. The change in conductivity is 10 times greater than can be accounted for by the temperature increase. The increase in conductivity over the upper 40 cm is similar to that found in an experiment at Site 1248 (see "Physical Properties," p. 14, in the "Site 1248" chapter. It can most easily be accounted for by the dissociation of hydrate, in the shape of veins or veinlets rather than as multiple small nodules (disseminated hydrate). Vein structure of electrically insulating hydrate would provide significant resistance to current flow despite its relatively small volume, something that would not be expected from small nodules.

The IR anomaly in interval 204-1249F-9H-3, 80–95 cm, indicates a vein or layer of hydrate, confirmed by the X-ray images and the digital photograph taken from the split archive half after the experiment was finished (Fig. F26). The images show a fracture dipping across the liner at an angle of ~45°. The fracture appears as a sharp boundary in the X-ray image, taken just after the core was recovered on deck. The digital core photograph shows a mousselike texture of the sediments, typical for sediments that contained gas hydrates. Onshore analyses will be

F26. Vein or layer of hydrate, p. 62

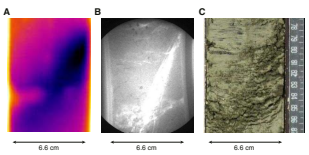

conducted to model the change in resistivity associated with various hydrate concentrations and the thermal anomaly.

Summary and Discussion

Physical properties were acquired at Site 1249 from three different holes, which were combined to provide downhole profiles. The measurements were strongly affected by poor core recovery and gas expansion effects. Data interpretation and correlation to lithostratigraphic units is, therefore, limited. In general, the MAD samples provide the highest quality data and correlate well with the LWD data. IR thermal imaging provided the best method to detect the presence of hydrates in the core liners. A complete downhole temperature profile was acquired only in Hole 1249F.

DOWNHOLE TOOLS AND PRESSURE CORING

Downhole Temperature Measurements

Ten in situ temperature runs were made at this site: eight using the APCT tool and two using the DVTPP (Table T15; Fig. F27). APCT data were modeled using the software program TFIT (as described in "Downhole Tools and Pressure Coring," p. 34, in the "Explanatory Notes" chapter) on the basis of measured thermal conductivities (see "Physical Properties," p. 17). Temperatures were measured directly from the DVTPP data because the tool was deployed long enough to approach equilibrium.

The resulting temperature estimates are shown vs. depth below the seafloor in Figure F28A. In determining the temperature gradient from these measurements, we did not include the temperature of 11.5°C measured at 90 mbsf using DVTPP tip 3 because of uncertainties in the calibration of this tool (see "Downhole Tools and Pressure Coring," p. 29, in the "Site 1244" chapter). The thermal gradient of 0.054°C/m derived from these data is similar to the thermal gradients at other sites and is not sensitive to whether the mudline temperature is included.

The scatter in the data, however, is greater than that at most other sites, especially in the depth range of 20–40 mbsf, where other observations indicate the presence of high concentrations of gas hydrate (see "Interstitial Water Geochemistry," p. 11, "Organic Geochemistry," p. 14, and "Downhole Logging," p. 29). This scatter may have several sources, including different calibration for APCT 11 and 12, the effect of gas hydrate on in situ thermal conductivity, and possible dissociation of gas hydrate in situ in response to probe insertion. To evaluate the importance of calibration effects, we added 0.51°C to temperatures derived from APCT 11, as indicated by the ice-bath tests discussed in "Downhole Tools and Pressure Coring," p. 14, in the "Site 1246" chapter. This reduced the scatter in the data and led to a lower estimate for thermal gradient (Fig. F28B).

The possible effect of in situ gas hydrate on estimates of in situ temperature was considered because we observed that the misfit between the observed temperature decay and the decay predicted by the software program TFIT was larger than normal for data of this quality for several APCT tool runs. One possible explanation for this misfit is that the conductivity determined on board is not representative of the in situ conductivity. Because the thermal conductivity of gas hydrate is

T15. Temperature measurements, p. 95.

F27. Estimating in situ temperature, p. 63.

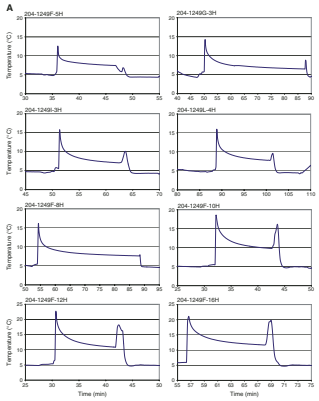

F28. Subsurface temperatures plotted vs. depth, p. 65.

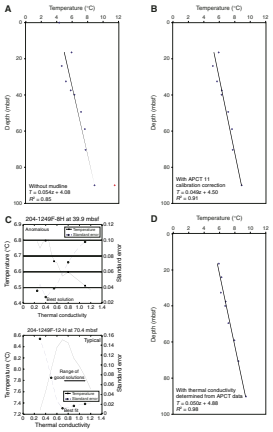

~0.4 W/(m·K) (Ruppel, 2000), the in situ thermal conductivity will be quite different from the conductivity measured on board if a high concentration of hydrate is present in the subsurface. Figure F28C shows the results of a preliminary effort to determine whether in situ thermal conductivity as well as in situ temperature can be independently resolved. The equilibrium temperature was determined using TFIT for thermal conductivity ranging from 0.3 to 1.2 W/(m·K) in steps of 0.05 W/(m·K). For "typical" measurements, where in situ conductivities are in the range of 0.7–1.2 W/(m·K), equilibrium temperature and thermal conductivity cannot be independently resolved and an independent measurement of thermal conductivity is required (Core 204-1249F-12H in Fig. F28C). For "anomalous" measurements, however, the best fit to the data occurs for low thermal conductivity and the in situ temperature corresponding to the best solution for thermal conductivity is higher than that derived using the shipboard measurements (Core 204-1249-8H in Fig. F28C). If in situ temperatures at Site 1249 are recalculated, solving simultaneously for in situ temperature and in situ thermal conductivity (Table T15), in situ temperatures are generally higher and the fit of the data to a linear temperature gradient is improved. Additional analysis of this phenomenon and of other possible effects of the presence of gas hydrate on in situ temperature will be undertaken postcruise. For example, the frictional heat pulse resulting from probe insertion can raise the temperature above in situ hydrate stability for as long as 1 min.

In summary, although there is considerable uncertainty about the in situ temperature gradient at this site, it is clear that the temperature gradient is not significantly higher and may even be lower than those at other sites drilled during Leg 204. This implies that upward advection of warm fluid from greater depths must be relatively slow (probably <1 cm/yr) (Tréhu et al., 2003) and represents an additional constraint on models for the dynamics of hydrate formation at this summit. The low in situ thermal conductivities derived for some of the temperature measurements are consistent with other data, indicating large concentrations of gas hydrate in the subsurface at Site 1249.

In Situ Pressure Measurements

Pressure data measured by the DVTPP are shown in Figure F27B. Analysis is pending.

Pressure Core Sampler

The ODP PCS was deployed seven times at Site 1249. Only three of these deployments were successful (i.e., a core under pressure was recovered). The ball valve failed to actuate during the other four deployments. The main objectives of the deployments were (1) to construct a detailed profile of concentration and composition of natural gases in the upper part of the section (0–80 mbsf) and (2) to identify the presence/absence and concentration of gas hydrate within the GHSZ.

Specific depth intervals were targeted for deployment of the PCS. All three cores (Cores 204-1249C-6P [33.5–34.5 mbsf] and 14P [71.4–72.4 mbsf] and 204-1249F-4P [13.5–14.5 mbsf]) were recovered from above the BSR at ~115 mbsf.

The time to degass the three PCS chambers ranged from 967 to 11,268 min (Table T16). Pressure was recorded during degassing experiments (Fig. F29). Gas was collected in a series of sample increments

T16. Degassing experiments, p. 96.

F29. Volume-pressure-time plots for PCS, p. 66.

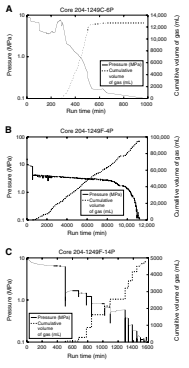

(splits), and most were analyzed for molecular composition (see "Organic Geochemistry," p. 14). In addition, gas splits were subsampled for onshore analyses. After degassing, the PCS chambers were disassembled. The lengths of the cores were measured (Table T16), and samples were taken for analysis of physical properties (see "Physical Properties," p. 17).

Gas was collected in 2- to 1300-mL increments. The measured incremental and cumulative volumes are plotted vs. time (Fig. F29). The cumulative volume of released gas varies from 4,800 (Core 204-1249F-14P) to 95,110 mL (Core 4P) (Table T16). The volume of the last gas splits varies from 2 (Core 204-1249C-6P) to 20 mL (Core 204-1249F-4P). This measurement suggests that almost all gas present in the cores was collected.

Gases released from the PCS are mixtures of air (N_2 and O_2), CH_4, CO_2, and C_{2+} hydrocarbon gases (see "Gas Hydrate and Pressure Cores," p. 15, in "Organic Geochemistry"). The abundance of air components in the PCS gas samples (0.6%–6.9% of gas mixtures) suggests that air was not always properly displaced from the PCS by seawater during deployments. Methane is the dominant natural gas present in collected gas splits. The molecular composition of gases from the PCS is similar to the composition of gas voids at adjacent depths (Fig. F30).

Sediments in cores recovered by the PCS have lithologies that are similar to sediments recovered by the APC and XCB at adjacent depths (see "Physical Properties," p. 17). Porosity values measured on samples from APC and XCB cores taken near the PCS were averaged and used to estimate the methane concentration in situ (Table T16).

The concentration of in situ methane was estimated based on data from the degassing experiments (i.e., total volume of methane) and core examination (i.e., length of recovered core and the porosity of sediments). The calculation yields equivalent concentrations varying from 215.7 to perhaps >5000 mM of methane in pore water (Table T16). These concentrations have been compared with the theoretical methane-solubility curve extrapolated from values calculated for higher pressures (depths) (Handa, 1990; Duan et al., 1992) (Fig. F30).

Preliminary analysis suggests that gas hydrates have been present in relatively high concentrations (perhaps >40% of pore volume) in the shallowest Core 204-1249F-4P recovered from ~14 mbsf. In addition to high gas concentrations, strong evidence of the presence of gas hydrate was found in the pressure record of core degassing (Fig. F29B). Gas hydrate concentration in Core 204-1249C-6P (~34 mbsf) is estimated to be >5% of pore volume. Unfortunately, the core was not maintained at 0°C during the degassing experiment, and no information about the presence of gas hydrate in the core can be obtained from the pressure record.

The wide range in the estimates of methane concentrations is related to the uncertainty about the lengths of the recovered core (Table T16). Full 1-m-long cores were recovered during successful deployments at Site 1249; therefore, the lowest methane concentration values presented in Table T16 are the most reliable. Relatively low gas hydrate concentrations (~2% of pore volume) are estimated in Core 204-1249F-14P (~72 mbsf). Interestingly, the pressure record suggests that only dissolved gas was present in the core (Fig. F29C).

The estimated decrease of gas hydrate saturation with increasing depth at Site 1249 is consistent with similar trends proposed based on well logging data (see "Downhole Logging," p. 29) and Cl^- anomalies (see "Interstitial Water Geochemistry," p. 11). Additional compari-

F30. Methane concentrations, p. 67.

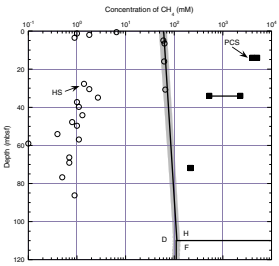

sons of measured methane concentrations with theoretical methane solubility both above and below the BSR will be performed on shore to better estimate if methane was present in situ in solution, in free phase, or as gas hydrate.

HYACINTH Pressure Coring

Coring Summary

We deployed the HYACINTH pressure coring tools five times at Site 1249 near the summit of Hydrate Ridge (Table T17) (see "Operations," p. 2). During the middle of Leg 204, the FPC and HRC tools were each used in an effort to capture massive hydrate samples under pressure from 8 mbsf. This experiment was repeated at the very end of Leg 204, again using both the FPC and HRC at 13.5 mbsf. In addition, a further HRC core was taken deeper in more disseminated hydrate at 37.5 mbsf.

T17. HYACINTH pressure coring summary, p. 97.

Core 204-1249D-2Y (FPC 5) recovered a core from 8 mbsf that was initially thought to be under in situ pressure. However, it transpired that the pressure had been released during the ascent, only to build up once the core was at the surface. These difficulties culminated in an exploding core that still contained some remnants of hydrate. Core 204-1249F-13Y (FPC 6) recovered a nearly full core from a depth of 70.4 mbsf. However, difficulties with the lower autoclave valve again prevented the core from being recovered at in situ pressures.

Core 204-1249F-2E (HRC 4) was taken at the same depth (8 mbsf) as Core 204-1249D-2Y (FPC 5). Despite some difficulties at the surface (see "HYACE Rotary Corer Operations," p. 24), a 80- to 90-cm-long core (as determined by core logging) was recovered under full pressure. It was cooled in the ice bath to maintain stability and successfully sheared and transferred into the HYACINTH logging chamber. It was subsequently logged repeatedly in the Geotek V-MSCL while being degassed over the following 2 days (see "Core Logging and Analysis," p. 26).

Core 204-1249G-2E (HRC 7) was taken a little deeper (13.5 mbsf) than Core 204-1249F-2E (HRC 4) (see "HYACE Rotary Corer Operations," p. 24). A successful 75-cm core containing massive hydrate layers (see "Core Logging and Analysis," p. 26) was recovered at full pressure and transferred into a HYACINTH storage chamber. It was subsequently frozen in He under pressure and successfully transferred into liquid nitrogen for preservation. It is probably the most pristine sample of natural gas hydrate ever recovered and preserved.

Core 204-1249H-2Y (FPC 10) was taken at the same depth as Core 204-1249G-2E (HRC 7) (13.5 mbsf). A successful (75 cm) core was recovered at full pressure, and a good GRA log was obtained from the core in the storage chamber showing massive hydrate layers. This core was designated as a "reference core" and companion to the APC and XCB cores that were taken and repressurized under methane. It was kept in the refrigerator ready for transportation to TAMU for further study.

Core 204-1249L-5E (HRC 8) was taken from deeper at this site (37.5 mbsf) in an attempt to recover pristine material under pressure from a region where the hydrate is present in lower concentrations and may be more disseminated. Some pressure was lost during disassembly (see "HYACE Rotary Corer Operations," p. 24), but it was rapidly repressurized to in situ pressures before being transferred to the logging chamber.

HYACE Rotary Corer Operations

Three HRC deployments were made at Site 1249 (Table T17). Core 204-1249F-2E (HRC 4) was taken at Site 1249, which was near the summit of Hydrate Ridge at 777 meters below sea level (mbsl). It is well known that massive hydrate exists near the surface and core recovery using regular APC and XCB coring through the upper 50 m was particularly poor in the previous holes. The purpose of this pressure coring attempt was to recover an undisturbed sample from massive hydrate just below the seafloor. Although the sediments in this near-surface environment would normally be extremely soft and highly unsuited to pressure coring with the HRC, it was thought possible that the massive hydrate ice structure would be hard enough to lend itself to rotary coring.

Core 204-1249F-2E (HRC 4) was deployed at 8 mbsf after an APC core was shot at the surface. Drilling procedures at these shallow depths mean that in practice these are separate holes. The tool was prepared on the piperacker and lifted into the vertical position and lowered into the drill string as in previous deployments. The DSA tool was attached and run in the hole at 40 m/min. After landing and lowering the HRC to TD, 5 m of slack wire was payed out to ensure that no tension was accidentally applied to the tool. The bottom of pipe (BOP) was closed and pumping started at 50 gallons per minute (gpm), causing the pressure to rise to 620 psi, which indicated that the tool had been activated (started rotating). With almost no load on bit we pumped for 12 min with 80 gpm before pumping for 8 min with 120 gpm. The drill string was lifted about 4 m, followed by a further 1-min pumping at 80 gpm. Slowly the wireline was pulled at 8 m/min for the first 16 m, after which it was increased to 74 m/min.

At the surface the tool was disassembled on the pipe racker, which took ~35 min before the tool could be moved to the transfer area outside the downhole tools shop. While breaking out the accumulator it was clear that there was high pressure inside the autoclave, which was measured with the pressure gauge. While mounting the pressure gauge, a very short high pressure burst was heard. Pressure was measured at ~220 kbar, and the autoclave chamber was then cooled down in the ice trough where the pressure soon dropped to ~120 kbar. Once the core was stable it was transferred through the shear transfer chamber and into the logging chamber, which was in turn placed in the ice trough for cooling and was left there and monitored overnight. The following morning the temperature and pressure was stable at around 0°C and 110 kbar. It was transferred to the Geotek V-MSCL, where it was degassed and logged over the next 2 days (see below). It transpired that the core (~90 cm long; 90% recovery) contained ~40% methane hydrate, which accounted for the rapid pressure rise at the surface (presumably caused by the partial dissociation of hydrate). During disassembly of the tool we discovered that the burst disk (230–270 kbar) had failed. This presumably occurred on deck, but rapid expulsion of sediment had immediately blocked the small orifice and, hence, no significant pressure had been lost.

Following the success of the HRC at this site earlier in the leg (Core 204-1249F-2E [HRC 4]), a second HRC core (Core 204-1249G-2E [HRC 7]) was taken at 13.5 mbsf. This is the same depth as Core 204-1249H-2Y (FPC 7) but in a different hole. The tool was deployed as in previous deployments.

Once on the trestles it was clear that the valve had closed, and ice bags were placed along the length of the autoclave to keep the system cold during the breakdown of the tool. Once outside the downhole tools laboratory the autoclave was kept under ice bags while the pressure was measured at ~80 kbar (the same as in situ pressures). The core was successfully transferred from the autoclave into the shear transfer chamber and then into the storage chamber at full pressure before being placed in an ice bath prior to logging. The logging revealed that a core about 75 cm long was retrieved and contained significant amounts of hydrate (the lower 25 cm appeared to be water) (see "Core Logging and Analysis," p. 26).

Having recovered good pressure cores at this site from near the top of the section where the hydrates were relatively massive (10 and 13.5 mbsf), there was interest in recovering a core from slightly lower in the section where the hydrates were thought to be more disseminated. Consequently, the final deployment of the HRC during this leg was at the bottom of Hole 1249L (Core 204-1249L-5E [HRC 9]). The only real issue was whether the nature of the sediment in this region would lend itself to being cored by the HRC and held by the core catcher. The deployment was run similarly to previous deployments with the DSA tool. It was run into the hole at 70 m/min while circulating and rotating. Pumping and rotation was stopped while the tool was landed, and 5 m of slack wire was payed out. The drill string was lowered to TD, followed by the wireline. Weight on bit was set at 7,000–10,000 klb. Again, the active heave was not working effectively (max heave = ~2 m), and, therefore, we relied only on the passive heave compensator. The BOP was closed and pumping began slowly. Coring continued after the first pressure peak (450 psi) for 20 min at 90 gpm and ~360 psi. A second spike was observed (indicating full stroke) after the drill string had been lifted 3 m above TD. Pumping continued at 100 gpm for 1 min before the tool was lifted on the wireline slowly at 7 m/min for the first 20 m and then continued at 70 m/min while circulating. Once the tool was broken out of the drill string and laid on the trestle, the flapper valve was observed to have closed and care was taken to ensure that the autoclave was cooled with ice bags during the disassembly. However, during the later part of the disassembly some pressure leaked away when the connecting rod was removed. The leak was occurring in the piston extension rod. Only 30 kbar remained when measured, and the autoclave was immediately pumped up to 80 kbar to stabilize any hydrate. The core was then transferred under pressure into the logging chamber and kept in the ice bath until logged in the V-MSCL (see "Core Logging and Analysis," p. 26). We found a 30-cm-long core without any significant hydrate layers. It is thought that these sediments were too soft to be retained by the type of sleeve catcher used.

Fugro Pressure Corer Operations

Three FPC cores were taken at Site 1249 (Table T17). The first deployment of the FPC at Site 1249 was Core 204-1249D-2Y (FPC 5). The purpose of attempting a shallow core at this site was the same as for Core 204-1249F-2E (HRC 4), to recover massive hydrate from just below the seafloor at ~8 mbsf. This deployment proceeded smoothly with the same operational procedures being used as previously. Active heave compensation was used throughout. On recovery it was clear that a full stroke had been achieved and that the autoclave had sealed. However, when the onboard FPC data logger was analyzed, it was clear that it was

not sealed and had depressurized coming to the surface. The autoclave had then sealed at the surface, allowing the pressure to rise to ~20 kbar.

The rapid rise in pressure to 20 kbar indicated that hydrate was present in Core 204-1249D-2Y (FPC 5). We connected the autoclave to the shear transfer chamber, pressurized the complete system to ~70 kbar (to stabilize the system and put any hydrate back into the stability field), and attempted to make the transfer. However, problems with the transfer (caused by expansion) meant that the core had to be depressurized and removed manually. Having done this, the liner then burst under internal pressure and some very soupy mud was collected from the floor in a plastic bag. It was clearly cold to the touch and even contained a few remnants of hydrate. Some optimism was gained from this deployment, as it was clear that the valve had seated properly during the handling of the tool at the surface allowing a build up of pressure to occur.

A second FPC deployment (Core 204-1249F-13Y [FPC 6]) was made at 70.4 mbsf. At this depth, the hydrate was less massive and a core with virtually full recovery was achieved. Everything worked perfectly other than the sealing valve that had not fully closed. It would appear from an analysis that the sleeve might be coming down too quickly on top of the valve, causing it to jam on the edge of the sleeve in the "nearly closed" position. It was thought that removing the spring above the sleeve and lifting the pipe string more slowly after coring might help prevent this jamming.

Following the success of the FPC at Site 1244 (Core 204-1244E-8Y [FPC 9]), a third FPC core (Core 204-1249H-2Y [FPC 10]) was taken at a depth of 13.5 mbsf in Hole 1249H. This is the same depth as Core 204-1249G-2E (HPC-7) but in a different hole. The tool was deployed as in previous deployments. With the tool at TD (801 mbsl), the pressure was increased to 700 psi, and, after shearing, the pressure was raised to 800 psi and the tool hammered smoothly for ~6 min. At the end of the run the pressure was increased briefly to 850 psi, but this caused the hammering to become irregular. The same lifting procedure was followed as with the successful Core 204-1244E-8Y (FPC 9). However, to assist in the closing of the lower valve the FPC was stopped as it came out off the landing shoulder. We then pumped and rotated to provide some string vibration, which may have helped the valve to seat and seal properly. Half a minute later we continued to lift the FPC out of the drill string in the normal manner. Once on the trestle, it was clear that the valve had closed. Analysis of the data logger showed we had full in situ pressure (~80 kbar) so the autoclave was attached to the shear transfer chamber and manipulator. After considerable difficulty, caused by the tight tolerances in the ball valves, the core was transferred, cut, and moved into a HYACINTH storage chamber, where it was logged showing that a core ~75 cm long was retrieved containing significant amounts of hydrate (the lower 25 cm appeared to be water).

Core Logging and Analysis

Core 204-1249F-2E (HRC 4) was stored within the logging chamber in the refrigerator at 5°C overnight before being loaded into the V-MSCL. The core was first logged at low resolution to get a quick impression of what type of core had been recovered. It was immediately clear that a nearly full core (85–90 cm) had been recovered with relatively low average densities. Interpretation of V_P continued to prove difficult (see "Downhole Tools and Pressure Coring," p. 34, in the "Explana-

tory Notes" chapter). Over the next few hours, more detailed logs were run while the core warmed up slowly and increased in pressure. Temperature measurements were taken by inserting a probe in the ball-valve spindle. This provided only an approximation of the core temperature, even though the logging chamber was insulated by foam whenever possible and the chamber ends were insulated with "bubble wrap" as far as practically possible. When the temperature and pressure had increased to 16°C and 160 kbar, respectively, the complete chamber was again returned to the refrigerator to stabilize overnight. In the morning (at 5°C), the pressure had dropped to 85 kbar (close to in situ conditions again).

Over the next 2 days, the GRA density logs were obtained repeatedly during the process of degassing (Fig. **F31**). Gas was collected using an inverted measuring cylinder in water as was used to degas the PCS (see **"Downhole Tools and Pressure Coring,"** p. 34, in the "Explanatory Notes"). Temperature was allowed to rise slowly while the pressure was varied in an effort to control the rate at which gas was released during the process of depressurization and hydrate dissociation. At the end of day 2, the chamber was again left in the refrigerator to stabilize overnight. Throughout day 3, the core was completely degassed, warmed to room temperature, and completely depressurized.

Over the course of the measurement period, >101.5 L of gas was collected, and 24 GRA density logs were obtained along the length of the core. The gas was subsampled during the degassing process for compositional analysis in the onboard chemistry laboratory (see **"Interstitial Water Geochemistry,"** p. 11). The GRA density logs clearly showed how the physical structures within the core changed during the measurement period. Characteristic features interpreted as gas, hydrate, sediment, and water could be correlated and traced between logs. It was clear from these logs where gas was forming and where and when it was escaping from the core. Methane hydrate and water are difficult to distinguish via density alone, but when hydrate dissociates, the gas layers generated are easily apparent in the GRA density logs. Figure **F31** shows three density logs at different stages of the experiment. Run 1 was collected prior to the degassing process at full pressure, showing the in situ density structure, which reveals low densities throughout with some layers interpreted as massive hydrate. Run 8 was in the early stages of degassing, showing distinct gas layers developing and the complete core structure being expanded by gas. Run 15 was in the middle of the degassing process (43 L of gas collected), showing how the complete structure had changed with sediment falling from the top and a water interval in the center of the core. By the time all the gas had been removed at the end of the process, the sediment had completely liquefied and most of it was removed from the chamber by bleeding it as a slurry through the pipework. It was collected, allowed to settle, and dried, and the total weight enabled a mass balance calculation to be performed. It was calculated that the core consisted of ~40% by volume of methane hydrate and 60% by volume of fine-grained sediment with an average bulk density of 1.3 g/cm³ (67% porosity). If hydrate is expressed as a percentage of pore volume, as is done elsewhere in this volume, then this core contained ~50% hydrate by pore volume.

Core 204-1249G-2E (HRC 7) was logged inside the storage chamber after having been stabilized at ~6°C. The density log is shown in Figure **F32** (run 1). The log shows that ~25 cm of material may have fallen out of the end of the core, but the remainder shows detailed structure indicating several layers of massive hydrate above a water interval. It was

F31. Density profiles of HRC 5, p. 68.

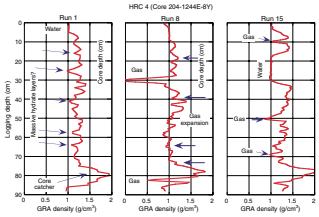

F32. Density profiles of HRC 7, p. 69.

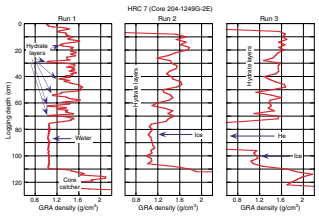

decided to attempt to preserve this core as a "pristine example" in liquid nitrogen for study in the laboratory. This could then be used as a reference core to compare with samples taken without pressure preservation and as a complementary reference core to Core 204-1249H-2Y (FPC 10) (see below). The problem was, of course, how to remove the core from the pressure vessel without the gas in solution instantly coming out of solution and without the hydrate starting to dissociate. We decided to freeze the core. First, the core was cooled in the storage chamber to 0°C in an ice bath for several hours. Following this, the seawater pressurizing fluid was replaced by He using a high-pressure regulator after the pressure inside the chamber was first reduced to 63 kbar (maximum regulator pressure). Despite some difficulties caused by small amounts of sediment in the pipes, the operation was successful and the storage chamber with core was then rapidly logged as a check (see Fig. **F32**) (run 2), which showed that the sediment section had not moved and that the water section still remained in the core. The chamber was then placed in the freezer at –10°C for more than 24 hr before being rapidly logged again. Run 3 (Fig. **F32**) showed that some of the water had escaped and some had frozen. This caused some concern because it left a gas pocket inside the liner. To remove the core, the chamber was connected to manipulator and wrapped in ice bags. Hot water and rags were applied to the manipulator end of the chamber to unfreeze the contact between the core and the inside of the chamber. Hot water was also applied at the ball-valve end to free the bleed pipes and pressure gauge, which was frozen, and did not read the inside gas pressure correctly. Once clear, the pressure inside the chamber was measured at ~62 kbar. This pressure was then released slowly (~5 min) so as to allow time for the pressure inside the core liner to escape. When the pressure was zero, the ball valve was opened and the manipulator extended slowly to push the core from the chamber. Rapid gas expansion shot some frozen core containing massive hydrate from the chamber. However, this was easily collected and placed directly in liquid nitrogen. The core was further extruded with care (surrounded by steel tube), and further core sections were cut off and placed in liquid nitrogen. It was clear that a substantial part of this core contained massive hydrate, as could be clearly seen from the core ends and through the core liner during its brief exposure.

Core 204-1249H-2Y (FPC 10) was logged inside a HYACINTH storage chamber, after having been stabilized at ~6°C. The density log is shown in Figure **F33** and shows a 75-cm-long core above a water interval of ~25 cm, indicating that some material may have fallen out of the end of the core. However, the sediment section shows detailed structure indicating several layers of massive hydrate. A thicker layer of hydrate (60- to 80-cm logging depth) shows a small interval where the average density is only ~0.75 g/cm^3, clearly demonstrating that free gas does exist in situ inside the massive hydrate structure.

Core 204-1249L-5E (HRC 8) was logged inside a HYACINTH logging chamber. The GRA density log revealed a short core at the top of the liner (~30 cm), with a column of water beneath. There were no apparent signs of low-density layers that would be interpreted as hydrate. Consequently, the core was depressurized and the gas collected (total volume = 2.325 L). Two samples were collected and analyzed in the onboard chemistry laboratory.

F33. Density profiles of FPC 10, p. 70.

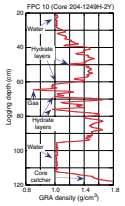

DOWNHOLE LOGGING

Logging While Drilling

Operations

LWD operations at Site 1249 consisted of drilling two dedicated LWD boreholes: Holes 1249A and 1249B. LWD operations at Site 1249 began at 1700 hr Universal Time Coordinated (UTC) on 21 July 2002 by spudding Hole 1249A at a water depth (drillers depth) of 788.50 meters below rig floor (mbrf) on the crest of southern Hydrate Ridge. The LWD tools deployed in Hole 1249A included the GeoVision Resistivity (GVR; RAB), MWD (Powerpulse), Nuclear Magnetic Resonance (NMR-MRP) tool, and Vision Neutron Density (VND) tool. Drilling proceeded at reduced ROP of 15 m/hr and lower fluid circulation rates of 15 spm to minimize formation washout in the unconsolidated sediments below seafloor. No real-time MWD or NMR-MRP data were recorded over this interval, as the pump rate was insufficient to activate the turbines in the downhole tools. The ROP was increased to ~25 m/hr and fluid circulation was returned to more normal levels at a bit depth of 30 mbsf, and real-time MWD and NMR data were recorded to TD (90 mbsf). The LWD tools were pulled to ~60 m clear of the seafloor at 2400 hr UTC on 21 July for the dynamic positioning move to Site 1250. The total bit run took ~7 hr.

On 24 July, we returned to Site 1249 to deploy and test the RAB-8 tool and coring system. LWD operations for Hole 1249B began with the initialization of the RAB-8 tool at 2115 hr UTC (24 July). The RAB-8 bottom-hole assembly (BHA) used for this test is described in **"Downhole Logging,"** p. 43, in the "Explanatory Notes" chapter. Though the RAB-8 BHA was extensively tested before sea deployment, the inner mandrel in the RAB-8 BHA was too high to connect with the $6^{5}/_{8}$-in full-hole pin above. The internal diameter of the pin was ground down, and the clear passage of the MDCB was tested before downhole deployment. Hole 1249B was spudded at 0400 hr UTC on 25 July in 788.50 mbrf water depth (drillers depth) on the summit of southern Hydrate Ridge. Drilling proceeded ahead to 30 mbsf, where RAB coring operations began with sequential 4.5-m-long (with liners) and 9-m-long (without liners) core recoveries through the shallow gas hydrate–bearing sedimentary sequence to 90 mbsf. Bit rotation varied from 15 to 45 rpm (increasing with depth), and the average ROP using this system was ~8 m/hr. The RAB-8 was recovered at the rig floor at 2000 hr on 25 July, and the downhole log data recorded in computer memory were downloaded. Total testing time was ~22 hr.

Logging Quality

Figure **F34** shows the quality control logs for GVR (RAB), MWD, NMR-MRP, and VND LWD tool string deployed in Hole 1249A. Other than about a 3-m-thick zone immediately below the seafloor, the upper ~32 m of Hole 1249A was drilled at an ROP of 15 m/hr (±3 m/hr). From a depth of ~32 mbsf to the bottom of the hole, the ROP was more variable, but it generally averaged ~25 m/hr (±3 m/hr). The ROP of 25 m/hr, which was sufficient to record one sample per 4-cm interval (~25 samples per meter), was obtained over 85% of the total section of the hole. The quality of RAB images is, thus, quite high, and no significant resolution loss is observed with variation in ROP in Hole 1249A. The in-

F34. Quality control LWD logs, p. 71.

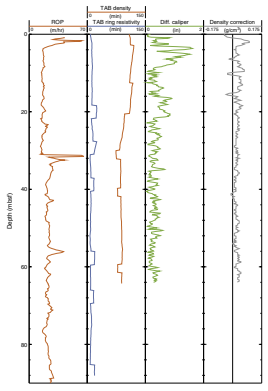

creased pump rates below 30 mbsf and a ROP of 25 m/hr yielded enhanced NMR-MRP porosity data, with a data sampling resolution of ~1 sample per 15-cm interval.

The differential caliper log (DCAL), which gives the distance between the tool sensor and the wall of the borehole as recorded by the LWD density tool, is the best indicator of borehole conditions. The differential caliper values are <1 in over 90% of the total drilled and cored sections in Hole 1249A. Only the uppermost ~10 mbsf of the hole contains washouts >1 in. The density correction, calculated from the difference between the short- and long-spaced density measurements, varies from 0 to 0.1 g/cm³ (Fig. **F34**), which suggests very high quality density measurements. A standoff of <1 in between the tool and the borehole wall also indicates high-quality density measurements, with an accuracy of ±0.015 g/cm³. In Hole 1249A, the time-after-bit (TAB) measurements were 10 ± 5 min for ring resistivity and gamma ray logs and 80 to 120 min for the density and neutron porosity logs (Fig. **F34**). The TAB values remained relatively constant over most of the hole, coinciding with the steady ROP.

The LWD RAB-8 tool in Hole 1249B yielded high-quality data over the drilled and cored interval of the hole to a TD of 90 mbsf. Eight rotary cores were recovered from Hole 1249B with 32.9% recovery, on average, through the 45-m cored interval (Table **T18**). The RAB-8 test cores were normally processed and archived and will be correlated to the RAB-8 logs over the same depth interval. RAB-8 images and logs from Hole 1249B are of high quality but require additional postcruise depth corrections and analysis to account for the coring process. Preliminary observations suggest, however, that the recorded RAB data from Hole 1249B correlates well with the LWD logging curves in Hole 1249A. In the future, when drilling in harder formations with faster rotary coring, core recovery and logging data quality are expected to improve using the RAB-8 coring system. This successful test marks the first ever logging-while-coring experiment, which is new technology that allows for precise core-log depth calibration and core orientation within a single borehole and without a pipe trip.

The depths relative to seafloor for the LWD logs from Hole 1249A were fixed by identifying the gamma ray signal associated with the seafloor and shifting the log data to the appropriate depth as determined by the drillers pipe tallies. For Hole 1249A, it was determined that the gamma ray log pick for the seafloor was at a depth of 787.0 mbrf. The rig floor logging datum was located 11.0 m above sea level.

Interpretation of Logging-While-Drilling Logs

The RAB-8 log data from Hole 1249B were not available on the ship for immediate analysis. Therefore, only the downhole LWD logs from Hole 1249A were used to assess the geology of Site 1249 (Figs. **F35, F36**). As discussed above, the LWD logs from Hole 1249A are of excellent quality. Lower pump rates through the shallow subsurface section greatly reduced the effect of borehole washouts on the logs in the near-surface unconsolidated sediments. At Site 1249, the downhole LWD logs dramatically reveal a thick, almost-continuous, gas hydrate–bearing sedimentary section throughout the entire drilled interval in Hole 1249A (Fig. **F37**).

T18. RAB-8 coring test summary, p. 98.

F35. LWD-logging data, p. 72.

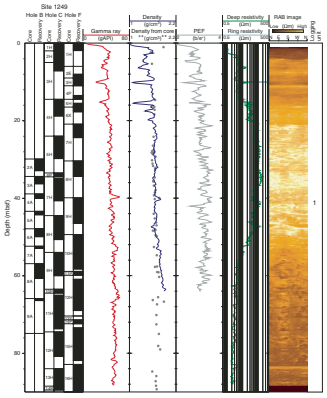

F36. LWD log- and core-derived porosities, p. 73.

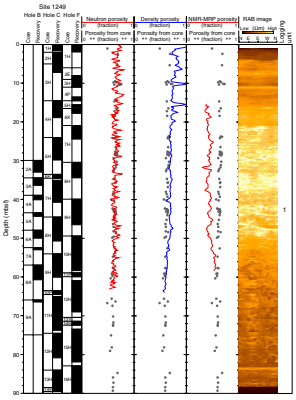

F37. Gas hydrate saturations, p. 74.

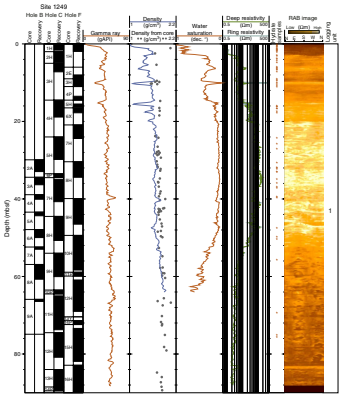

Logging Units

The logged section in Hole 1249A consists of one "logging unit" based on the analysis of the acquired downhole LWD log data (Fig. F35).

Logging Unit 1 (0–90 mbsf; TD of Hole 1249A) is characterized by numerous intervals of very high electrical resistivity, with measured average peak values exceeding 160 Ωm. The gamma ray log generally increases with depth from ~40 American Petroleum Institute gamma ray units (gAPI) near the top to >70 gAPI near the bottom of the hole. Logging Unit 1 at Site 1249 is included within lithostratigraphic Unit I-II (0–89.50 mbsf), which was described by the shipboard sedimentologists as diatom-bearing clay to silty clay stratigraphic sequences (see "Lithostratigraphy," p. 5). The downhole logging-measured density increases with depth in the hole (1.3 at the top to near 1.8 g/cm³ at the bottom). Near the top of Hole 1429A, the density log reveals several conspicuous low-density intervals (ranging from ~1.1 to 1.5 g/cm³). Because of drilling safety concerns, none of the holes at Site 1249 were cored or drilled through the predicted depth of the BSR (estimated at ~115 mbsf).

Resistivity-at-the-Bit Images

The RAB tool produces high-resolution images of the electrical resistivity characteristics of the borehole wall that can be used for detailed sedimentological and structural interpretations. The RAB tool can also be used to make high-resolution electrical images of gas hydrate in the borehole, thus yielding information about the nature and texture of gas hydrate in sediments. The RAB image in Figure F38 has a mottled appearance and is characterized by light (high resistivity) bands, which in many cases can be traced across the display. These light continuous high-resistivity bands likely represent gas hydrate occupying high-angle (40°–80°) fractures in Hole 1249A. In addition, the bright mottled appearance of the RAB image in Figure F38 may also reflect the presence of disseminated gas hydrate in the sediments.

F38. RAB image, p. 75.

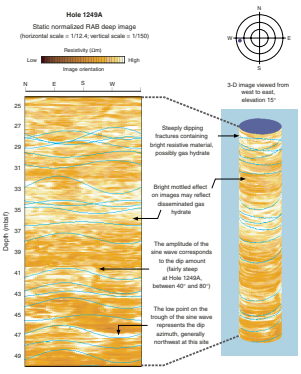

Logging Porosities

Sediment porosity can be determined from analysis of recovered cores and from numerous borehole measurements (see "Physical Properties," p. 22, and "Downhole Logging," p. 43, both in the "Explanatory Notes" chapter). Data from the LWD density, neutron, and NMR logs have been used to calculate porosity for Hole 1249A. Core-derived physical property data, including porosities (see "Physical Properties," p. 17), have been used to both calibrate and evaluate the log-derived sediment porosities.

The VND LWD log-derived measurements of bulk density in Hole 1249A (Fig. F35) increase with depth and are relatively consistent (as discussed above); however, the density log measurements are much more variable near the top of the hole (0–15 mbsf). The LWD log-derived density measurements from Hole 1249A were used to calculate sediment porosity (ϕ) using the standard density-porosity relation,

$$\phi = (\rho_m - \rho_b)/(\rho_m - \rho_w).$$

Water density (ρ_w) was assumed to be constant and equal to 1.05 g/cm^3; however, variable core-derived grain/matrix densities (ρ_m) were assumed for each logging density porosity calculation. The core-derived grain densities (ρ_m) in Hole 1249B range from an average value at the seafloor of 2.69 to ~2.71 g/cm^3 at the bottom of the hole (see "Physical Properties," p. 17). The density logging–derived porosities in Hole 1249A generally range from ~60% to 75% (Fig. F36). However, the density log porosities in the upper part of the hole (0–15 mbsf) are more variable, ranging from 70% to near 100%. The zones near the top of the hole that exhibit very high density log porosities (i.e., very low formation densities) are also characterized by very high resistivities (in one case exceeding 500 Ωm), which suggests the presence of massive gas hydrate layers.

The LWD neutron porosity log from Hole 1249A (Fig. F36) yielded sediment porosities ranging from an average value at the top of the logged section of ~70% to ~60% near the bottom of the hole. The "total" sediment porosities derived by the LWD NMR tool in Hole 1249A (Fig. F36) ranged from ~30% at a depth of 16 mbsf to ~55% near the bottom of the hole (56 mbsf).

The comparison of core- and log-derived porosities in Figure F36 reveals that the density and neutron log-derived porosities are generally higher than the core-derived porosities in Hole 1249A (16–56 mbsf). However, the NMR-MRP porosities are lower than the core-derived porosities throughout the entire hole. The higher value of density- and neutron log–derived porosities compared to NMR-MRP porosities can be attributed to the presence of gas hydrate. Porosities calculated from NMR-MRP tool, density, or neutron logs in gas hydrate–bearing reservoirs are subject to error because most downhole porosity devices are calibrated to the physical properties of water-bearing sediments (as reviewed by Collett and Ladd, 2000). Therefore, downhole log-derived porosities need to be corrected for the presence of gas hydrate. The required correction for density- and neutron-derived porosities is relatively small, but NMR-MRP porosities are more significantly affected by the presence of gas hydrate. The effect of gas hydrate on the downhole logging-derived porosities from Site 1249 will be further examined after the cruise.

Gas Hydrate

The presence of gas hydrate at Site 1249 was documented by direct sampling, with numerous specimens of gas hydrate recovered from near the seafloor to a depth of 75.07 mbsf in Holes 1249B–1249F. From these occurrences of gas hydrate, it was inferred, based on geochemical core analyses (see "Interstitial Water Geochemistry," p. 11), IR image analysis of cores (see "Physical Properties," p. 17), and downhole logging data that massive and disseminated gas hydrate is present throughout the logged and cored interval at Site 1249. As previously discussed in "Downhole Logging," p. 43, in the "Explanatory Notes" chapter, the presence of gas hydrate is generally characterized by increases in logging-measured electrical resistivities and acoustic velocities. Hole 1249A is characterized by intervals of high electrical resistivities, but we have no acoustic data (because no wireline logging was conducted at Site 1249) to further evaluate the occurrence of gas hydrate or free gas at this site.

Resistivity logging data were used to quantify the amount of gas hydrate at Site 1249. For the purpose of discussion, it is assumed that the high resistivities measured in Hole 1249A are due to the presence of gas hydrate. Archie's Relation,

$$S_w = (aR_w/\phi^m R_t)^{1/n}$$

(see "Downhole Logging," p. 43, in the "Explanatory Notes" chapter), was used with resistivity data (R_t) from the LWD RAB tool and porosity data (ϕ) from the LWD density tool to calculate water saturations in Hole 1246A. It should be noted that gas hydrate saturation (S_h) is the measurement of the percentage of pore space in sediment occupied by gas hydrate, which is the mathematical complement of Archie-derived S_w, with

$$S_h = 1 - S_w.$$

For Archie's Relation, the formation water resistivity (R_w) was calculated from recovered core water samples and the Archie a and m variables were calculated by a crossplot technique that compares the downhole log-derived resistivities and density porosities. See Collett and Ladd (2000) for the details on how to calculate the required formation water resistivities and Archie variables. The values used for Site 1249 were a = 1, m = 2.8, and n = 1.9386. The Archie Relation yielded water saturations (Fig. F37) ranging from a minimum average value of only ~8% in Hole 1249A to a maximum of 90% near the seafloor, which implies gas hydrate saturations at Site 1249 ranging from 10% to 92%.

REFERENCES

Boetius, A., Ravenschlag, K., Schubert, C.J., Rickert, D., Widdel, F., Gieseke, A., Amann, R., Jørgensen, B.B., Witte, U., and Pfannkuche, O., 2000. Microscopic identification of a microbial consortium apparently mediating anaerobic methane oxidation above marine gas hydrate. *Nature,* 407:623–626.

Clague, D., Maher, N., and Paull, C.K., 2001. High-resolution multibeam survey of Hydrate Ridge, offshore Oregon. In Paull, C.K., and Dillon, W.P. (Eds), *Natural Gas Hydrates: Occurrence, Distribution, and Detection.* Am. Geophys. Union, Geophys. Monogr. Ser., 124:297–306.

Collett, T.S., and Ladd, J., 2000. Detection of gas hydrate with downhole logs and assessment of gas hydrate concentrations (saturations) and gas volumes on the Blake Ridge with electrical resistivity log data. *In* Paull, C.K., Matsumoto, R., Wallace, P.J., and Dillon, W.P. (Eds.), *Proc. ODP, Sci. Results,* 164: College Station, TX (Ocean Drilling Program), 179–191.

Duan, Z., Møller, N., Greenberg, J., and Weare, J.H., 1992. The prediction of methane solubility in natural waters to high ionic strengths from 0° to 250°C and from 0 to 1600 bar. *Geochim. Cosmochim. Acta,* 56:1451–1460.

Freifeld, B.M., Keafsey, T.J., Tomutsa L., Stern, L.A., and Kirby, S.H., 2002. Use of computed X-ray tomographic data for analyzing the thermodynamics of a dissociating porous sand/hydrate mixture. *Proc. 4th Int. Conf. Gas Hydrates,* 750–755.

Freifeld, B.M., Kneafsey, T.J., Tomutsa L., and Pruess, J., in press. Development of a portable X-ray computed tomographic imaging system for drill-site investigation of recovered core. *Proc. 2003 Int. Symp. Soc. Core Analysts,* 21–24.

Handa, Y.P., 1990. Effect of hydrostatic pressure and salinity on the stability of gas hydrates. *J. Phys. Chem.,* 94:2652–2657.

Heeschen, K.U., Tréhu, A.M., Collier, R.W., Suess, E. and Rehder, G., 2003. Distribution and height of methane bubble plumes on the Cascadia margin characterized by acoustic imaging. *Geophys. Res. Lett.,* 30:1643.

Hesse, R., and Harrison, W.E., 1981. Gas hydrates (clathrates) causing pore-water freshening and oxygen isotope fractionation in deep-water sedimentary sections of terrigenous continental margins. *Earth Planet. Sci. Lett.,* 55:453–462.

Johnson, J.E., Goldfinger, C., and Suess, E., in press. Geophysical constraints on the surface distribution of authigenic carbonates across the Hydrate Ridge region, Cascadia margin. *Mar. Geo.*

Reeburgh, W.S., 1976. Methane consumption in Cariaco Trench waters and sediments. *Earth Planet. Sci. Lett.,* 28:337–344.

Ruppel, C., 2000. Thermal state of the gas hydrate reservoir. *In* Max, M.D. (Ed.), *Natural Gas Hydrate in Oceanic and Permafrost Environments:* Dordrecht (Kluwer Academic Publishers), 29–42.

Sahling, H., Rickert, D., Lee, R.W., Linke, P., and Suess, E., 2002. Macrofaunal community structure and the sulfide flux at gas hydrate deposits from the Cascadia convergent margin, NE Pacific. *Mar. Ecol.: Prog. Ser.,* 231:121–138.

Suess, E., Torres, M.E., Bohrmann, G., Collier, R.W., Rickert, D., Goldfinger, C., Linke, P., Heuser, A., Sahling, H., Heeschen, K., Jung, C., Nakamura, K., Greinert, J., Pfannkuche, O., Tréhu, A., Klinkhammer, G., Whiticar, M.J., Eisenhauer, A., Teichert, B., and Elvert, M., 2001. Sea floor methane hydrates at Hydrate Ridge, Cascadia margin. *In* Paull, C.K., and Dillon, W.P. (Eds.), *Natural Gas Hydrates: Occurrence, Distribution, and Detection.* Am. Geophysical Union, Geophys. Monogr. Ser., 124:87–98.

Torres, M.E., Bohrmann, G., and Suess, E., 1996. Authigenic barites and fluxes of barium associated with fluid seeps in the Peru subduction zones. *Earth Planet. Sci. Lett.,* 170:1–15.

Torres, M.E., McManus, J., Hammond, D.E., de Angelis, M.A., Heeschen, K.U., Colbert, S.L., Tryon, M.D., Brown, K.M., and Suess, E., 2002. Fluid and chemical fluxes

in and out of sediments hosting methane hydrate deposits on Hydrate Ridge. *Earth Planet. Sci. Lett.,* 201:525–540.

Tréhu, A.M., and Bangs, N., 2001. 3-D seismic imaging of an active margin hydrate system, Oregon continental margin, report of cruise TTN112. Oregon State Univ. Data Rpt., 182.

Tréhu, A.M., Bangs, N.L., Arsenault, M.A., Bohrmann, G., Goldfinger, C., Johnson, J.E., Nakamura, Y., and Torres, M.E., 2002. Complex subsurface plumbing beneath southern Hydrate Ridge, Oregon continental margin, from high-resolution 3-D seismic reflection and OBS Data. *Fourth Int. Conf. Gas Hydrates:* Yokohama, Japan, 19023:90–96.

Tréhu, A.M., Stakes, D.S., Bartlett, C.D., Chevallier, J., Duncan, R.A., Goffredi, S.K., Potter, S.M., Salamy, K.A., 2003. Seismic and seafloor evidence for free gas, gas hydrates, and fluid seeps on the transform margin offshore Cape Mendocino. *J. Geophys. Res.,* 108:10.1029/2001JB001679.

Tryon, M.D., Brown, K.M., and Torres, M.E., 2002. Fluid and chemical flux at Hydrate Ridge, II. Observations and long-term records reveal insights into dynamic driving mechanisms. *Earth Planet. Sci. Lett.,* 201:541–557.

Figure F1. Bathymetric map showing locations of holes drilled at Site 1249. Bathymetry from EM300 data acquired by Monterey Bay Aquarium Research Institute (MBARI) (Clague et al., 2001).

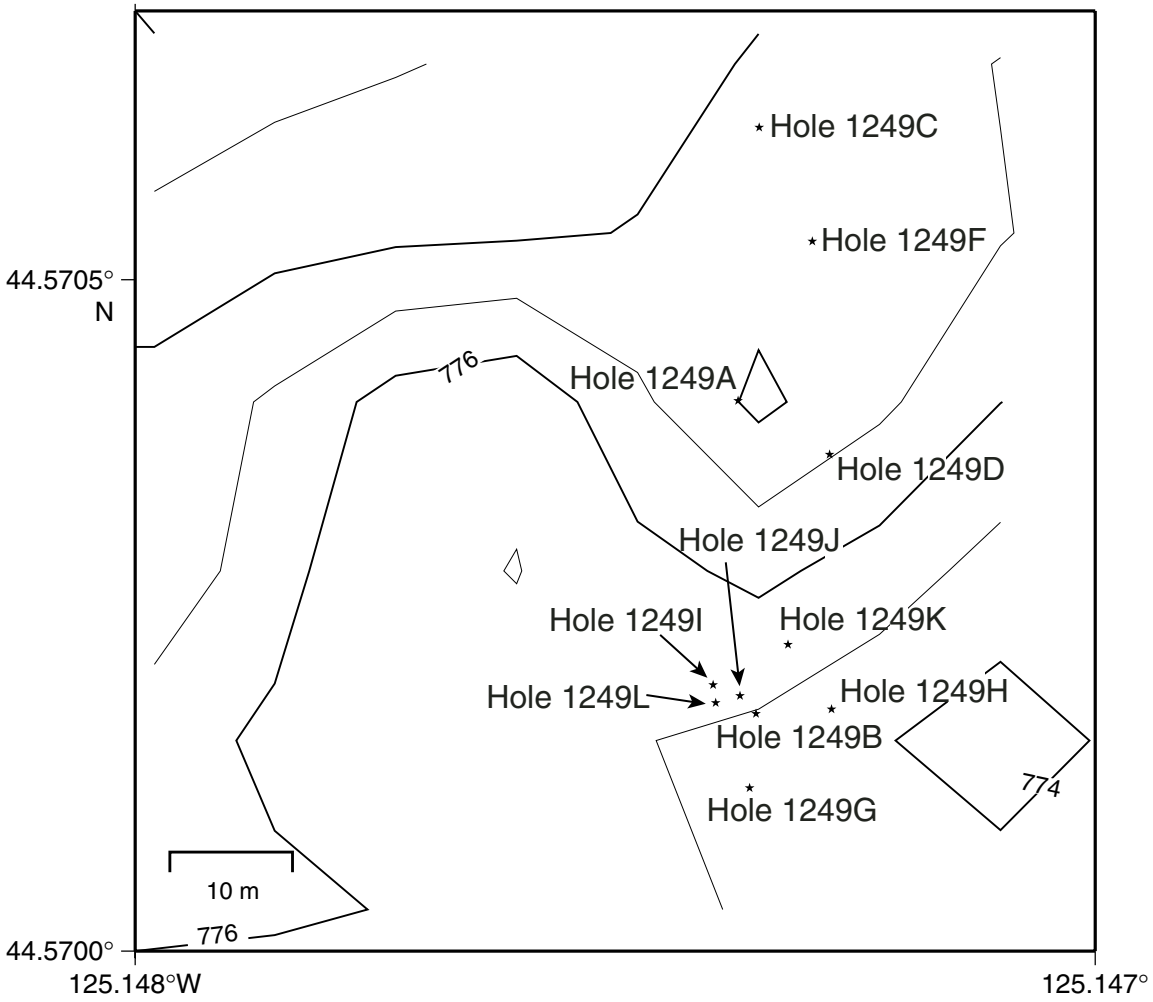

Figure F2. Lithostratigraphic summary for Site 1249.

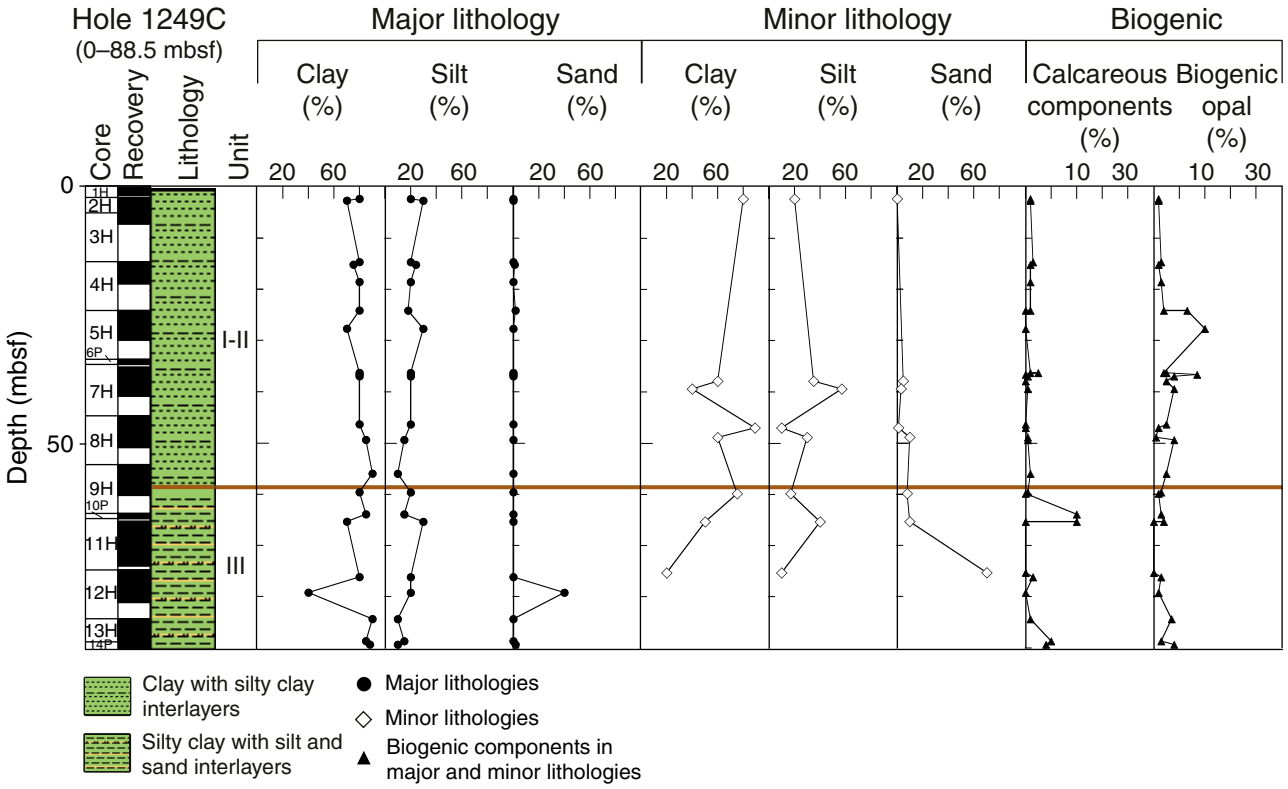

Figure F3. Close-up photograph of sediment from lithostratigraphic Unit I-II (interval 204-1249C-7H-5, 20–50 cm), showing a mottled texture. Dark color is due to sulfide precipitates.

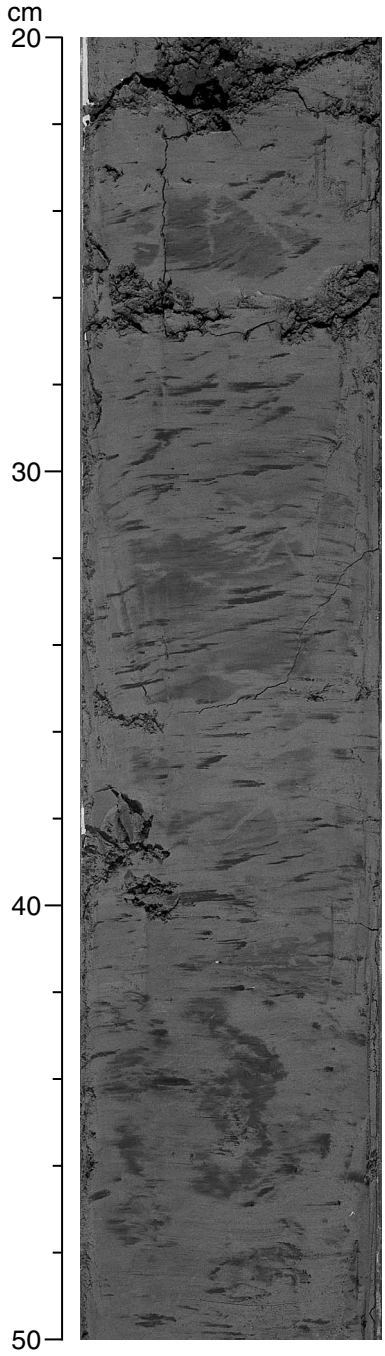

Figure F4. Close-up photographs of lithostratigraphic Unit III. **A.** Thin (<2 mm), inclined silt layers (interval 204-1249C-11H-5, 114–133 cm). **B.** A ~4-cm-thick sand layer (interval 204-1249F-12H-5, 34–41 cm).

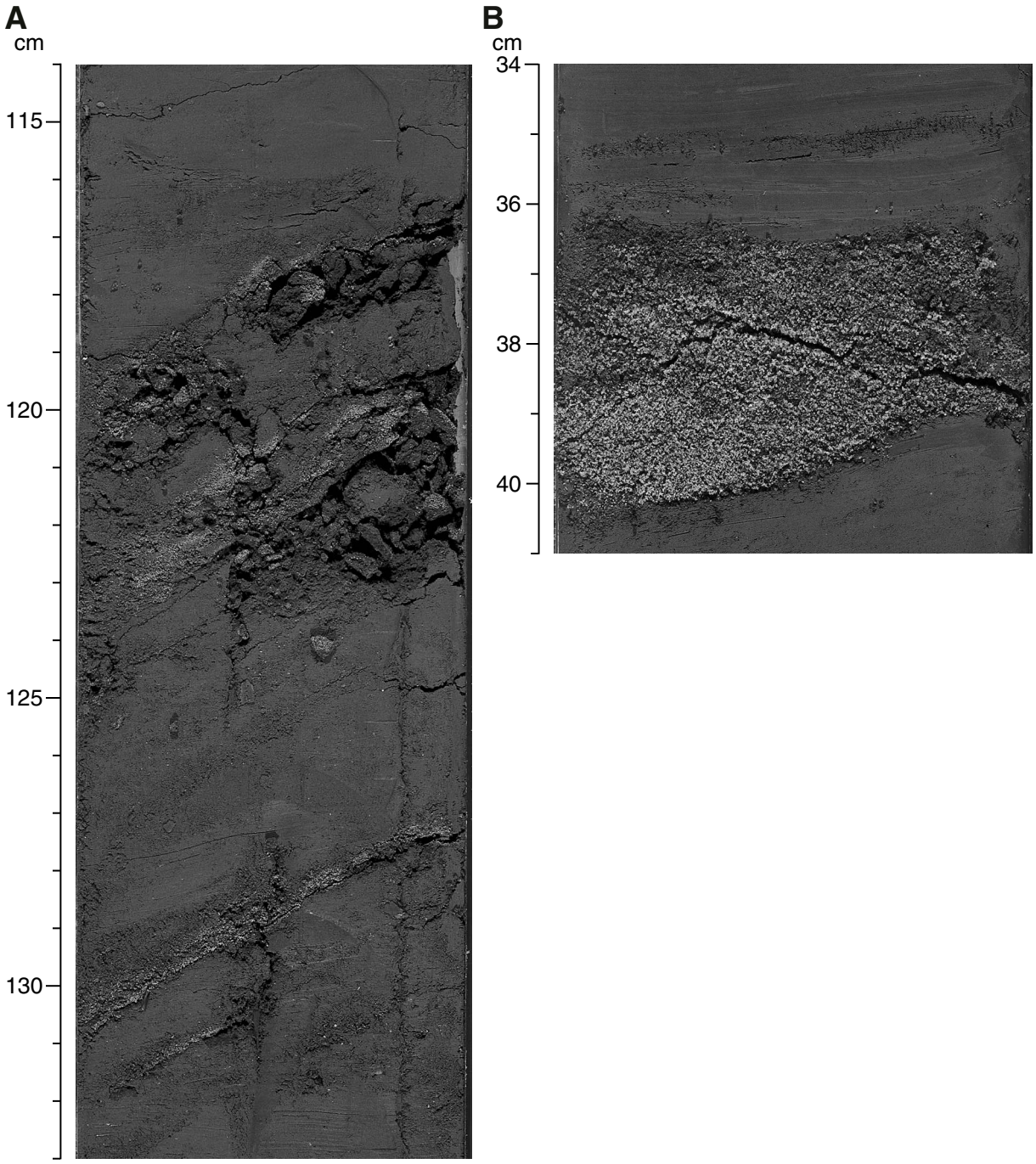

Figure F5. Graph showing the distribution of soupy (black) and mousselike textured (blue) sediments for lithostratigraphic Units I-II and III as observed during core description in Holes 1249B, 1249C, 1249D, 1249E, and 1249F. For indications of core recovery, see Figure F38, p. 75.

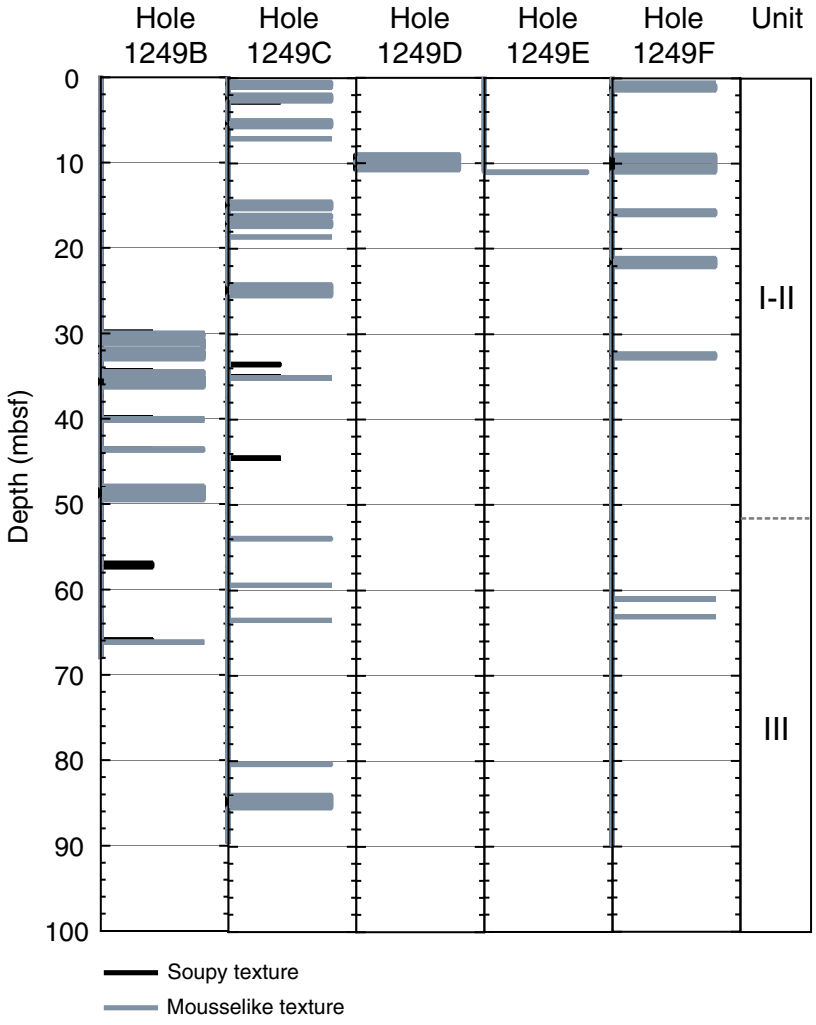

Figure F6. Close-up photographs of sediment from lithostratigraphic Unit I-II. **A.** A very disrupted section with mousselike textured sediment (interval 204-1249F-3H-1, 35–50 cm). **B.** Disrupted sediments resulting from gas hydrate dissociation or gas expansion upon recovery (interval 204-1249F-9H-3, 64–93 cm).

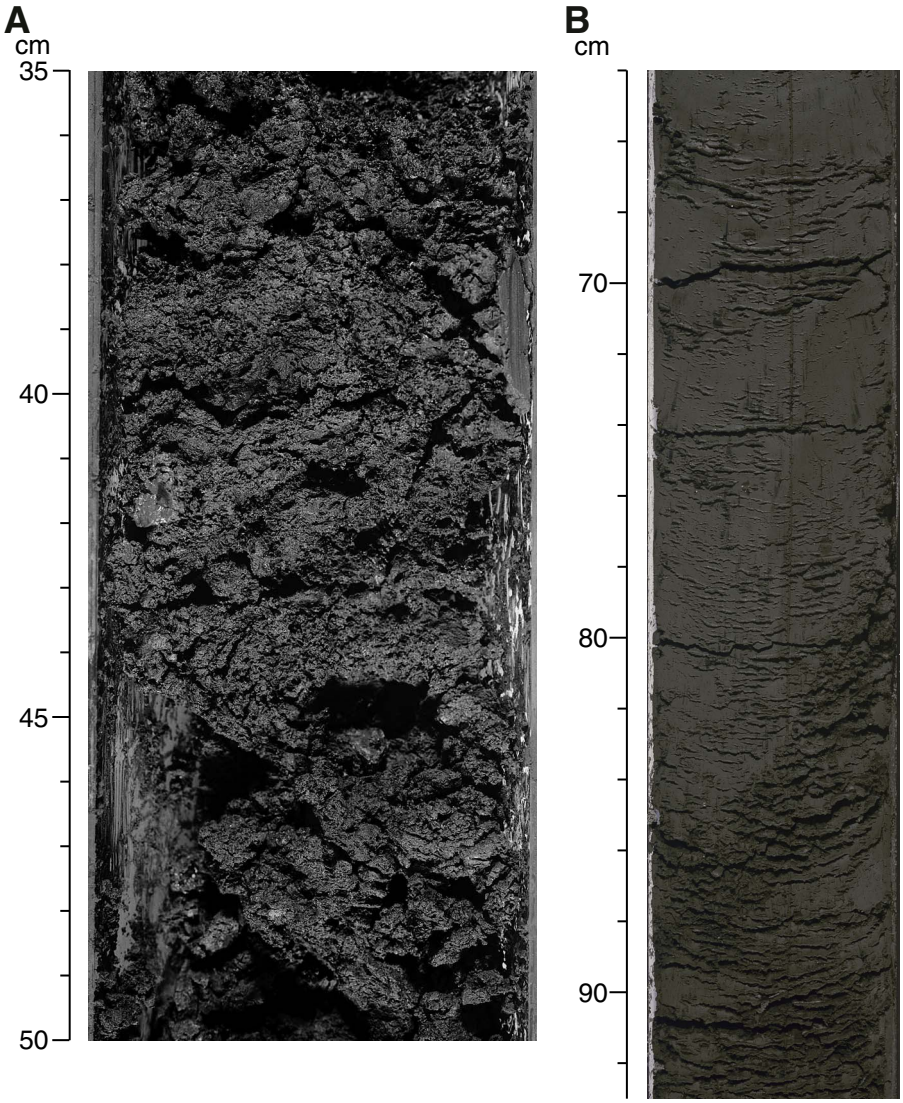

Figure F7. Close-up photographs of sediment from lithostratigraphic Unit III. **A.** A well-defined zone of mousselike textured sediments (interval 204-1249C-12H-5, 13–32 cm). **B.** A zone of dry mousselike textured sediments disrupted by gas hydrate dissociation or gas expansion upon recovery (interval 204-1249C-13H-1, 60–90 cm).

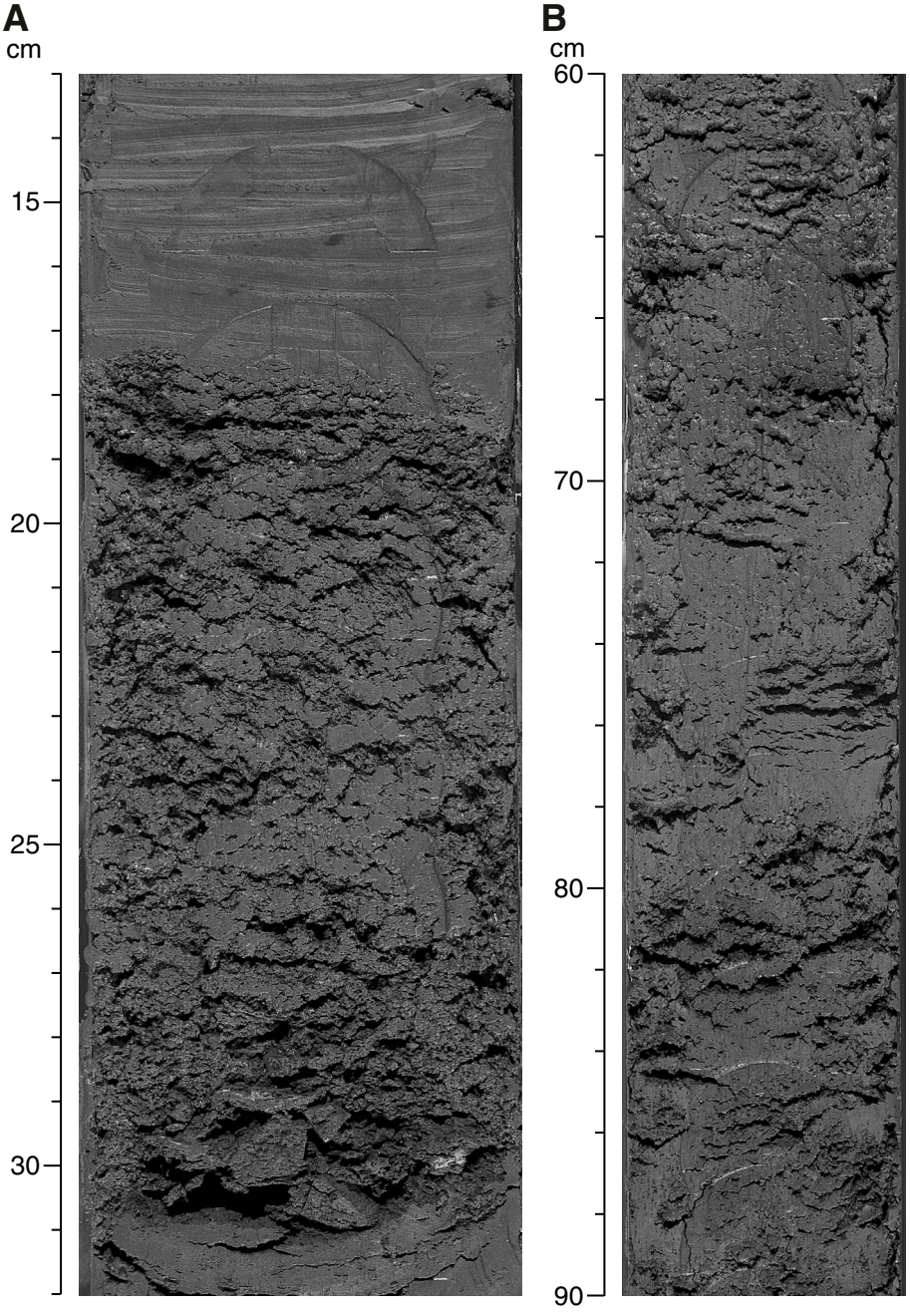

Figure F8. Photographs of Sample 204-1249F-8H-2, 117–127 cm. **A.** Shows the top of the whole-round sample before splitting (diameter of whole-round sample is 6.6 cm). Large red arrow marks a thin vein of gas hydrate. The grayish white cover on the sediment is ice. **B.** After splitting the whole-round core perpendicular to the core axis. The large red arrow marks the enlarged gas hydrate vein and the small red arrow a thinner subparallel vein. The yellow arrow marks a spot of black sulfide precipitates. **C.** Second split of the bottom part of the whole-round sample. The large red arrow marks the dominate vein, spanning almost the whole sample. The small red arrow indicated a second smaller vein. The surface is covered by a very thin layer of gas hydrate. Black spots of sulfide precipitates are marked by yellow arrows.

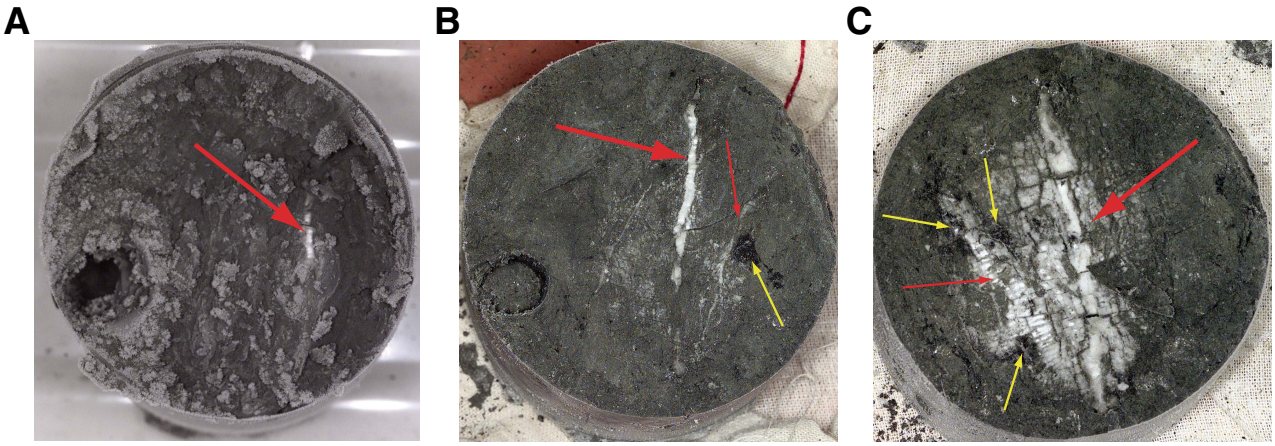

Figure F9. Close-up photograph of Sample 204-1249F-8H-2, 117–127 cm, showing a split gas hydrate vein (diameter of whole-round sample is 6.6 cm). Top and bottom of sample are indicated.

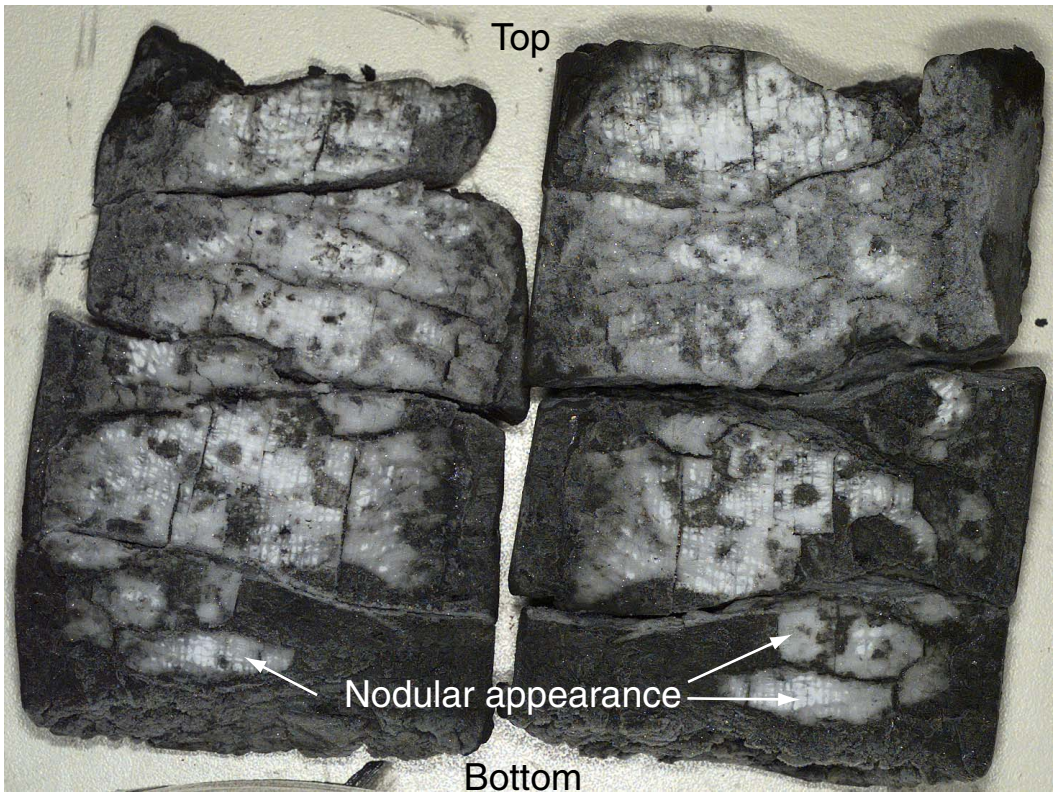

Figure F10. Close-up photograph of Sample 204-1249F-8H-2, 117–127 cm (diameter of whole-round sample is 6.6 cm). Blue lines = closely spaced cleavage planes. Red lines = planes with an offset.

Figure F11. Photograph of Sample 204-1249F-8H-4, 41–49 cm, after complete dissociation of gas hydrate vein. Note the mousselike sediment texture.

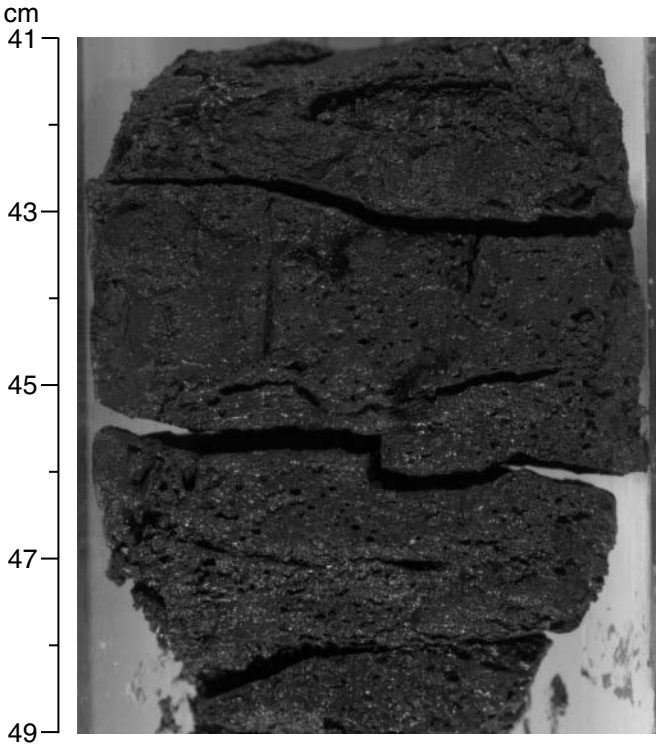

Figure F12. Age-depth plot based on diatom and calcareous nannofossil bioevents for Hole 1249C. The detailed age and depth of control points are shown in Table T3, p. 82. D = diatom event, N = nannofossil event.

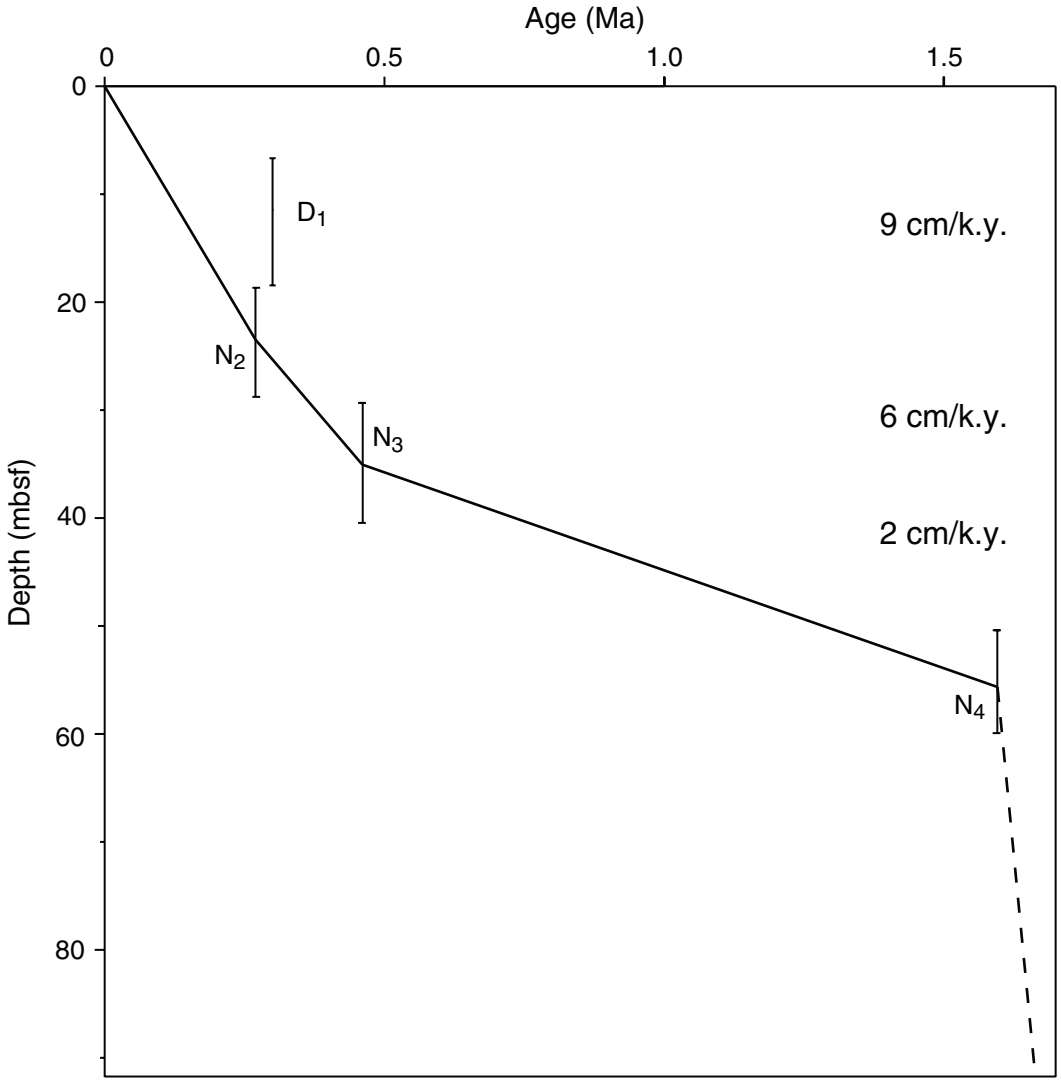

Figure F13. Concentration profiles of various dissolved species in pore waters from Holes 1249B, 1249C, 1249D, 1249E, and 1249F. DOC = dissolved organic carbon. (Continued on next page.)

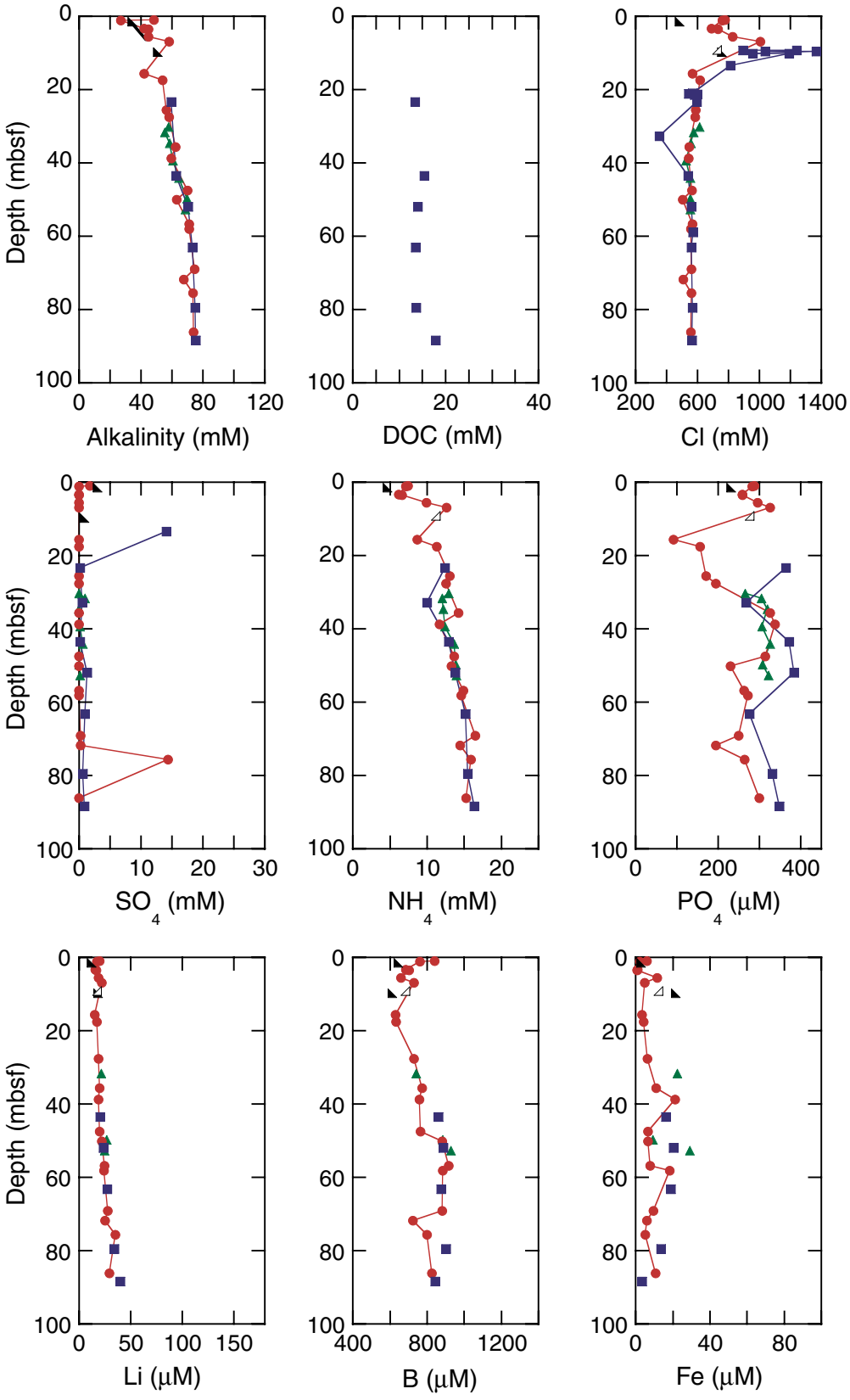

Figure F13 (continued).

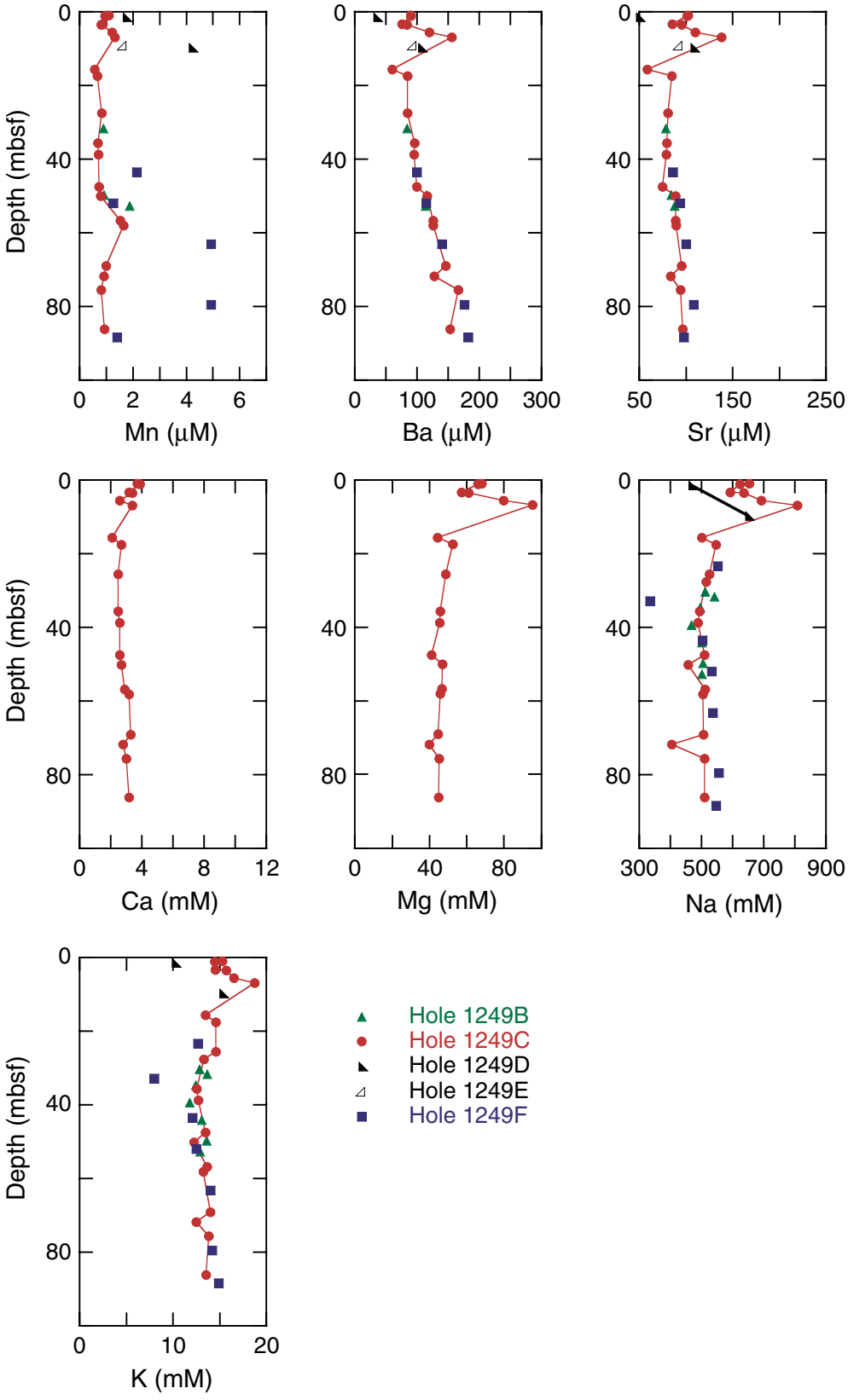

Figure F14. Chloride (Cl^-) concentration profile at Site 1249 (red circles) is shown with data from Site 1245 (fine orange line) for comparison. **A.** Chloride concentration data below ~30 mbsf show excursions to fresher values as defined by a vertical baseline of chloride values from Site 1245. Chloride data above 15 mbsf show positive chloride anomalies with respect to the vertical baseline. We infer that these saltier pore waters result from gas hydrate formation at rates that exceed those of salt removal by diffusion and advection. **B.** Chloride concentration in pore fluids collected from whole-round samples (gray circles) and data from special samples collected to quantify the difference between dry-looking and wet-looking sediment textures (see Table T5, p. 84) in the upper 40 mbsf. Fine orange line represents Cl^- concentrations measured in samples from Site 1245. The color-coded closed and half-open squares identify sample pairs taken in close proximity to one another within either dry or wet sediment. In all cases, the dry-looking samples have significantly higher dissolved chloride than the wet-looking samples. The wet-looking samples also have a higher water content (Table T5, p. 84). These data clearly identify the presence of a brine in the upper 10 mbsf. IW = interstitial water.

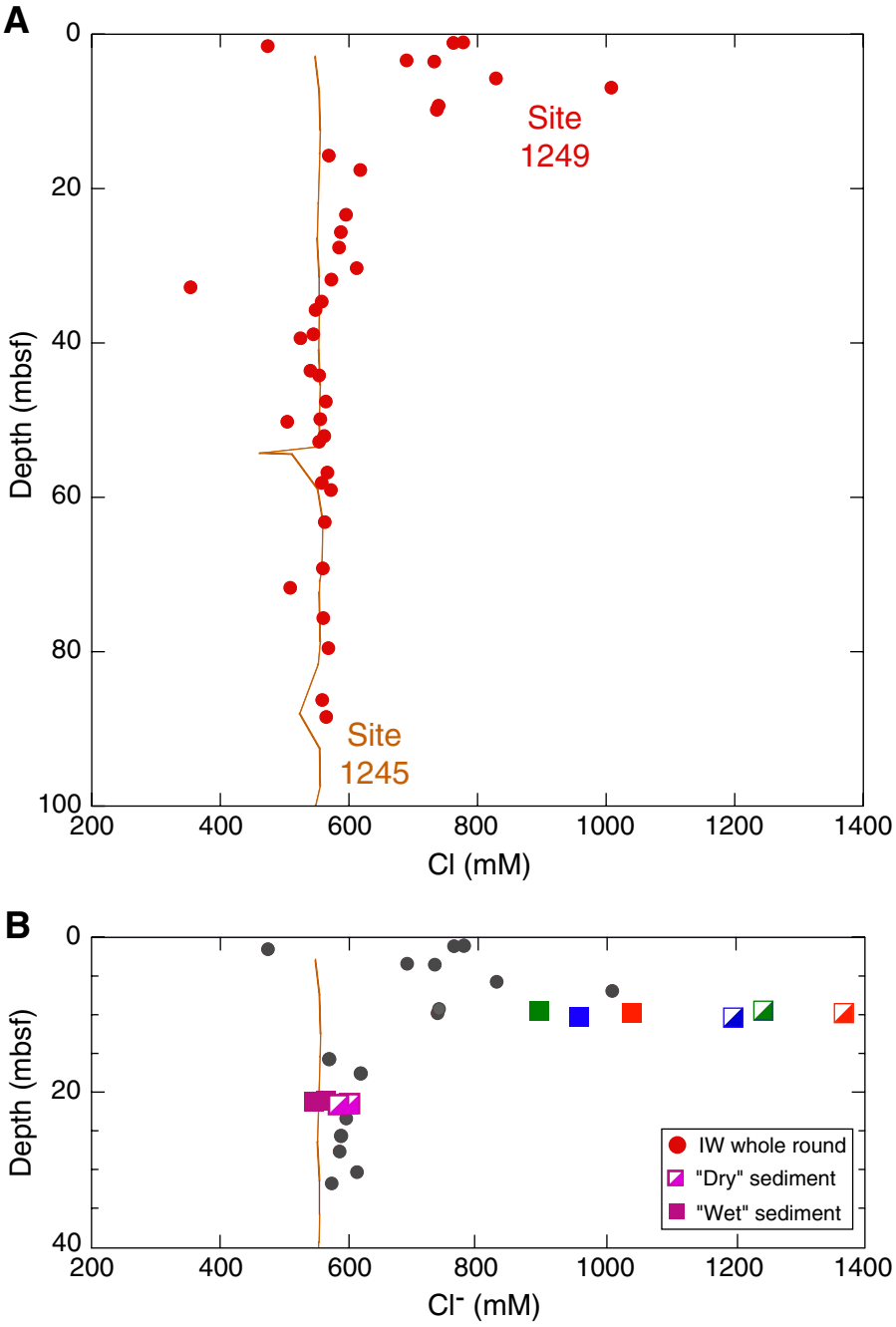

Figure F15. Close-up photograph of sediment from Hole 1249F (interval 204-1249E-7H-3, 37–48 cm) illustrating sediment disturbance by gas hydrate dissociation (38–42 cm) and undisturbed sediments (45–48 cm).

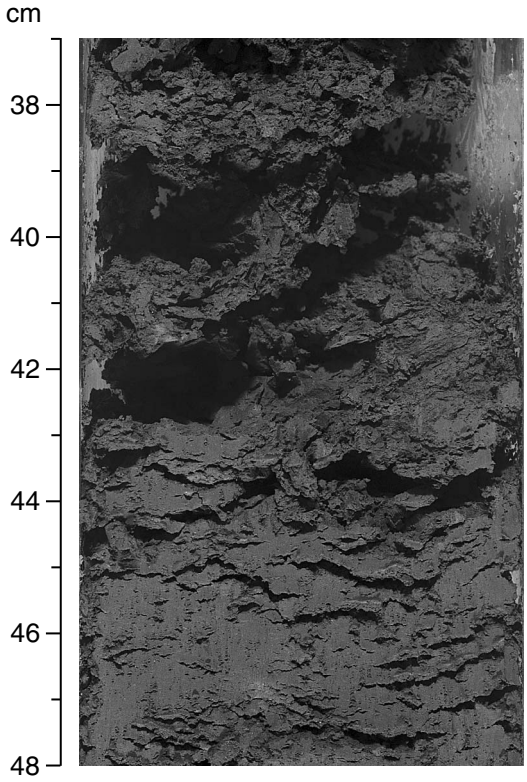

Figure F16. Headspace gas concentrations of C_1, C_2, $C_{2=}$, and C_3 vs. depth for Site 1249.

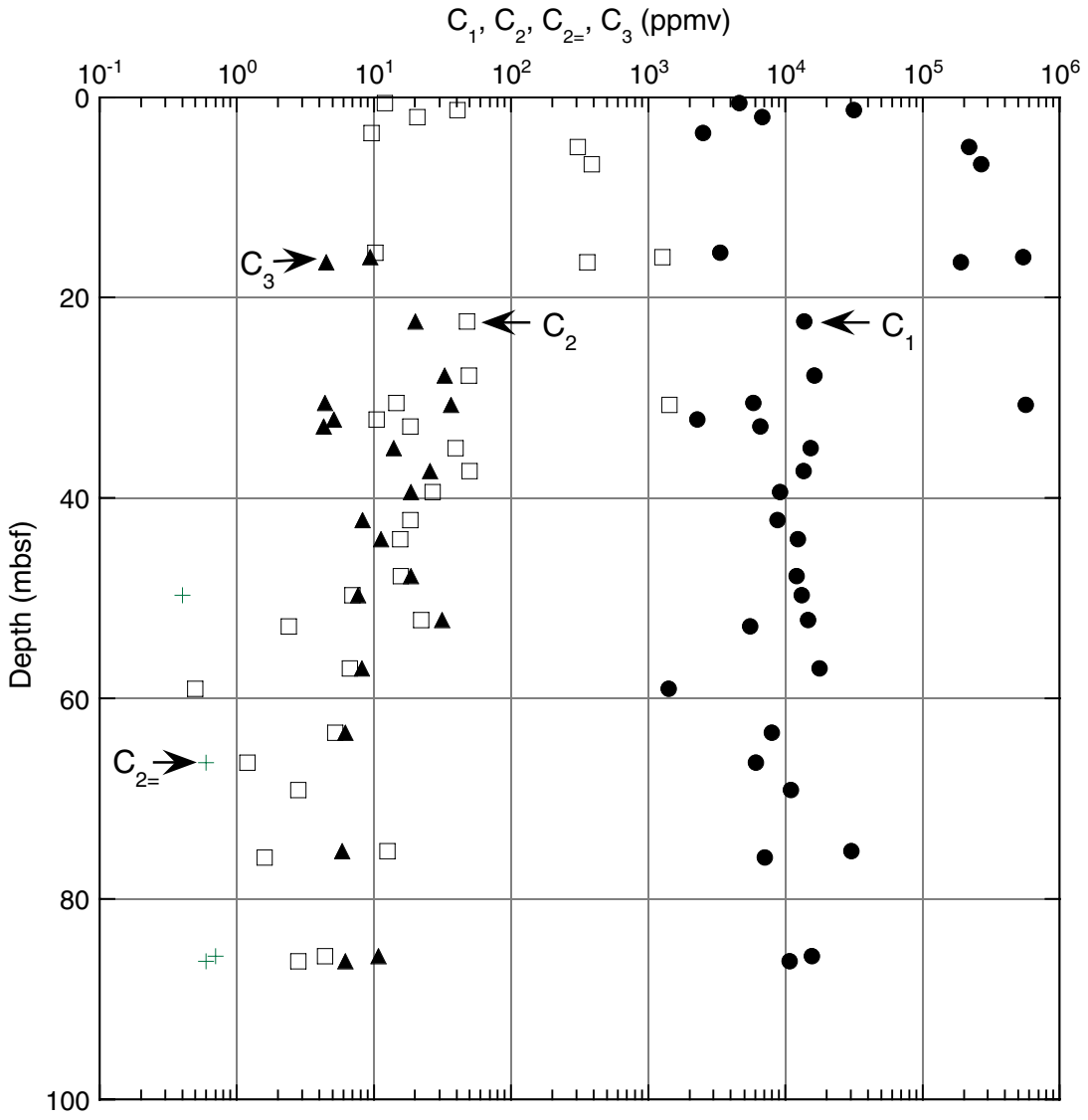

Figure F17. Concentrations of C_1, C_2, C_3, *n*-C_4, *i*-C_4, and *i*-C_5 in core void gas vs. depth for Site 1249.

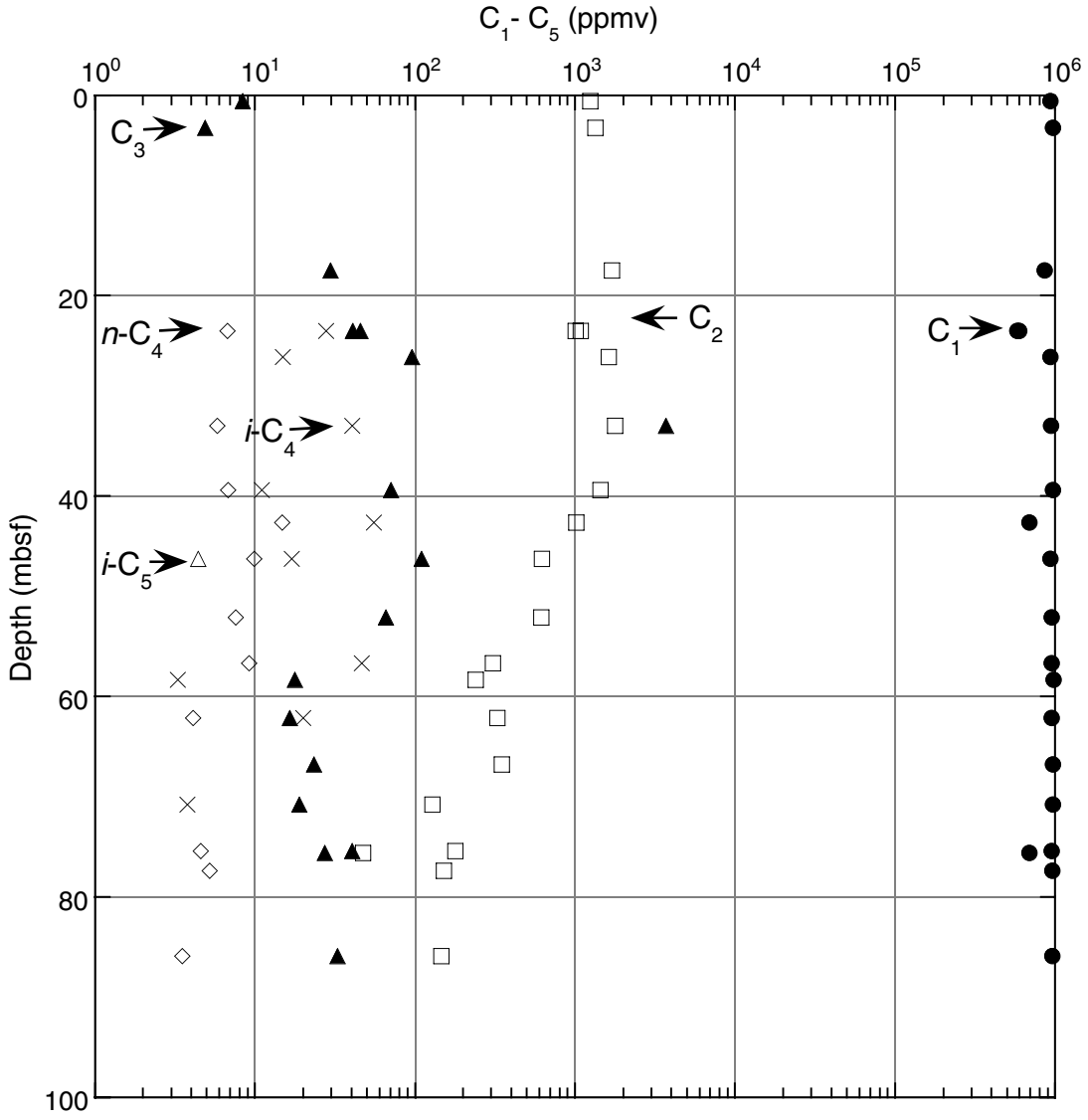

Figure F18. C_1/C_2 ratio vs. depth for Site 1249. VAC = void gas, HS = headspace gas, GH = gas hydrate, PCS = pressure core sampler.

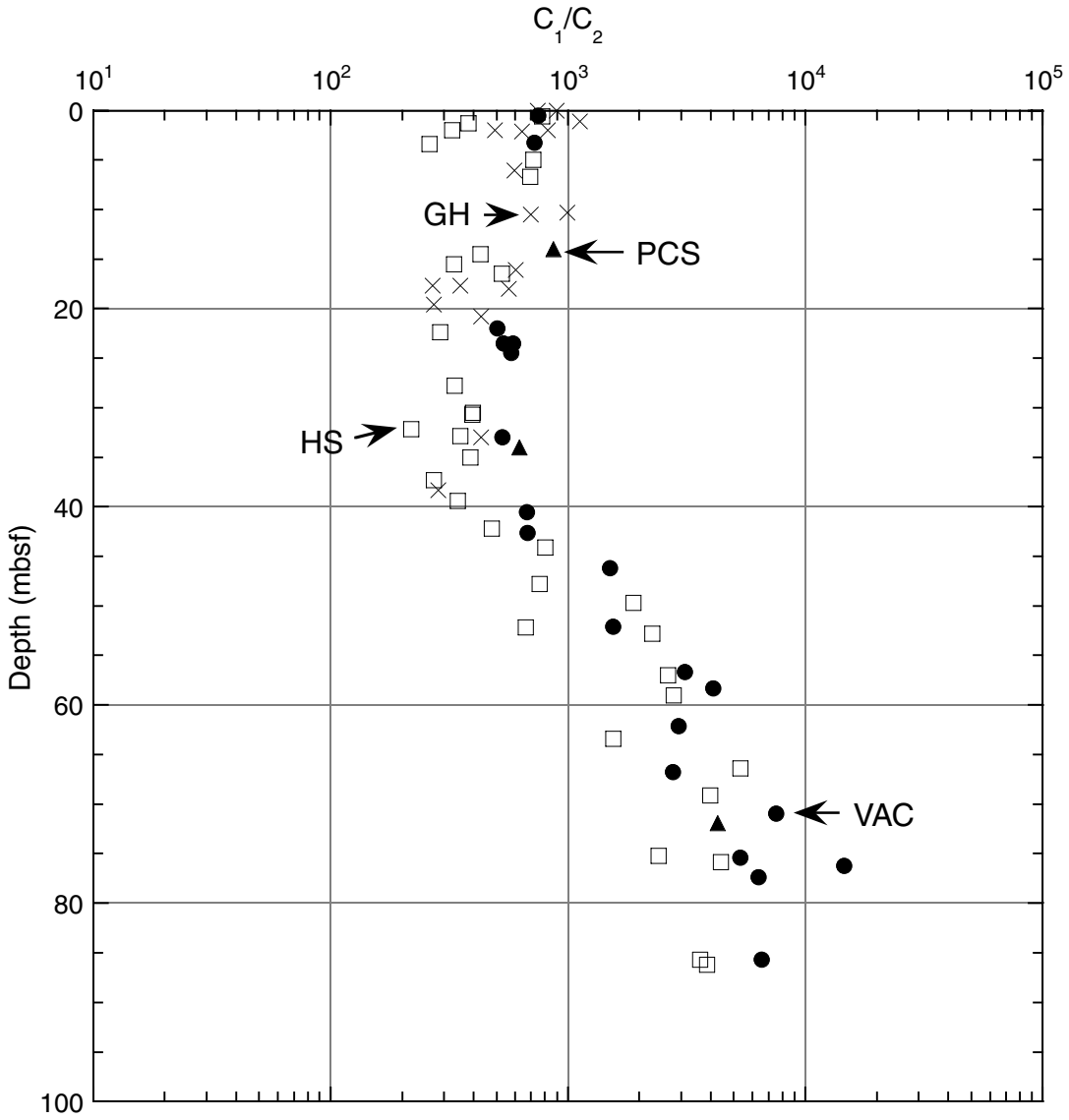

Figure F19. C_1/C_2 ratio vs. temperature for Site 1249. VAC = void gas, HS = headspace gas.

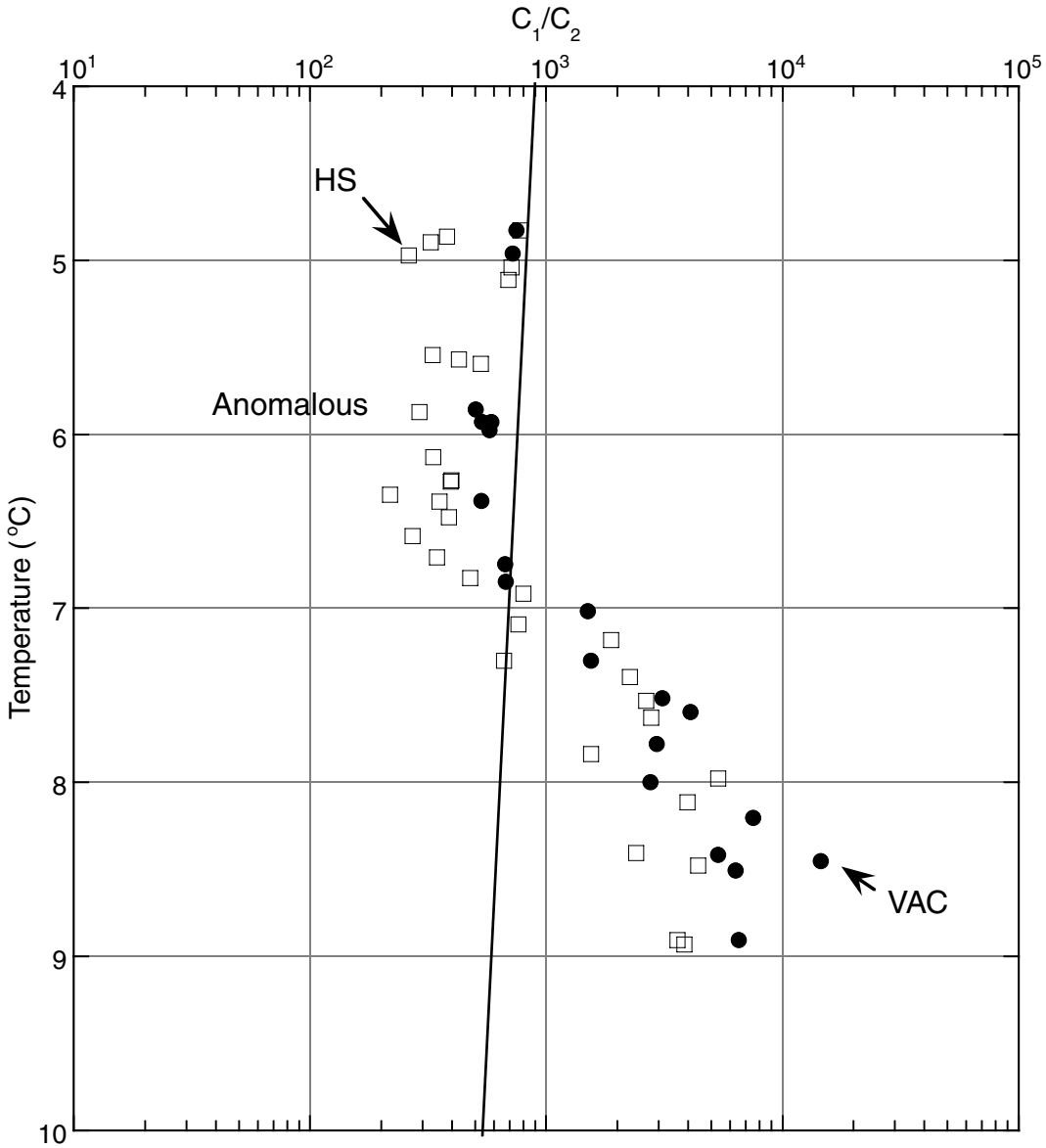

Figure F20. Examples of IR images. **A.** Nodular texture. **B.** Vein or lens.

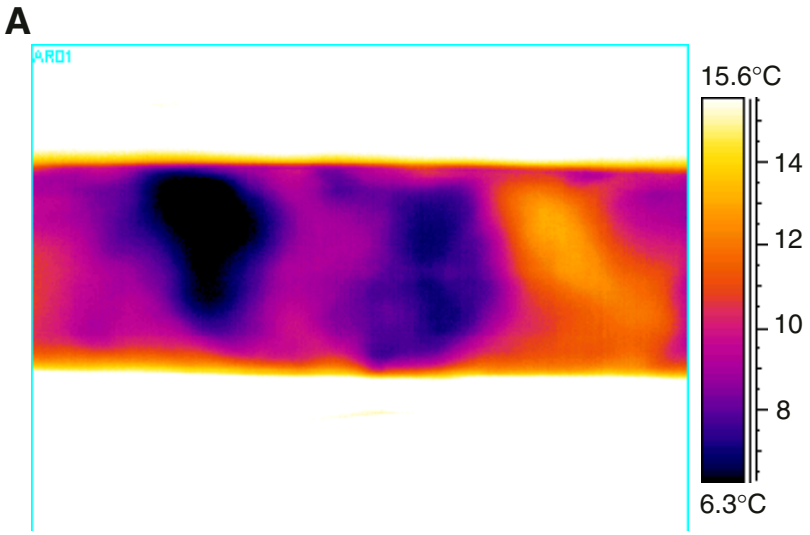

Figure F21. Downhole IR temperature profiles from Holes 1249B, 1249C, and 1249F.

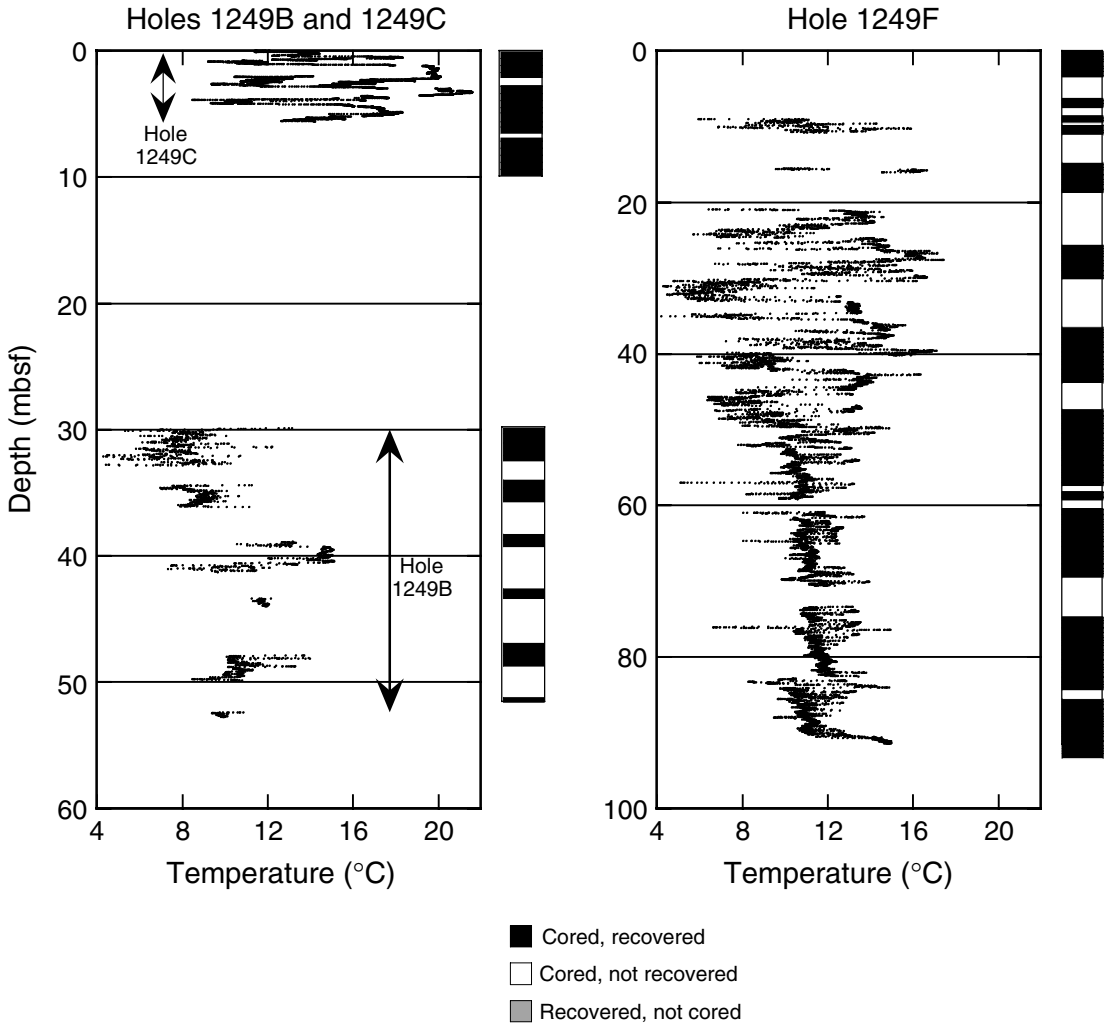

Figure F22. IR temperature anomalies in Hole 1249F compared to S_w from LWD data in Hole 1249A. Resistivity data are plotted in terms of apparent S_w using Archie's Relation; the estimated hydrate concentration is 1.0 – S_w (see **"Downhole Logging,"** p. 29).

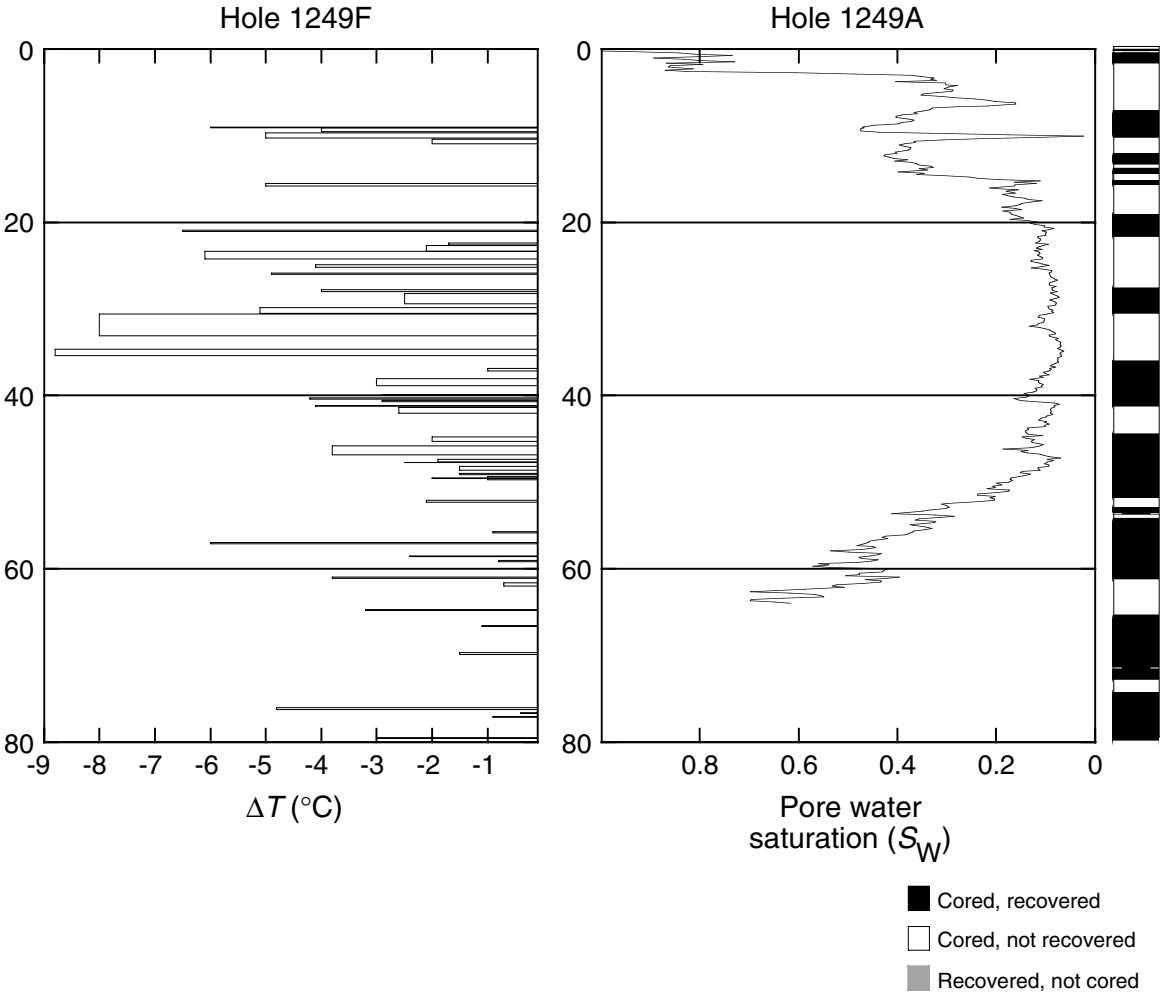

Figure F23. Overview of physical properties measured in Holes 1249B, 1249C, and 1249F. LWD = logging-while-drilling, GRA = gamma ray attenuation, MAD = moisture and density.

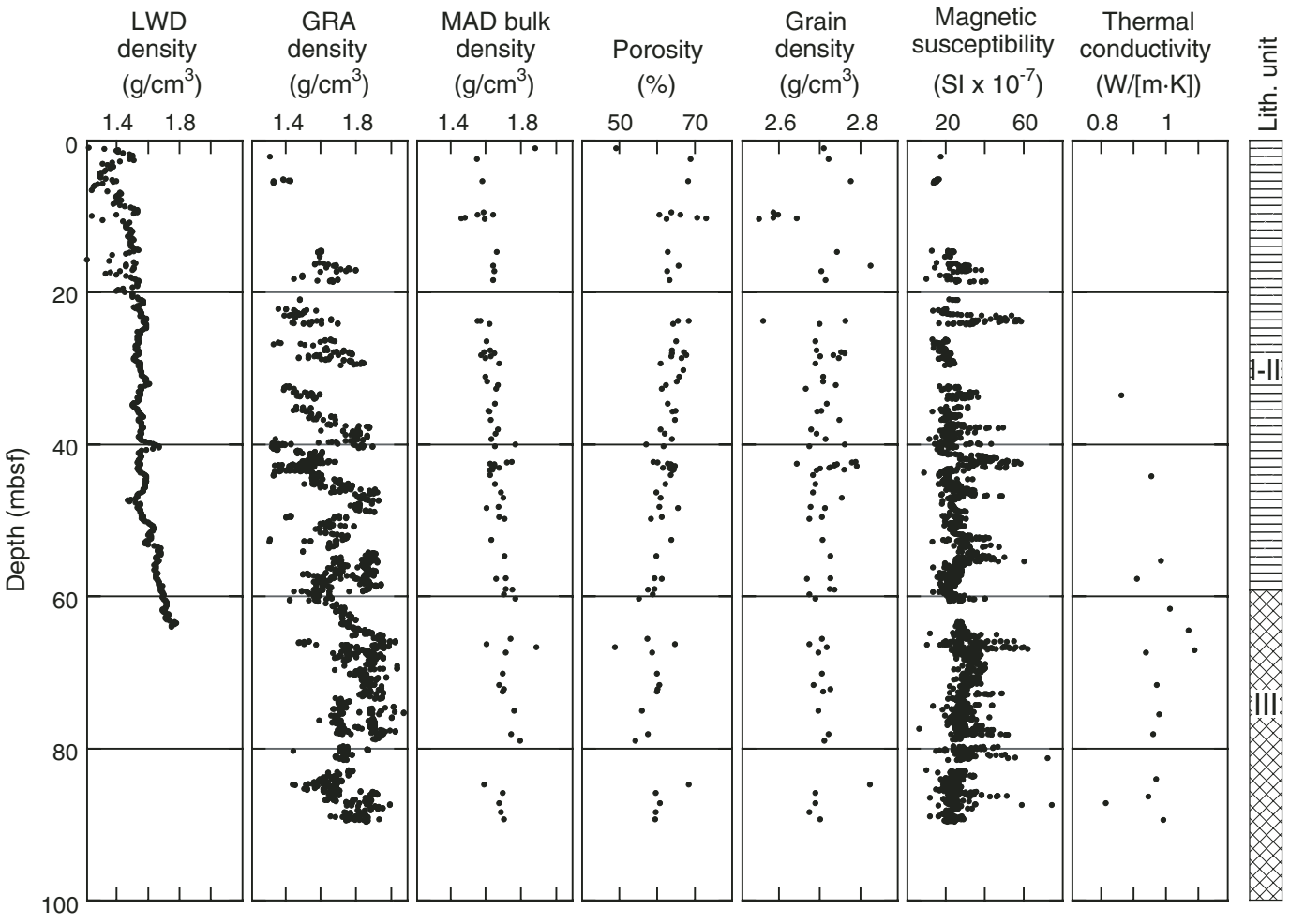

Figure F24. Comparison of physical properties with 3-D seismic data at Site 1249. LWD = logging-while-drilling, MAD = moisture and density, BSR = bottom-simulating reflector.

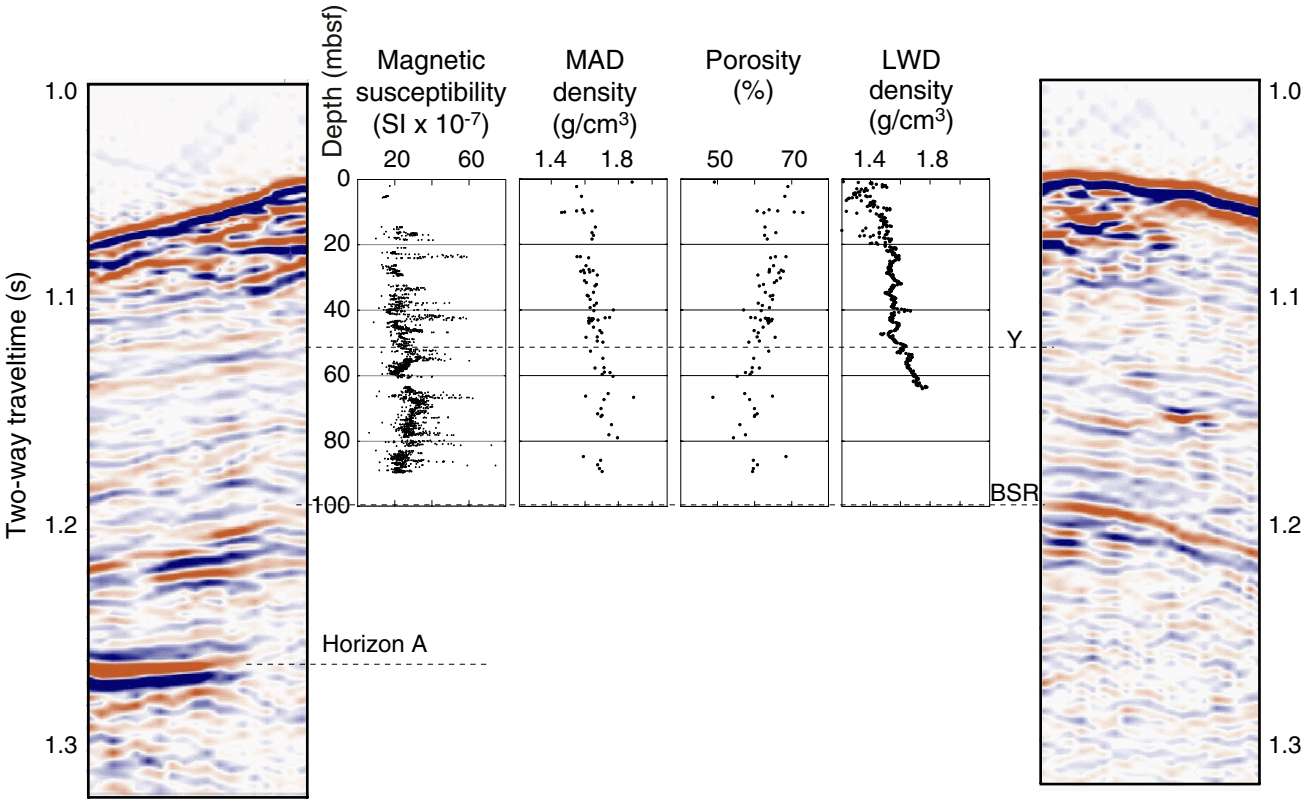

Figure F25. Hydrate dissociation experiment on Section 204-1249F-9H-3. Hydrate is present in discrete intervals, which show a change in electrical conductivity over time. The experiment took 3 hr between runs 1 and 7.

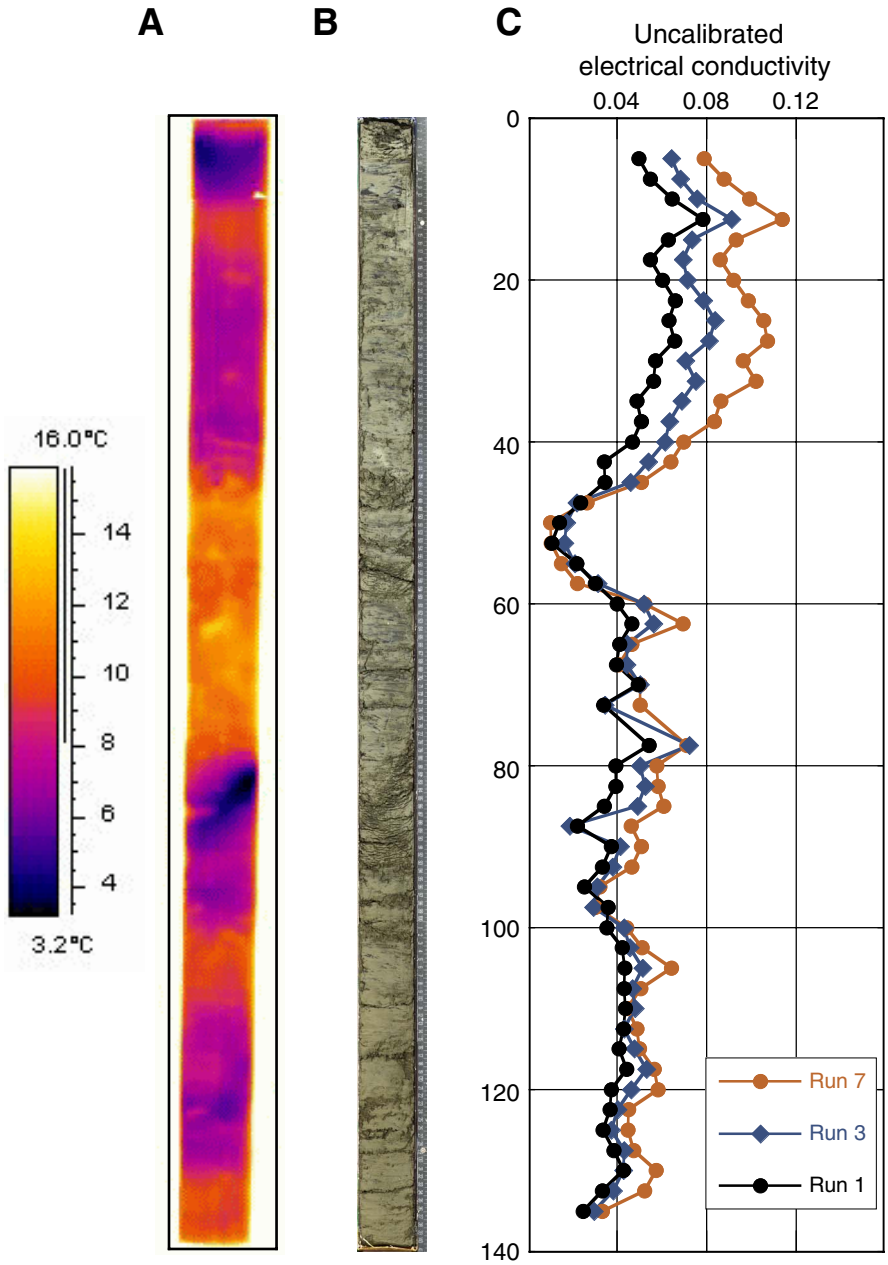

Figure F26. Close-up images of a vein or layer of hydrate in Section 204-1249F-9H-3. **A.** Thermal IR image before start of experiment. The hydrate is associated with –6°C temperature decrease relative to the gas hydrate–free interval. **B.** X-ray image before start of experiment showing fracture dipping at ~45°. **C.** Digital photograph of the split-core archive half at the end of the experiment, showing mousselike texture of the sediments.

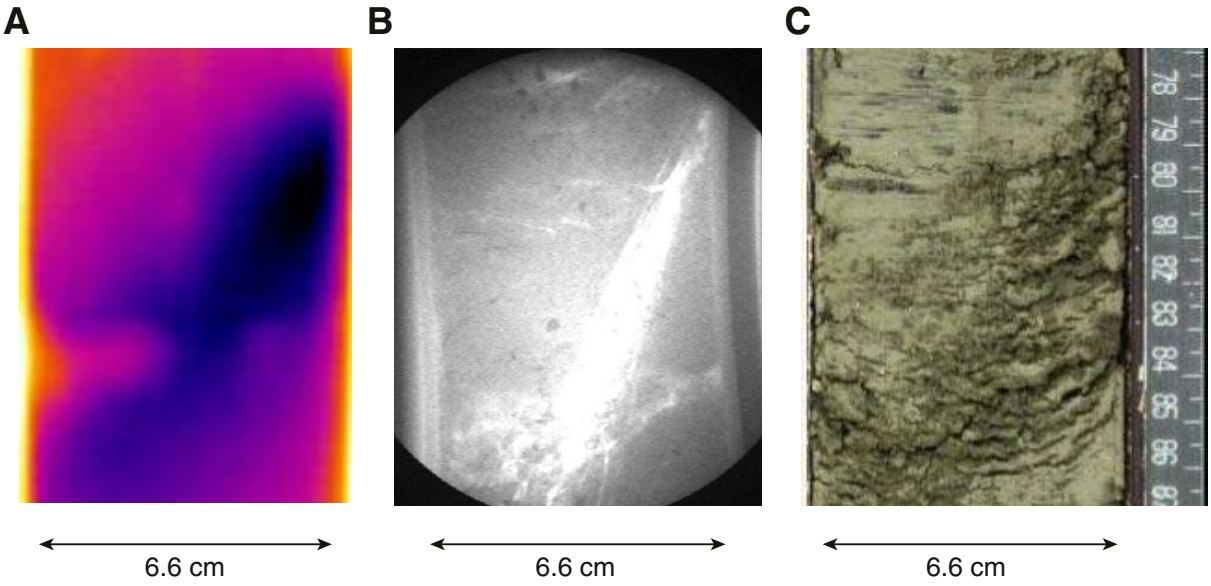

Figure F27. Raw APCT tool data for estimating in situ temperatures. Only the portion of data immediately before, during and immediately after penetration of the probe into the subsurface is shown. For an example of the entire temperature history of a deployment, see **"Downhole Tools and Pressure Coring,"** p. 34, in the "Explanatory Notes" chapter. The ODP core identification number associated with each run of the APCT tool is indicated in the upper left corner of the graph. **B.** DVTPP temperature data. The ODP identification for the cores preceding and following tool deployment is indicated. (Continued on next page.)

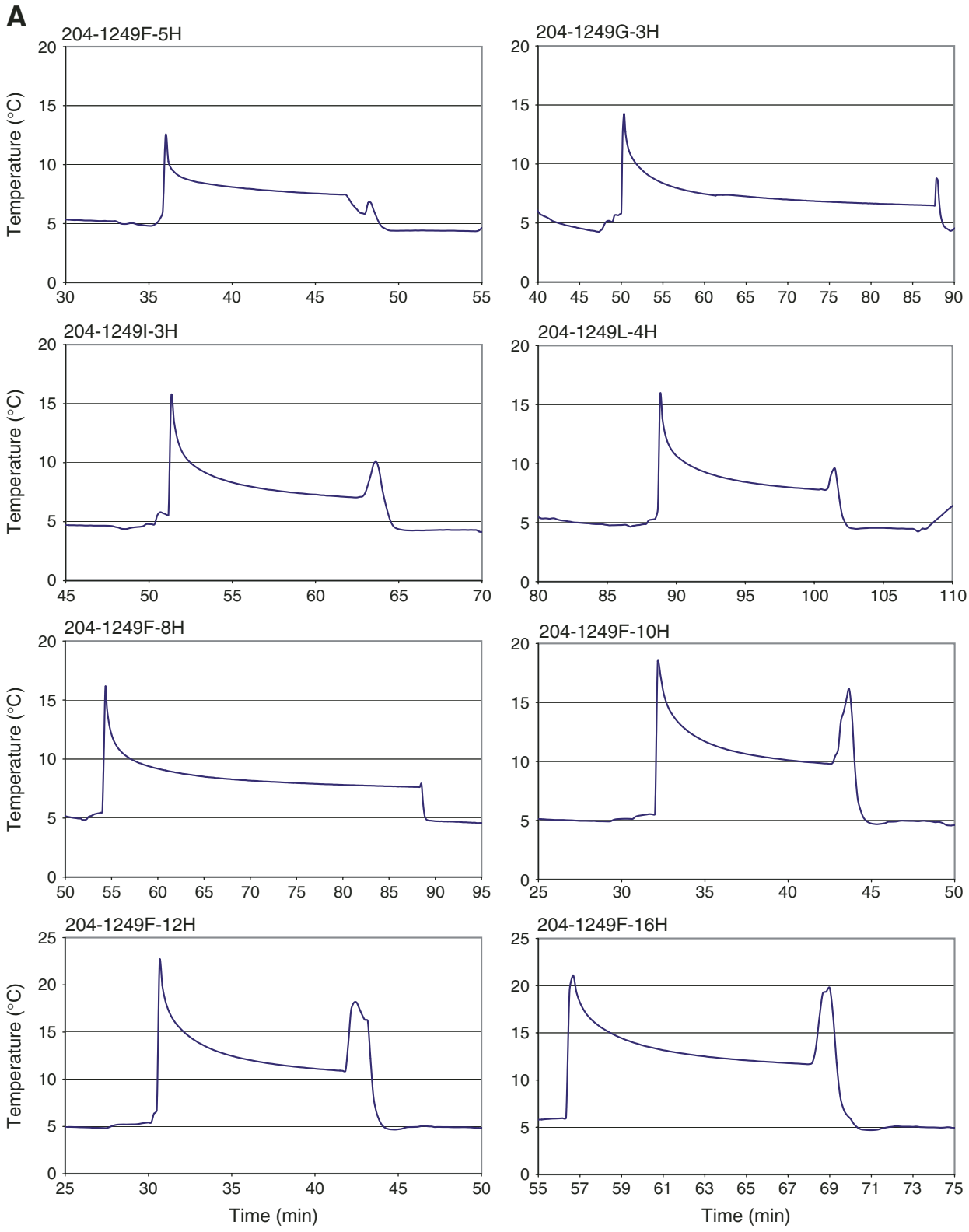

Figure F27 (continued).

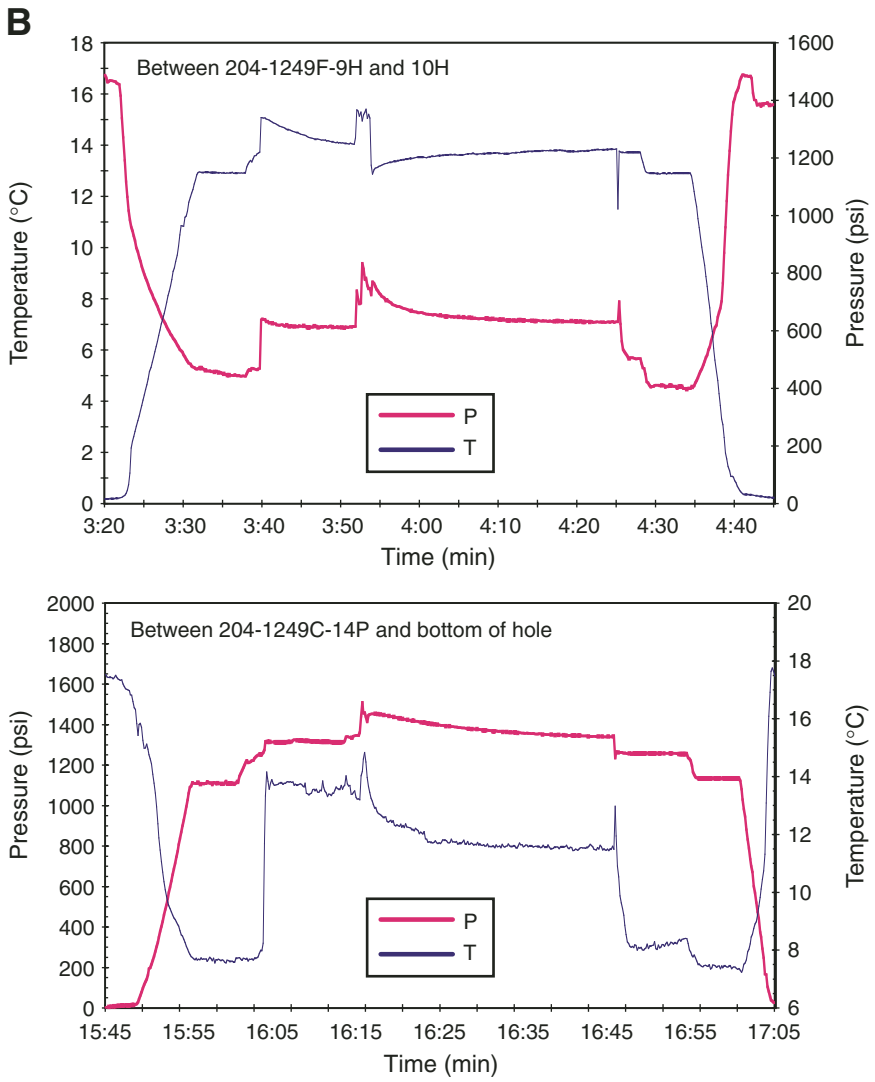

Figure F28. A. Subsurface temperatures plotted vs. depth beneath the seafloor at Site 1249. The equation for the best fitting linear thermal gradient for all the data is also shown. **B.** Effect of adding 0.051°C to all temperatures derived from APC temperature (APCT) tool 11. **C.** Best fitting temperature and the misfit of the data for that temperature as a function of the assumed thermal conductivity assumed. See **"Downhole Tools and Pressure Coring,"** p. 34, in the "Explanatory Notes" chapter for further explanation. **D.** Effect on the apparent thermal gradient of simultaneously determining in situ temperature and thermal conductivity.

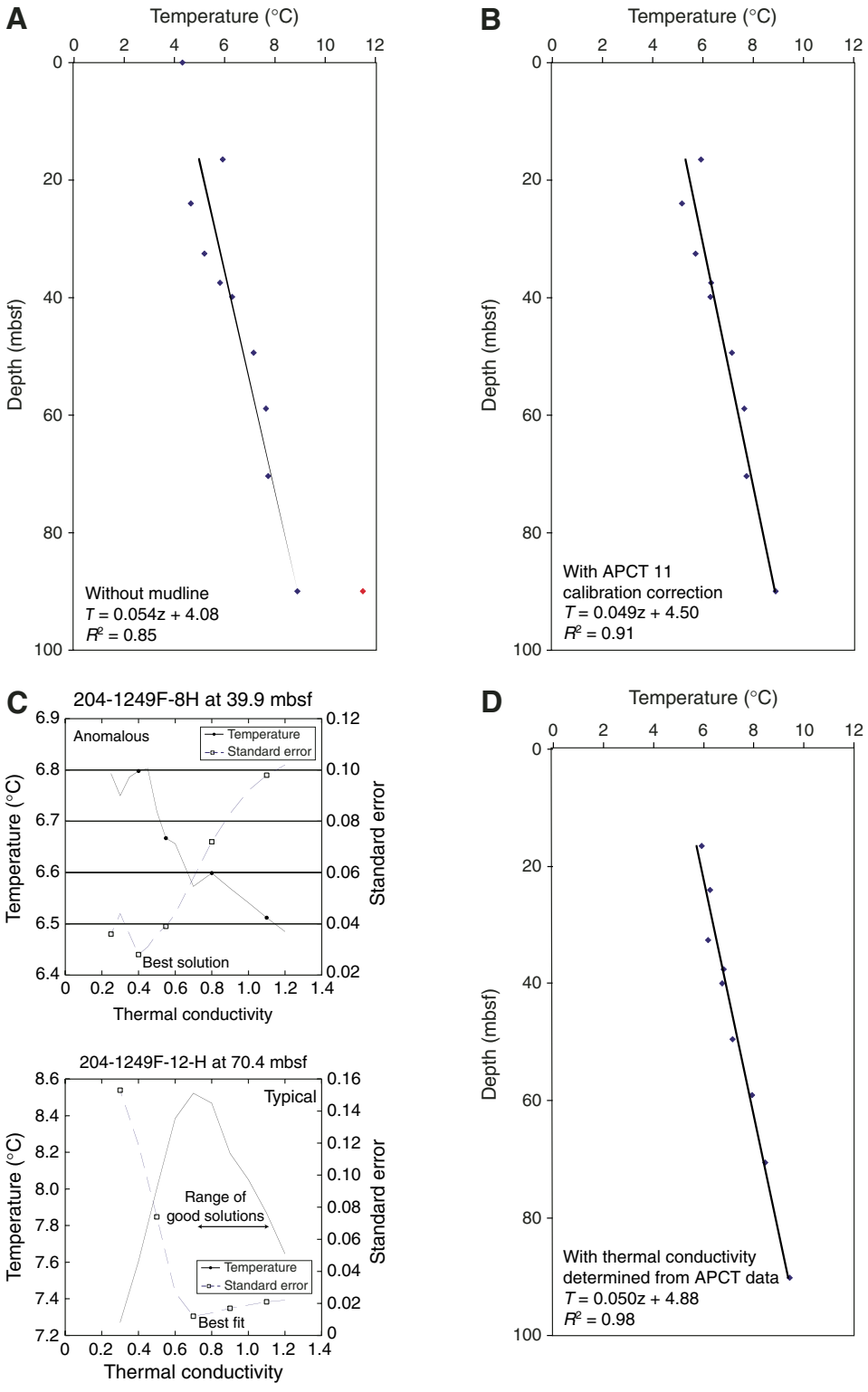

Figure F29. Volume-pressure-time plots for the PCS deployed at Site 1249. **A.** Core 204-1249C-6P. **B.** Core 204-1249F-4P. **C.** Core 204-1249F-14P.

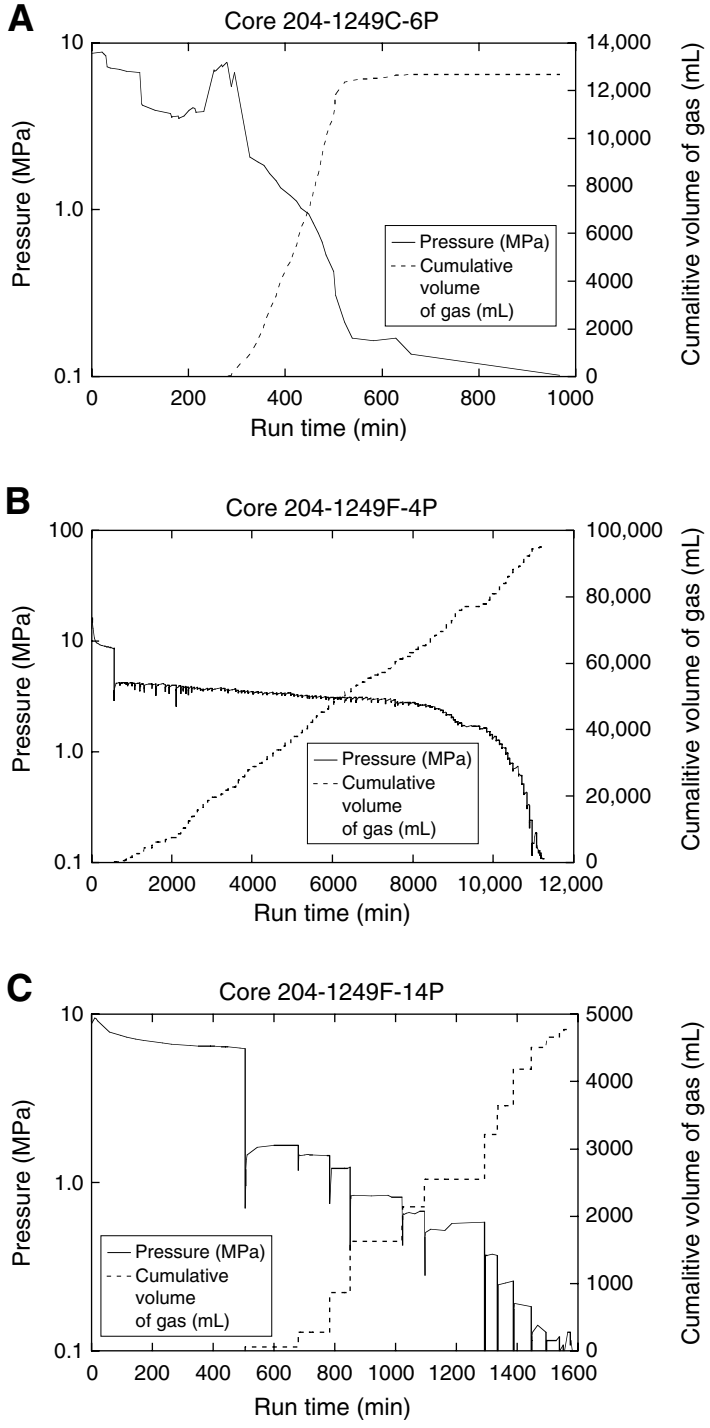

Figure F30. Methane concentration in sediments at Site 1249 based on headspace (HS) and pressure core sampler (PCS) data. Estimated theoretical solubility of methane in pore water (extrapolated from values calculated for higher pressures) (Handa, 1990; Duan et al., 1992) is shown, and fields of dissolved methane (D), methane hydrate (H), and free methane (F) are depicted. Note that the headspace technique fails to determine accurate concentration values above ~2 mM because methane is relatively abundant in situ and it rapidly escapes from sediments upon core retrieval.

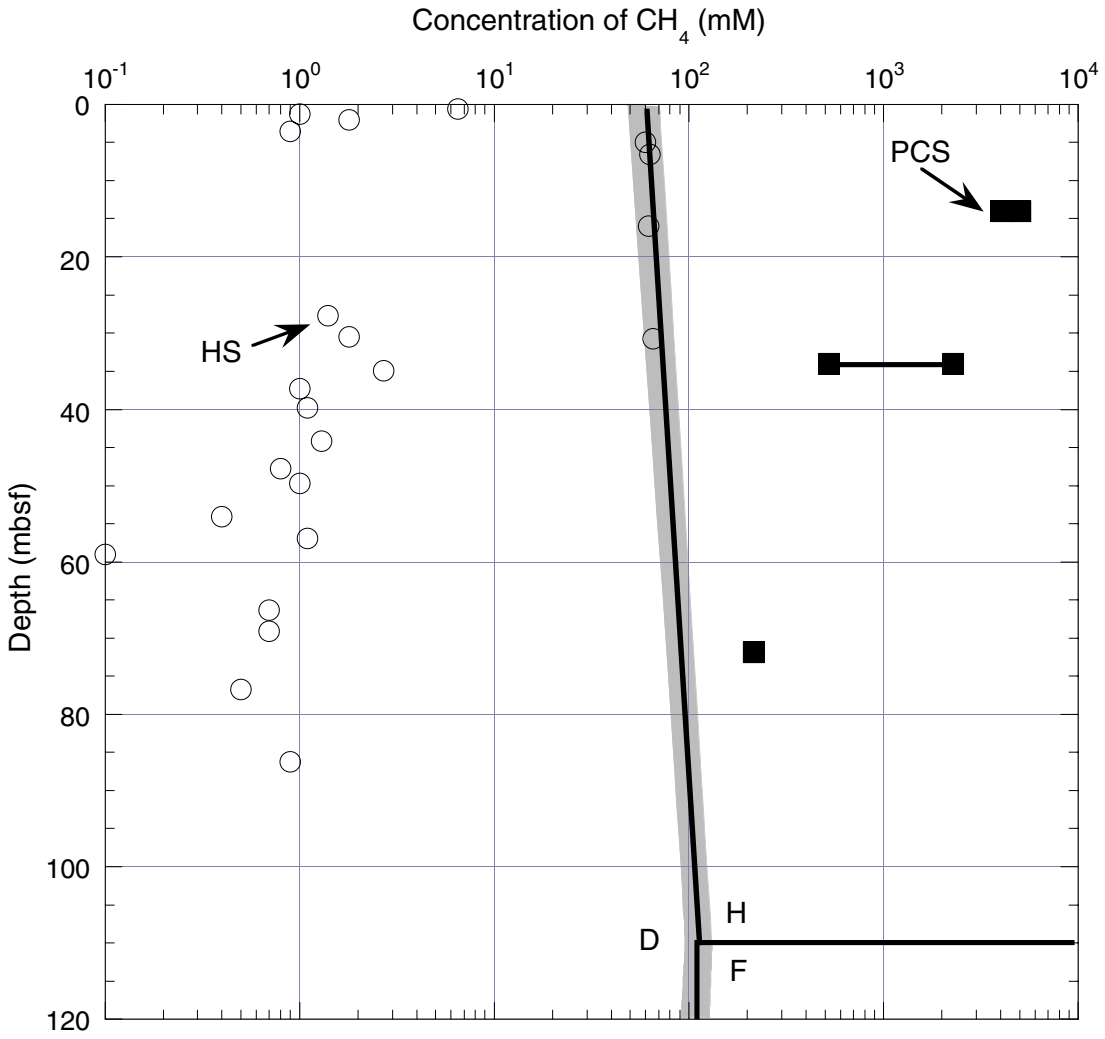

Figure F31. Density profiles of HRC 4 (Core 204-1244E-8Y) showing the initial in situ density profile (run 1), a profile during early degassing (run 8), and a profile during the later stages of degassing (run 15).

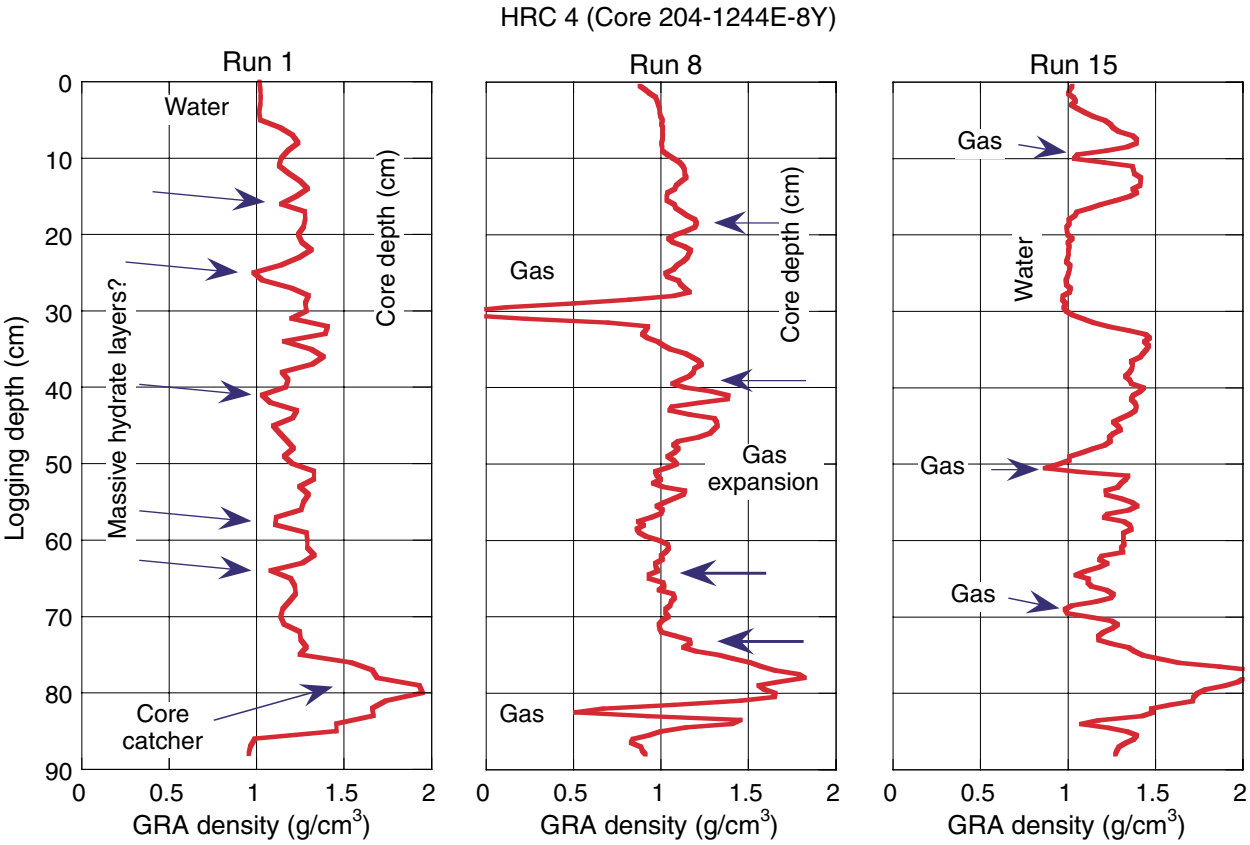

Figure F32. Density profiles of HYACE Rotary Corer (HRC) 7 (Core 204-1249G-2E) showing the initial profile (run 1), a rapid profile after replacing the chamber water with He (run 2), and a rapid density profile after freezing (run 3). GRA = gamma ray attenuation

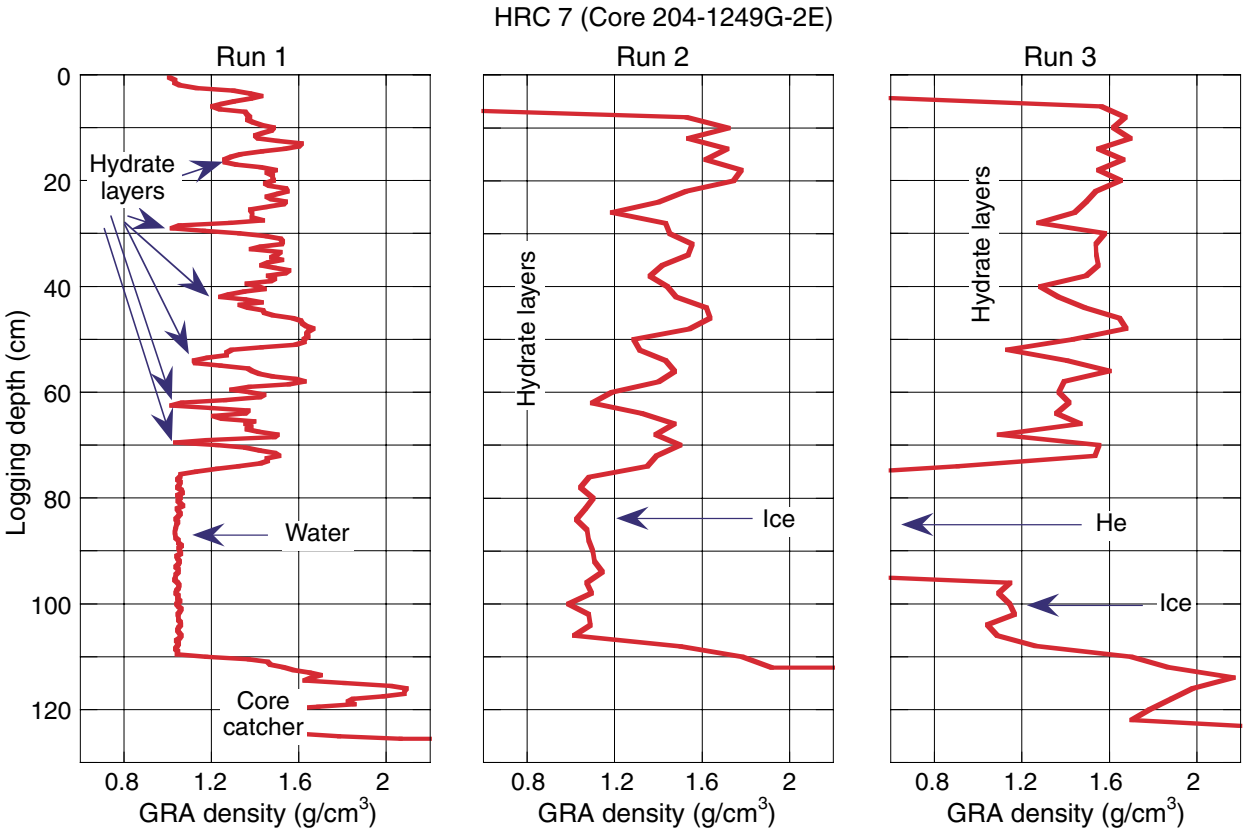

Figure F33. Density profile of Fugro Pressure Corer (FPC) 10 (Core 204-1249H-2Y) showing the interpretation of massive hydrate layers and free gas. GRA = gamma ray attenuation.

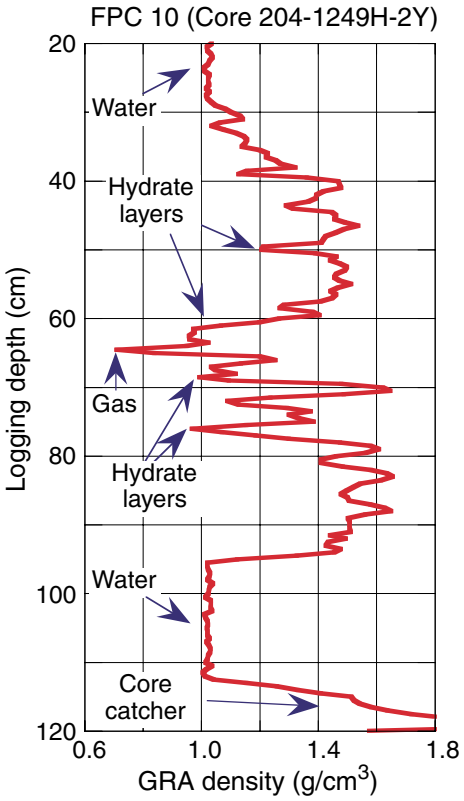

Figure F34. Quality control LWD logs from Hole 1249A. ROP = rate of penetration, TAB = time after bit, Diff. = differential.

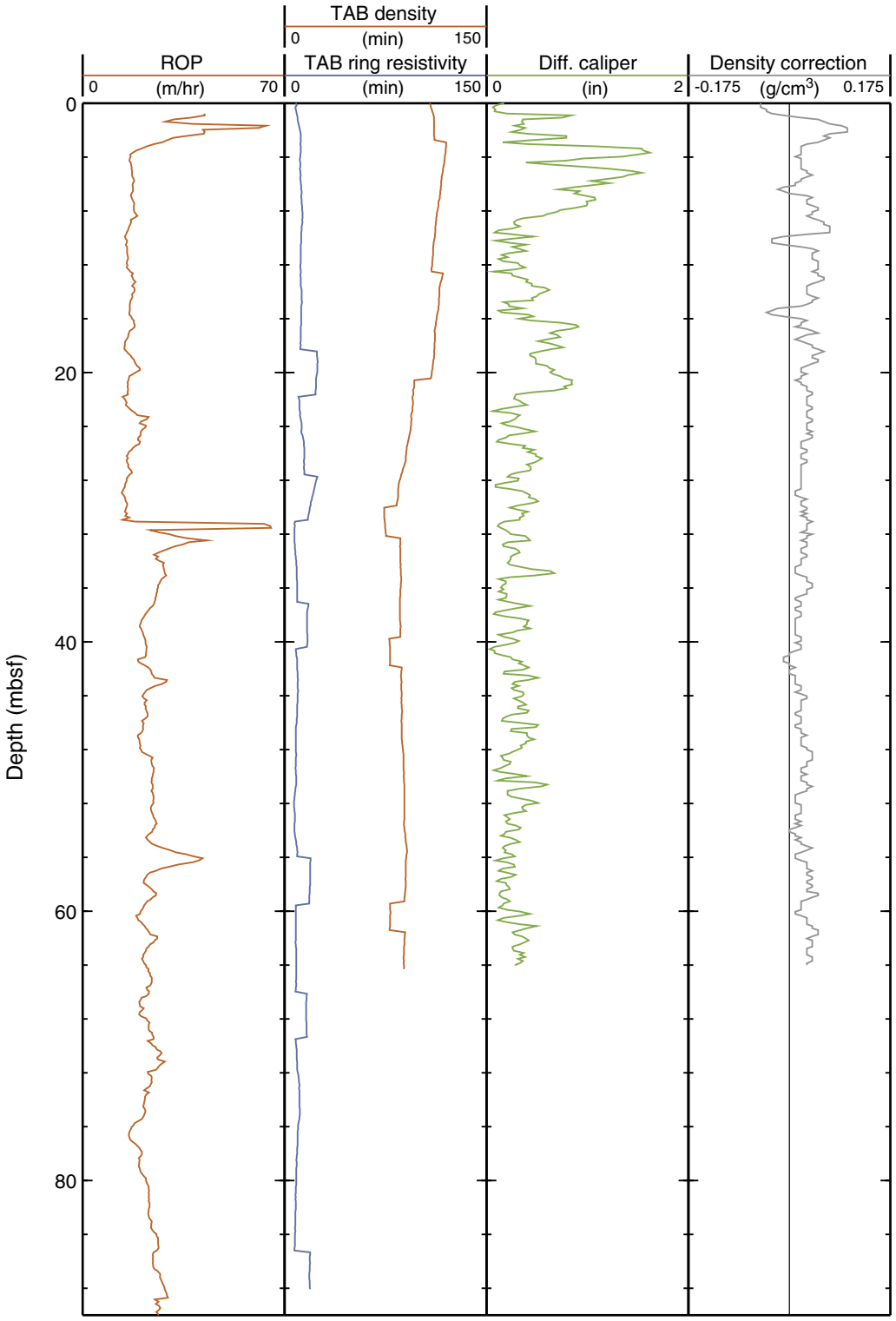

Figure F35. Summary of LWD data from Hole 1249A. gAPI = American Petroleum Institute gamma ray units, PEF = photoelectric effect factor, RAB = resistivity at the bit.

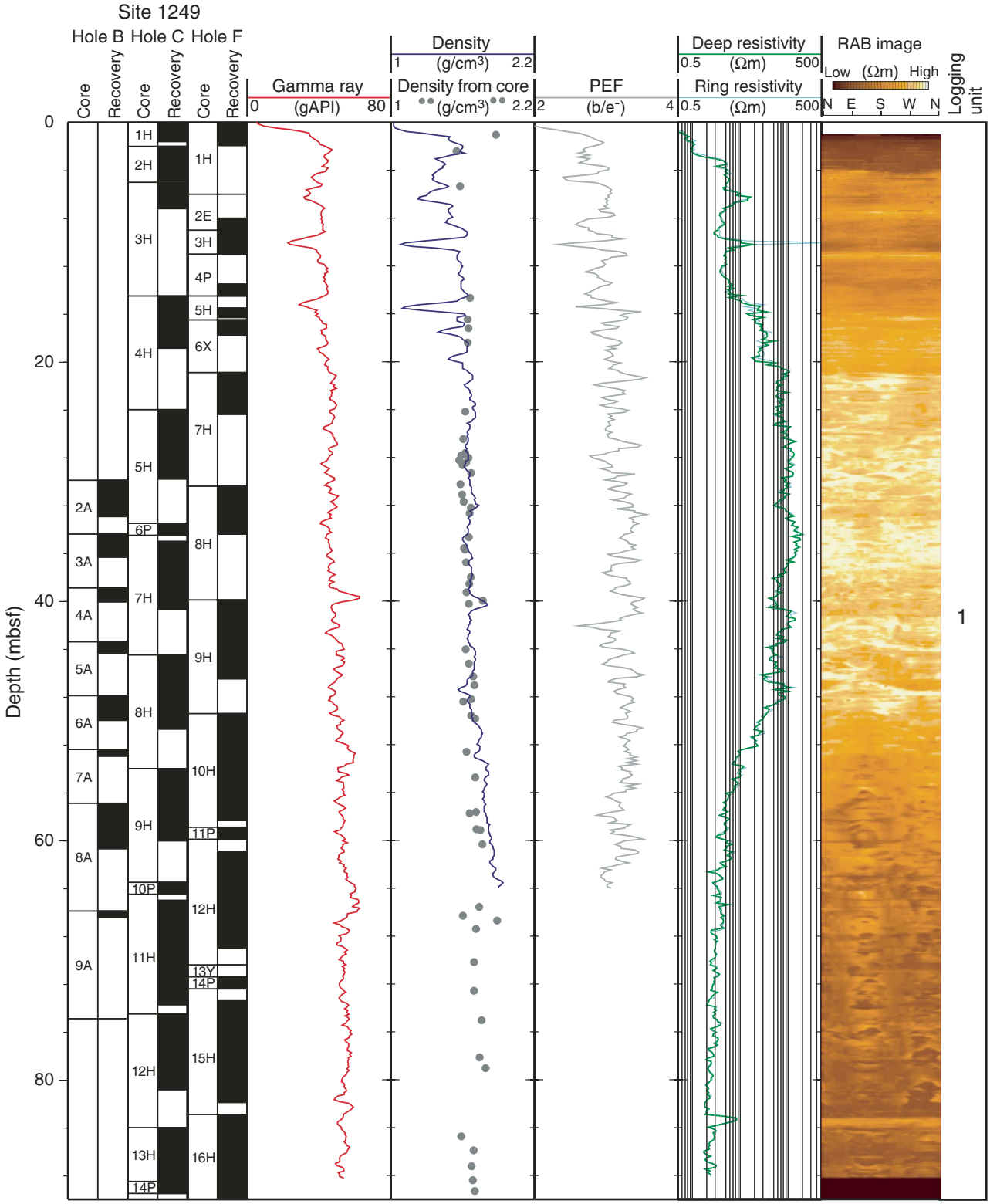

Figure F36. LWD- and core-derived porosities for Hole 1249A. NMR-MRP = Nuclear Magnetic Resonance tool, RAB = resistivity at the bit.

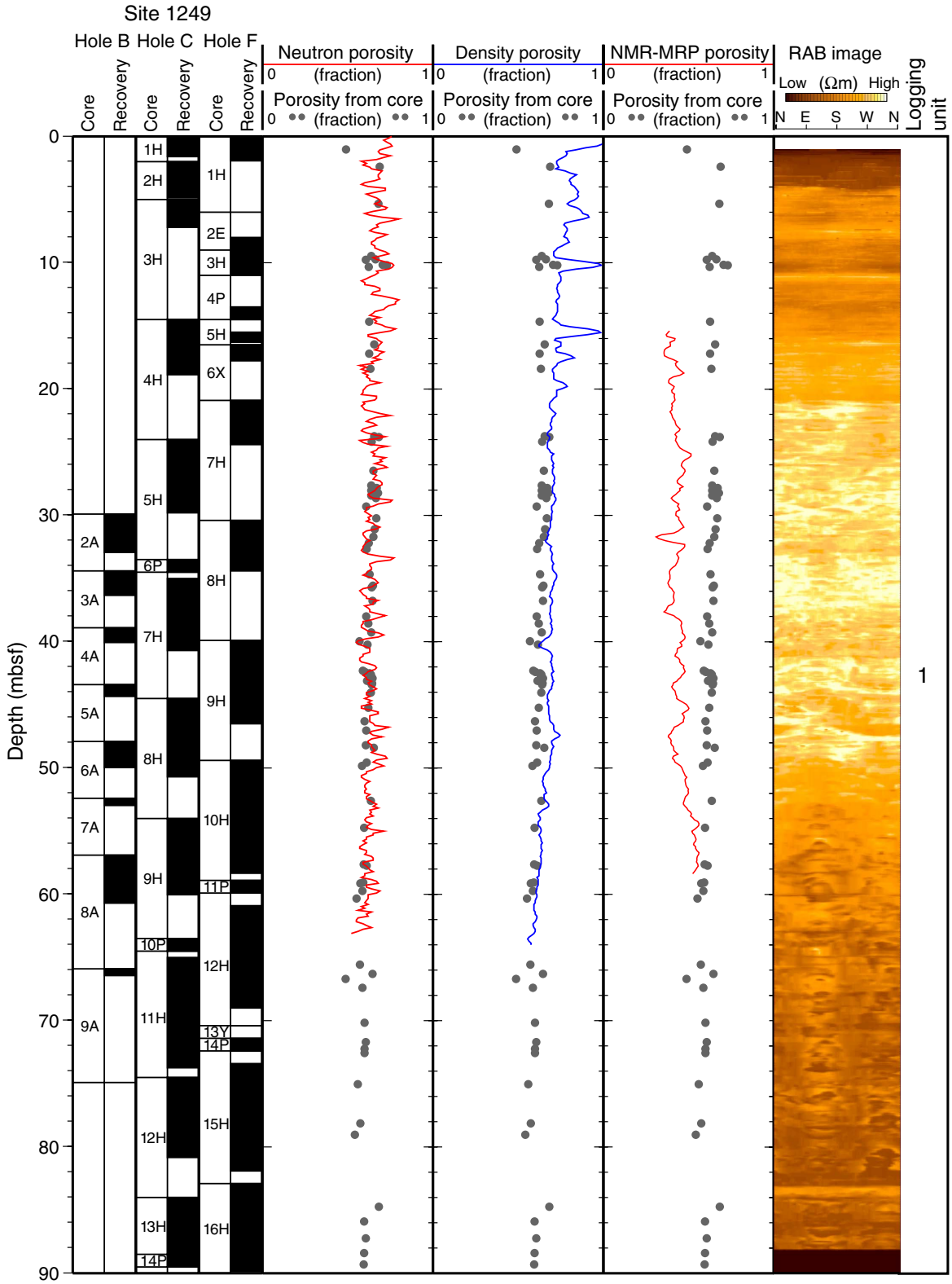

Figure F37. Logging-derived gas hydrate saturations for Hole 1249A. gAPI = American Petroleum Institute gamma ray units, RAB = resistivity at the bit.

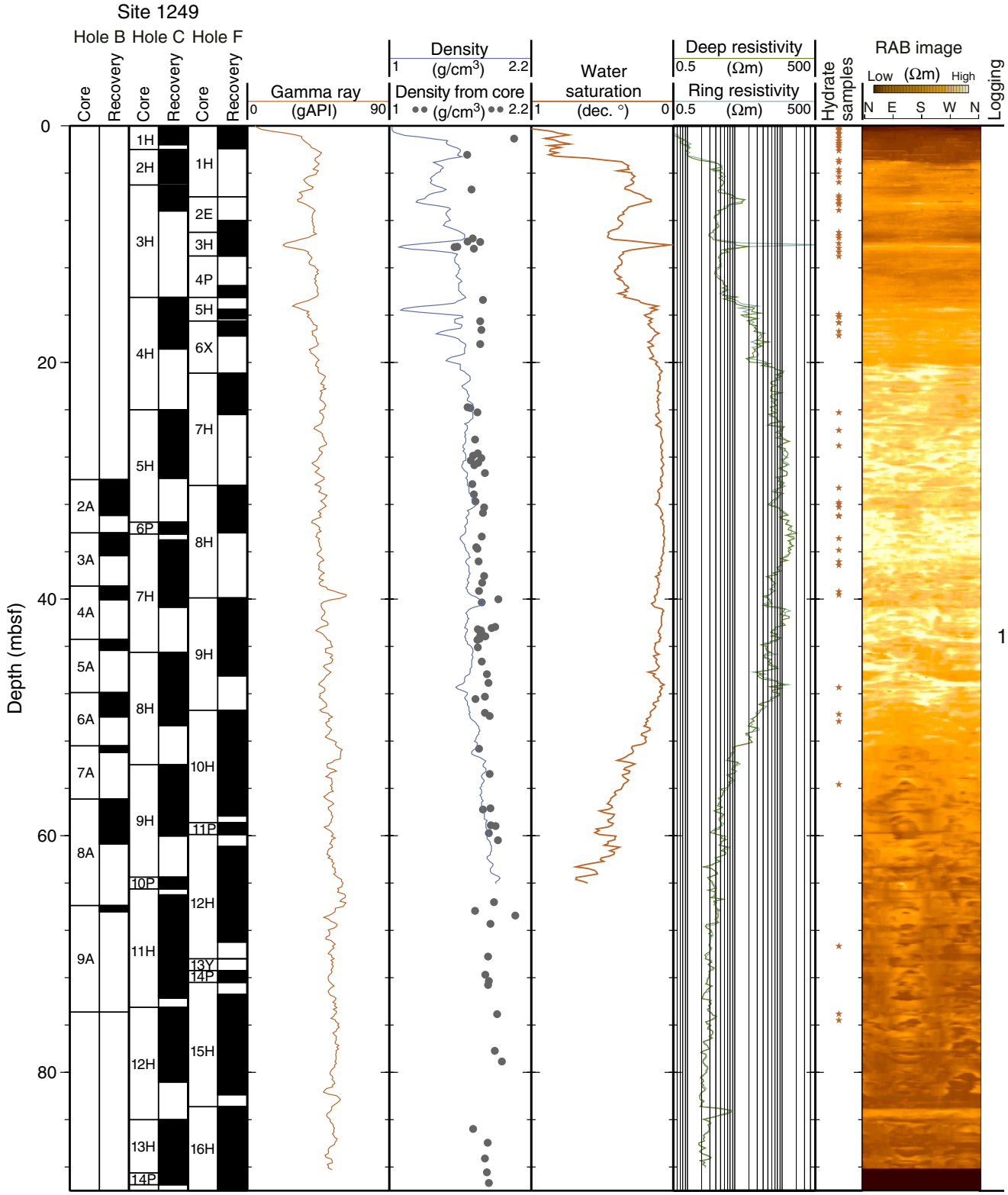

Figure F38. Resistivity-at-the-bit (RAB) image showing the possible presence of gas hydrate as bright resistive material occupying low-angle fractures, nearly flatlying stratigraphic horizons, and disseminated throughout the formation in Hole 1249A. 3-D = three-dimensional.

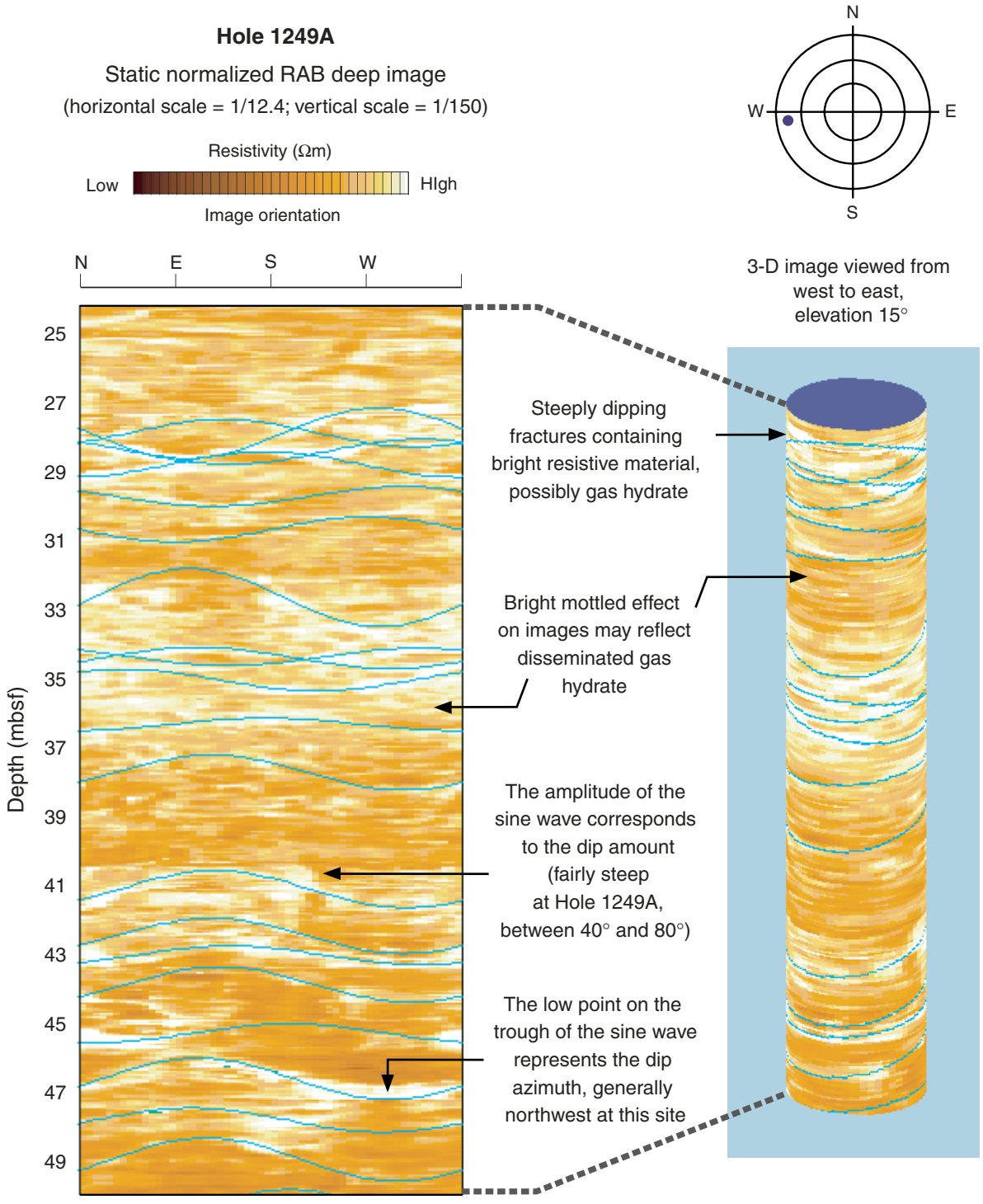

Table T1. Coring summary, Site 1249. (Continued on next four pages.)

Hole 1249A
Latitude: 44°34.2246′N
Longitude: 125°8.8423′W
Time on site (hr): 140.25 (0645 hr, 21 Jul–1650 hr, 21 Jul 2002)
Time on hole (hr): 9.75 (0645 hr, 21 Jul–1650 hr, 21 Jul 2002)
Seafloor (drill pipe measurement from rig floor, mbrf): 788.5
Distance between rig floor and sea level (m): 11
Water depth (drill pipe measurement from sea level, m): 777.5
Total depth (drill pipe measurement from rig floor, mbrf): 878.5
Total penetration (meters below seafloor, mbsf): 90
Total number of cores: 0
Total number of drilled intervals: 1
Total length of cored section (m): 0
Total core recovered (m): 0
Core recovery (%): 0

Hole 1249B
Latitude: 44°34.2106′N
Longitude: 125°8.8412′W
Time on hole (hr): 28.00 (0930 hr, 24 Jul–1330 hr, 25 Jul 2002)
Seafloor (drill pipe measurement from rig floor, mbrf): 788.5
Distance between rig floor and sea level (m): 11.1
Water depth (drill pipe measurement from sea level, m): 777.4
Total depth (drill pipe measurement from rig floor, mbrf): 863.4
Total penetration (meters below seafloor, mbsf): 74.9
Total number of cores: 8
Total number of drilled intervals: 0
Total length of cored section (m): 45
Total core recovered (m): 14.01
Core recovery (%): 31.1

Hole 1249C
Latitude: 44°34.2368′N
Longitude: 125°8.8410′W
Time on hole (hr): 22.25 (1330 hr, 25 Jul–1145 hr, 26 Jul 2002)
Seafloor (drill pipe measurement from rig floor, mbrf): 788.5
Distance between rig floor and sea level (m): 11.1
Water depth (drill pipe measurement from sea level, m): 777.4
Total depth (drill pipe measurement from rig floor, mbrf): 878.5
Total penetration (meters below seafloor, mbsf): 90
Total number of cores: 14
Total number of drilled intervals: 3
Total length of cored section (m): 88.5
Total core recovered (m): 58.84
Core recovery (%): 66.5

Hole 1249D
Latitude: 44°34.2222′N
Longitude: 125°8.8366′W
Time on hole (hr): 5.25 (2230 hr, 4 Aug–0345 hr, 5 Aug 2002)
Seafloor (drill pipe measurement from rig floor, mbrf): 788.5
Distance between rig floor and sea level (m): 11.3
Water depth (drill pipe measurement from sea level, m): 777.2
Total depth (drill pipe measurement from rig floor, mbrf): 807
Total penetration (meters below seafloor, mbsf): 18.5
Total number of cores: 3
Total number of drilled intervals: 1
Total length of cored section (m): 16.5
Total core recovered (m): 4.78
Core recovery (%): 29

Hole 1249E
Latitude: 44°34.2270′N
Longitude: 125°8.369′W
Time on hole (hr): 4.75 (0345 hr, 5 Aug–0830 hr, 5 Aug 2002)
Seafloor (drill pipe measurement from rig floor, mbrf): 788.5
Distance between rig floor and sea level (m): 11.3
Water depth (drill pipe measurement from sea level, m): 777.2
Total depth (drill pipe measurement from rig floor, mbrf): 799.5
Total penetration (meters below seafloor, mbsf): 11
Total number of cores: 3
Total number of drilled intervals: 1
Total length of cored section (m): 9
Total core recovered (m): 4.38
Core recovery (%): 48.7

Table T1 (continued).

Hole 1249F
Latitude: 44°34.2317′N
Longitude: 125°8.8377′W
Time on hole (hr): 22.75 (0830 hr, 5 Aug–0715 hr, 6 Aug 2002)
Seafloor (drill pipe measurement from rig floor, mbrf): 788.5
Distance between rig floor and sea level (m): 11.3
Water depth (drill pipe measurement from sea level, m): 777.2
Total depth (drill pipe measurement from rig floor, mbrf): 878.5
Total penetration (meters below seafloor, mbsf): 90
Total number of cores: 16
Total number of drilled intervals: 5
Total length of cored section (m): 82.5
Total core recovered (m): 57.37
Core recovery (%): 69.5

Hole 1249G
Latitude: 44°34.2073′N
Longitude: 125°8.8416′W
Time on hole (hr): 9.00 (2130 hr, 27 Aug–0630 hr, 28 Aug 2002)
Seafloor (drill pipe measurement from rig floor, mbrf): 788.5
Distance between rig floor and sea level (m): 11.6
Water depth (drill pipe measurement from sea level, m): 776.9
Total depth (drill pipe measurement from rig floor, mbrf): 831.5
Total penetration (meters below seafloor, mbsf): 43
Total number of cores: 5
Total number of drilled intervals: 0
Total length of cored section (m): 43
Total core recovered (m): 11.24
Core recovery (%): 26.1

Hole 1249H
Latitude: 44°34.2108′N
Longitude: 125°8.8365′W
Time on hole (hr): 8.50 (0630 hr, 28 Aug–1500 hr, 28 Aug 2002)
Seafloor (drill pipe measurement from rig floor, mbrf): 788.5
Distance between rig floor and sea level (m): 11.7
Water depth (drill pipe measurement from sea level, m): 776.8
Total depth (drill pipe measurement from rig floor, mbrf): 841
Total penetration (meters below seafloor, mbsf): 52.5
Total number of cores: 6
Total number of drilled intervals: 0
Total length of cored section (m): 52.5
Total core recovered (m): 27.52
Core recovery (%): 52.4

Hole 1249I
Latitude: 44°34.2111′N
Longitude: 125°8.8437′W
Time on hole (hr): 6.00 (1500 hr, 28 Aug–2100 hr, 28 Aug 2002)
Seafloor (drill pipe measurement from rig floor, mbrf): 788.5
Distance between rig floor and sea level (m): 11.7
Water depth (drill pipe measurement from sea level, m): 776.8
Total depth (drill pipe measurement from rig floor, mbrf): 822.1
Total penetration (meters below seafloor, mbsf): 33.6
Total number of cores: 4
Total number of drilled intervals: 0
Total length of cored section (m): 33.6
Total core recovered (m): 8.69
Core recovery (%): 25.9

Hole 1249J
Latitude: 44°34.2114′N
Longitude: 125°8.8422′W
Time on hole (hr): 5.50 (2100 hr, 28 Aug–0230 hr, 29 Aug 2002)
Seafloor (drill pipe measurement from rig floor, mbrf): 788.5
Distance between rig floor and sea level (m): 11.7
Water depth (drill pipe measurement from sea level, m): 776.8
Total depth (drill pipe measurement from rig floor, mbrf): 821
Total penetration (meters below seafloor, mbsf): 32.5
Total number of cores: 3
Total number of drilled intervals: 0
Total length of cored section (m): 32.5
Total core recovered (m): 7.69
Core recovery (%): 23.7

Table T1 (continued).

Hole 1249K
Latitude: 44°34.2137′N
Longitude: 125°8.8392′W
Time on hole (hr): 8.25 (0230 hr, 29 Aug–1045 hr, 29 Aug 2002)
Seafloor (drill pipe measurement from rig floor, mbrf): 788.5
Distance between rig floor and sea level (m): 11.7
Water depth (drill pipe measurement from sea level, m): 776.8
Total depth (drill pipe measurement from rig floor, mbrf): 832.7
Total penetration (meters below seafloor, mbsf): 44.2
Total number of cores: 5
Total number of drilled intervals: 1
Total length of cored section (m): 43.2
Total core recovered (m): 16.87
Core recovery (%): 39.1

Hole 1249L
Latitude: 44°34.2119′N
Longitude: 125°8.8439′W
Time on hole (hr): 10.25 (1045 hr, 29 Aug–2100 hr, 29 Aug 2002)
Seafloor (drill pipe measurement from rig floor, mbrf): 788.5
Distance between rig floor and sea level (m): 11.7
Water depth (drill pipe measurement from sea level, m): 776.8
Total depth (drill pipe measurement from rig floor, mbrf): 827
Total penetration (meters below seafloor, mbsf): 38.5
Total number of cores: 5
Total number of drilled intervals: 0
Total length of cored section (m): 38.5
Total core recovered (m): 14.15
Core recovery (%): 36.8

Core	Date (2002)	Local time (hr)	Depth (mbsf) Top	Depth (mbsf) Bottom	Length (m) Cored	Length (m) Recovered	Recovery (%)
204-1249A-							
			*****Drilled from 0 to 90 mbsf*****				
204-1249B-							
1W	24 Jul	2305	0.0	29.9	29.9	0.00	0.0
2A	25 Jul	0140	29.9	34.4	4.5	3.05	67.8
3A	25 Jul	0315	34.4	38.9	4.5	1.92	42.7
4A	25 Jul	0355	38.9	43.4	4.5	1.15	25.6
5A	25 Jul	0440	43.4	47.9	4.5	0.93	20.7
6A	25 Jul	0525	47.9	52.4	4.5	2.06	45.8
7A	25 Jul	0615	52.4	56.9	4.5	0.57	12.7
8A	25 Jul	0730	56.9	65.9	9.0	3.81	42.3
9A	25 Jul	0845	65.9	74.9	9.0	0.52	5.8
				Cored totals:	74.9	14.01	18.7
				Drilled total:	0.0		
				Total:	74.9		
204-1249C-							
1H	25 Jul	1750	0.0	2.0	2.0	1.60	80.0
2H	25 Jul	1825	2.0	5.0	3.0	2.85	95.0
3H	25 Jul	2045	5.0	14.5	9.5	2.20	23.2
4H	25 Jul	2200	14.5	24.0	9.5	4.37	46.0
5H	25 Jul	2315	24.0	33.5	9.5	5.79	60.9
6P	26 Jul	0130	33.5	34.5	1.0	1.00	100.0
			*****Drilled from 34.5 to 35 mbsf*****				
7H	26 Jul	0150	35.0	44.5	9.5	5.69	59.9
8H	26 Jul	0240	44.5	54.0	9.5	6.21	65.4
9H	26 Jul	0340	54.0	63.5	9.5	6.02	63.4
10P	26 Jul	0445	63.5	64.5	1.0	1.00	100.0
			*****Drilled from 64.5 to 65 mbsf*****				
11H	26 Jul	0510	65.0	74.5	9.5	8.74	92.0
12H	26 Jul	0610	74.5	84.0	9.5	6.34	66.7
13H	26 Jul	0710	84.0	88.5	4.5	6.16	136.9
14P	26 Jul	0815	88.5	89.5	1.0	1.00	100.0
			*****Drilled from 89.5 to 90 mbsf*****				
				Cored totals:	88.5	58.97	66.6
				Drilled total:	1.5		
				Total:	90.0		

Table T1 (continued).

Core	Date (2002)	Local time (hr)	Depth (mbsf) Top	Depth (mbsf) Bottom	Length (m) Cored	Length (m) Recovered	Recovery (%)
204-1249D-							
1H	5 Aug	0045	0.0	6.0	6.0	2.16	36.0
			*****Drilled from 6 to 8 mbsf*****				
2Y	5 Aug	0305	8.0	9.0	1.0	0.80	80.0
3H	5 Aug	0350	9.0	18.5	9.5	1.82	19.2
			Cored totals:		16.5	4.78	29.0
			Drilled total:		2.0		
			Total:		18.5		
204-1249E-							
1H	5 Aug	0500	0.0	6.0	6.0	1.19	19.8
			*****Drilled from 6 to 8 mbsf*****				
2H	5 Aug	0730	8.0	9.0	1.0	0.00	0.0
3H	5 Aug	0820	9.0	11.0	2.0	2.19	109.5
			Cored totals:		9.0	3.38	37.6
			Drilled total:		2.0		
			Total:		11.0		
204-1249F-							
1H	5 Aug	0915	0.0	6.0	6.0	1.94	32.3
			*****Drilled from 6 to 8 mbsf*****				
2E	5 Aug	1130	8.0	9.0	1.0	0.80	80.0
3H	5 Aug	1235	9.0	11.0	2.0	2.05	102.5
			*****Drilled from 11 to 13.5 mbsf*****				
4P	5 Aug	1410	13.5	14.5	1.0	1.00	100.0
			*****Drilled from 14.5 to 15.5 mbsf*****				
5H	5 Aug	1455	15.5	16.5	1.0	0.80	80.0
6X	5 Aug	1655	16.5	20.9	4.4	1.28	29.1
7H	5 Aug	1735	20.9	30.4	9.5	3.50	36.8
8H	5 Aug	1915	30.4	39.9	9.5	4.01	42.2
9H	5 Aug	2000	39.9	49.4	9.5	6.59	69.4
10H	5 Aug	2235	49.4	58.9	9.5	8.93	94.0
11P	5 Aug	2350	58.9	59.9	1.0	1.00	100.0
			*****Drilled from 59.9 to 60.9 mbsf*****				
12H	6 Aug	0045	60.9	70.4	9.5	8.09	85.2
13Y	6 Aug	0230	70.4	71.4	1.0	0.91	91.0
14P	6 Aug	0340	71.4	72.4	1.0	1.00	100.0
			*****Drilled from 72.4 to 73.4 mbsf*****				
15H	6 Aug	0420	73.4	82.9	9.5	8.50	89.5
16H	6 Aug	0530	82.9	90.0	7.1	6.97	98.2
			Cored totals:		82.5	57.37	69.5
			Drilled total:		7.5		
			Total:		90.0		
204-1249G-							
1X	28 Aug	0045	0.0	13.5	13.5	3.36	24.9
2E	28 Aug	0230	13.5	14.5	1.0	0.75	75.0
3H	28 Aug	0345	14.5	24.0	9.5	4.44	46.7
4H	28 Aug	0440	24.0	33.5	9.5	2.69	28.3
5H	28 Aug	0535	33.5	43.0	9.5	0.00	0.0
			Cored totals:		43.0	11.24	26.1
			Drilled total:		0.0		
			Total:		43.0		
204-1249H-							
1X	28 Aug	0830	0.0	13.5	13.5	1.70	12.6
2Y	28 Aug	1000	13.5	14.5	1.0	0.75	75.0
3H	28 Aug	1035	14.5	24.0	9.5	4.60	48.4
4H	28 Aug	1145	24.0	33.5	9.5	4.97	52.3
5H	28 Aug	1240	33.5	43.0	9.5	5.70	60.0
6H	28 Aug	1355	43.0	52.5	9.5	9.80	103.2
			Cored totals:		52.5	27.52	52.4
			Drilled total:		0.0		
			Total:		52.5		
204-1249I-							
1X	28 Aug	1725	0.0	13.5	13.5	0.40	3.0
2H	28 Aug	1805	13.5	14.6	1.1	1.31	119.1
3H	28 Aug	1920	14.6	24.1	9.5	1.10	11.6
4H	28 Aug	2025	24.1	33.6	9.5	5.88	61.9
			Cored totals:		33.6	8.69	25.9
			Drilled total:		0.0		
			Total:		33.6		

Table T1 (continued).

Core	Date (2002)	Local time (hr)	Depth (mbsf) Top	Depth (mbsf) Bottom	Length (m) Cored	Length (m) Recovered	Recovery (%)
204-1249J-							
1X	29 Aug	0010	0.0	13.5	13.5	0.00	0.0
2H	29 Aug	0100	13.5	23.0	9.5	2.99	31.5
3H	29 Aug	0150	23.0	32.5	9.5	4.70	49.5
			Cored totals:		32.5	7.69	23.7
			Drilled total:		0.0		
				Total:	32.5		
204-1249K-							
1X	29 Aug	0535	0.0	13.5	13.5	0.82	6.1
2H	29 Aug	0625	13.5	14.7	1.2	1.20	100.0
			*****Drilled from 14.7 to 15.7 mbsf*****				
3H	29 Aug	0810	15.7	25.2	9.5	5.65	59.5
4H	29 Aug	0910	25.2	34.7	9.5	3.95	41.6
5H	29 Aug	1000	34.7	44.2	9.5	5.25	55.3
			Cored totals:		43.2	16.87	39.1
			Drilled total:		1.0		
				Total:	44.2		
204-1249L-							
1X	29 Aug	1315	0.0	11.9	11.9	2.00	16.8
2X	29 Aug	1430	11.9	18.5	6.6	4.65	70.5
3H	29 Aug	1530	18.5	28.0	9.5	3.75	39.5
4H	29 Aug	1715	28.0	37.5	9.5	3.40	35.8
5E	29 Aug	1925	37.5	38.5	1.0	0.35	35.0
			Cored totals:		38.5	14.15	36.8
			Drilled total:		0.0		
				Total:	38.5		

Table T2. Depth of penetration, cored interval, and core recovery, Holes 1249B, 1249C, 1249D, 1249E, and 1249F.

Hole	Penetration (m)	Cored (m)	Recovered (m)	Total recovery (%)	Unit I–II recovery (%)	Unit III recovery (%)
204-						
1249B	74.9	45.0	14.0	31.1	36.8	24.1
1249C	90.0	88.5	59.0	66.6	66.0	99.1
1249D	18.5	16.5	4.8	29.0	45.1	—
1249E	11.0	9.0	3.4	37.6	43.1	—
1249F	90.0	82.5	57.4	69.5	66.6	94.0

Note: Holes 1249G, 1249H, 1249J, 1249K, and 1249L were not included in this table because these cores went directly to pressure vessels and were not described.

Table T3. Bioevents, Hole 1249C.

Age (Ma)	Bioevent	Top		Bottom		Average depth (mbsf)	Event number*	Comment
		Core, section, interval (cm)	Depth (mbsf)	Core, section, interval (cm)	Depth (mbsf)			
		204-1249C-		204-1249C-				
0.30	LO *Proboscia curvirostris*	3H-CC	7.18	4H-CC	18.82	13.00	1	Diatom
0.27	FO *Emiliania huxleyi*	4H-CC	18.82	5H-CC	29.74	24.28	2	Nannofossil
0.46	LO *Pseudoemiliania lacunosa*	5H-CC	29.74	7H-CC	40.64	35.19	3	Nannofossil
1.59	FO *Calcydiscus macintyrei*	8H-CC	50.66	9H-CC	59.97	55.32	4	Nannofossil

Notes: FO = first occurrence, LO = last occurrence. * = number in Figure F6, p. 41.

Table T4. Interstitial water data, Holes 1249B, 1249C, 1249D, 1249E, and 1249F.

Core, section, interval (cm)	Depth (mbsf)	pH	Alkalinity (mM)	Salinity (g/kg)	Cl (mM)	SO_4 (mM)	NH_4 (mM)	PO_4 (µM)	Na (mM)	K (mM)	Mg (mM)	Ca (mM)	B (µM)	Ba (µM)	Fe (µM)	Li (µM)	Mn (µM)	Sr (µM)	DOC (mM)
204-1249B-																			
2A-1, 45–60	30.35	7.63	57.69	39	612	0.0	12.9	266	511	12.8	—	—	—	—	—	—	—	—	—
2A-2, 112–126	31.82	7.75	55.25	36	573	0.9	12.0	305	543	13.7	—	—	741	84.0	22.5	21	0.89	79	—
3A-1, 31–46	34.71	7.52	58.68	35	557	0.0	12.2	320	497	12.5	—	—	—	—	—	—	—	—	—
4A-1, 53–74	39.43	7.41	60.59	34	525	0.2	12.4	306	469	11.8	—	—	—	—	—	—	—	—	—
5A-1, 78–93	44.18	7.45	64.45	36	554	0.6	13.6	326	502	13.1	—	—	—	—	—	—	—	—	—
6A-2, 95–106	49.85	7.71	69.66	36	555	0.0	13.9	307	505	13.6	—	—	884	115.0	9.3	27	0.92	84	—
7A-1, 42–57	52.82	7.43	68.72	36	554	0.2	14.0	322	501	12.9	—	—	929	113.4	29.3	25	1.88	88	—
204-1249C-																			
1H-1, 110–118	1.10	7.44	48.31	49	778	1.7	7.5	288	654	15.3	68.1	3.7	841	90.0	6.1	20	1.10	103	—
1H-1, 118–125	1.18	7.84	27.13	49	762	0.0	7.2	283	624	14.5	66.1	3.9	761	90.1	2.4	17	0.95	101	—
2H-2, 0–15	3.40	7.66	41.95	42	690	0.0	6.2	259	592	14.6	57.2	3.2	685	76.3	1.0	16	0.87	86	—
2H-2, 15–30	3.55	7.68	44.74	45	733	0.0	6.6	259	636	15.7	61.0	3.4	704	84.1	0.9	17	0.81	95	—
3H-1, 74–89	5.74	7.70	44.76	51	829	0.0	9.9	296	693	16.6	79.8	2.6	659	120.4	11.7	19	1.23	110	—
3H-2, 41–51	6.96	7.52	58.20	62	1008	0.0	12.6	327	809	18.8	95.4	3.4	730	156.2	4.8	22	1.32	139	—
4H-2, 44–62	15.77	8.00	42.20	34	569	0.0	8.7	92	501	13.5	44.4	2.1	631	60.7	3.5	15	0.57	59	—
4H-5, 86–101	17.61	7.95	54.11	39	618	0.0	11.3	156	547	14.6	52.5	2.7	633	85.2	4.1	17	0.68	85	—
5H-2, 20–25	25.70	7.88	56.33	37	588	0.0	13.1	170	526	14.6	48.7	2.5	—	—	—	—	—	—	—
5H-4, 44–49	27.70	7.75	58.31	36	585	0.0	12.6	195	515	13.4	—	—	731	84.8	6.3	19	0.83	81	—
7H-1, 71–86	35.71	7.67	62.54	35	548	0.0	14.2	326	495	12.6	46.0	2.5	773	96.3	11.1	20	0.69	80	—
7H-5, 76–91	38.89	7.70	59.43	35	545	0.0	11.7	338	489	12.7	45.7	2.6	759	95.5	21.3	19	0.71	79	—
8H-3, 18–33	47.64	7.62	70.06	36	564	0.0	13.6	314	511	13.5	41.3	2.6	764	99.7	6.7	20	0.74	75	—
8H-4, 124–139	50.18	7.63	63.19	33	504	0.0	13.3	230	458	12.3	47.2	2.7	882	116.7	6.6	22	0.79	89	—
9H-2, 133–148	56.83	7.40	71.39	37	566	0.0	14.9	263	513	13.7	46.8	2.9	918	125.9	7.9	25	1.52	89	—
9H-3, 120–135	58.18	7.62	71.25	36	558	0.0	14.6	273	506	13.3	45.9	3.2	885	125.9	18.5	24	1.65	90	—
11H-4, 104–119	69.17	7.71	74.61	36	560	0.2	16.5	249	507	14.0	44.6	3.3	883	146.0	9.6	28	1.00	96	—
11H-6, 95–115	71.81	7.77	67.62	33	509	0.3	14.5	194	404	12.5	40.1	2.8	724	128.0	5.9	25	0.91	84	—
12H-1, 120–140	75.70	7.63	73.79	36	561	14.4	16.0	264	509	13.9	45.3	3.0	799	166.6	5.3	35	0.82	95	—
13H-2, 79–99	86.29	7.54	74.12	36	559	0.0	15.3	300	510	13.6	45.1	3.2	825	153.8	10.8	29	0.94	97	—
204-1249D-																			
1H-2, 25–40	1.52	7.85	33.38	32	474	2.7	4.4	228	468	10.2	—	—	635	34.5	1.9	10	1.74	50	—
3H-1, 79–94	9.79	7.57	49.91	45	747	0.6	—	—	650	15.3	—	—	605	107.0	20.7	17	4.22	109	—
204-1249E-																			
3H-1, 25–45	9.25	—	—	—	737	—	11.4	280	—	—	—	—	693	93.6	13.2	19	1.64	92	—
204-1249F-																			
4P-1, 0–80	13.50	—	—	—	—	—	—	—	—	—	—	—	—	—	—	—	—	—	—
7H-2, 106–116	23.41	7.64	59.77	39	595	0.2	12.4	365	552	12.7	—	—	—	—	—	—	—	—	13.37
8H-2, 102–112	32.84		—	—	354	0.5	10.0	269	334	8.0	—	—	—	—	—	—	—	—	—
9H-3, 140–150	43.61	7.40	62.81	36	540	0.2	12.9	372	504	12.1	—	—	862	100.0	16.4	21	2.15	86	15.45
10H-2, 140–150	52.09	7.38	70.32	36	562	1.3	13.8	385	533	12.5	—	—	887	114.8	20.4	23	1.26	94	13.99
11P-1, 20–30	59.10	—	—	—	572	—	—	—	—	—	—	—	—	—	—	—	—	—	—
12H-2, 131–146	63.20	7.48	73.44	41	563	0.9	15.2	276	537	14.0	—	—	876	140.5	18.9	27	4.94	100	13.53
15H-5, 135–150	79.57	7.32	75.03	36	568	0.6	15.5	332	556	14.2	—	—	904	176.0	13.8	34	4.93	108	13.72
16H-4, 135–150	88.50	7.33	75.29	36	565	0.8	16.4	348	548	14.9	—	—	845	182.8	3.6	40	1.40	98	17.93

Notes: DOC = dissolved organic carbon. — = no sample was available.

Table T5. Chloride concentration and MAD of samples collected with "dry-looking" and "wet-looking" texture, Hole 1249F.

Core, section, interval (cm)	Sediment appearance*	Depth (mbsf)	Chloride (mM)	Wet weight (%)	Density (g/cm^3)			Porosity (%)
					Bulk	Dry	Grain	
204-1249F-								
3H-1, 45–47	Wet	9.45	895	41.2	1.588	0.934	2.586	63.9
3H-1, 45–47	Dry	9.45	1242	—	—	—	—	—
3H-1, 76–78	Wet	9.76	1039	43.8	1.552	0.872	2.591	66.3
3H-1, 76–78	Dry	9.76	1368	37.8	1.643	1.021	2.598	60.7
3H-2, 18–20	Wet	10.18	—	48.9	1.481	0.757	2.586	70.7
3H-2, 20–21	Wet	10.20	—	51.2	1.461	0.713	2.644	73
3H-2, 33–35	Dry	10.33	957	40.1	1.596	0.956	2.551	62.5
3H-2, 33–35	Dry	10.33	1195	—	—	—	—	—
7H-1, 22–25	Dry	21.12	566	43.3	1.553	0.881	2.561	65.6
7H-1, 28–30	Wet	21.18	545	44.6	1.573	0.872	2.763	68.5
7H-1, 48–50	Dry	21.38	601	—	—	—	—	—
7H-1, 67–69	Wet	21.57	582	—	—	—	—	—

Note: * = associated with gas hydrate dissociation. — = no sample available.

Table T6. Concentrations of methane, ethane, ethylene, and propane in headspace gas, Holes 1249B, 1249C, and 1249F.

Core, section, interval (cm)	Depth (mbsf)	C_1 (ppmv)	C_2 (ppmv)	$C_{2=}$ (ppmv)	C_3 (ppmv)	C_1/C_2
204-1249B-						
2A-1, 75–80	30.5	5,813	14.6		4.4	398
2A-2, 0–5	30.7	564,829	1,426		36.6	396
3A-2, 0–5	35.0	15,318	39.5		13.9	388
4A-1, 53–58	39.4	9,188	26.7		18.7	344
5A-1, 73–78	44.1	12,414	15.5		11.3	801
6A-2, 78–83	49.7	13,206	7.0	0.4	7.7	1,887
7A-1, 37–42	52.8	5,529	2.4			2,266
8A-2, 61–66	59.0	1,419	0.5			2,782
9A-1, 45–50	66.4	6,140	1.2	0.6		5,339
204-1249C-						
1H-1, 55–60	0.6	4,613	12.1			381
1H-1, 125–130	1.3	31,602	40.7			776
2H-1, 0–5	2.0	6,756	20.8			325
2H-2, 0–5	3.4	2,507	9.6			261
3H-1, 0–5	5.0	220,058	307			716
3H-2, 10–15	6.7	268,569	388			693
4H-1, 0–5	14.5	542,810	1,271		9.4	427
5H-5, 0–5	27.8	16,421	49.3		33.0	333
7H-4, 0–5	37.3	13,541	49.7		25.6	272
8H-3, 33–38	47.8	12,033	15.8		18.6	762
9H-3, 0–5	57.0	17,717	6.7		8.2	2,644
11H-4, 99–104	69.1	10,924	2.8			3,972
12H-2, 0–5	75.9	7,108	1.6			4,415
13H-2, 74–75	86.2	10,732	2.8	0.6	6.2	3,860
204-1249F-						
5H-1, 0–5	15.5	3,369	10.2			331
6X-1, 0–5	16.5	189,786	360		4.5	527
7H-2, 0–5	22.4	13,767	47.5		20.1	290
8H-2, 42–47	32.2	2,291	10.5		5.1	218
8H-2, 107–112	32.9	6,537	18.5		4.3	353
9H-3, 0–5	42.2	8,756	18.3		8.3	478
10H-3, 0–5	52.2	14,729	22.2		31.5	663
12H-3, 0–5	63.4	8,002	5.2		6.2	1,551
15H-3, 0–5	75.2	30,303	12.6		5.9	2,407
16H-3, 0–5	85.7	15,702	4.4	0.7	10.8	3,610

Note: C_1 = methane, C_2 = ethane, $C_{2=}$ = ethylene, C_3 = propane.

Table T7. Concentration of light hydrocarbon and nonhydrocarbon gases in VAC samples of core gas voids, Holes 1249B, 1249C, and 1249F.

Core, section, interval (cm)	Depth (mbsf)	C_1 (ppmv)	C_2 (ppmv)	C_3 (ppmv)	*i*-C_4 (ppmv)	*n*-C_4 (ppmv)	*i*-C_5 (ppmv)	CO_2 (ppmv)	O_2 (ppmv)	N_2 (ppmv)	C_1/C_2
204-1249B-											
2A-1, 70–71	30.60	840,995	1,573	75.0	18.0	11.9	7.0	17,201	7,921	109,309	535
4A-1, 74–75	39.64	943,658	2,047	79.0	13.0	7.8		15,226	8,566	27,109	461
204-1249C-											
1H-1, 60–61	0.60	933,178	1,243	8.4							751
2H-1, 130–132	3.30	972,741	1,346	4.9				7,909	2,427	2,457	723
4H-5, 75–78	17.50	861,340	1,705	29.7							505
5H-3, 0–5	26.15	937,191	1,627	96.4	14.9			14,703	8,278	24,805	576
7H-6, 38–39	39.42	971,662	1,442	70.9	11.0	6.8		12,926	505	789	674
8H-2, 24–25	46.24	935,093	622	110	17.0	9.9	4.4	44,654	1,921	3,443	1,503
9H-3, 135–136	58.33	985,687	241	17.8	3.3			6,131	79	689	4,093
11H-5, 137–138	70.79	968,087	128	18.9	3.8			11,710	1,474	2,814	7,536
12H-1, 110–111	75.60	693,595	47.5	27.2							14,602
204-1249F-											
7H-3, 0–5	23.51	595,157	1,011	45.7	27.8	6.7		10,423	76,317	296,219	589
7H-3, 0–5	23.51	580,528	1,083	41.0							536
8H-2, 120–121	33.02	948,468	1,787	37.1	40.6	5.8		10,107	370	9,784	531
9H-3, 44–45	42.65	690,384	1,021		55.1	14.8		20,485	51,278	201,073	676
10H-2, 145–146	52.14	953,060	615	65.8		7.6		10,997	379	12,691	1,551
10H-6, 81–82	56.67	957,619	308		46.3	9.2		13,336	210	7,062	3,111
12H-2, 26–27	62.15	957,909	326	16.5	20.1	4.1		10,404	290	12,223	2,937
12H-5, 40–41	66.75	966,275	349	23.5				5,391	205	7,458	2,770
15H-3, 22–23	75.44	952,678	178	40.6		4.6		15,401	194	8,453	5,340
15H-4, 64–65	77.36	962,180	151			5.2		9,776	190	8,650	6,372
16H-3, 22–23	85.87	959,822	147	32.7		3.5		8,740	164	9,307	6,549

Note: C_1 = methane, C_2 = ethane, C_3 = propane, *i*-C_4 = isobutane, *n*-C_4 = normal butane, *i*-C_5 = isopentane, CO_2 = carbon dioxide, O_2 = oxygen, N_2 = nitrogen.

Table T8. Composition of gas from analyses of decomposed samples of gas hydrate, Holes 1249B, 1249C, 1249D, 1249E, and 1249F.

Core, section, interval (cm)	Depth (mbsf)	C_1 (ppmv)	C_2 (ppmv)	C_3 (ppmv)	*i*-C_4 (ppmv)	*n*-C_4 (ppmv)	*i*-C_5 (ppmv)	CO_2 (ppmv)	O_2 (ppmv)	N_2 (ppmv)	C_1/C_2
204-1249B-											
4A-1, 74–82	39.64	376,691	1,328	11.0				7,376	125,755	530,050	284
204-1249C-											
1H-1, 105–120	1.05	792,216	705	25.9	6.3	4.9		2,346	52,500	202,795	1,124
1H-1, 195–200	1.95	963,698	1,170	15.2				4,001	4,557	13,006	824
2H-1, 0–5	2.00	957,415	1,944	10.0				3,585	5,682	16,729	492
3H-1, 106–131	6.06	983,641	1,657	15.0				3,962	283	764	594
4H-2, 62–72	15.95	169,544	301					1,525	151,364	628,845	563
4H-3, 57–59	16.62	939,133	3,457	28.0							272
4H-4, 70–81	17.34	616,696	1,430	14.0	3.2			4,961	76,142	296,540	431
204-1249D-											
1H-CC	2.11	507,255	792	25.4				2,348	61,151	234,535	640
3H-1, 150–160	10.50	813,647	1,163					28,658	2,941	100,062	699
204-1249E-											
1H-1, 0–10	0.00	502,708	673		14.5	5.4		1,277	371,203	95,665	746
3H-2, 70–80	10.70	898,742	905	30.6				6,904	4,126	59,792	993
204-1249F-											
1H-1, 0–20*	0.00	924,696	1,029					2,046	1,561	45,097	898
5H-1, 64–70	16.14	510,840	849		6.8			3,600	23,439	102,073	602
6H-1, 100–110	17.50	969,616	2,754	17.1				5,144	19	1,112	352
6H-1, 100–110*	17.50	969,542	3,599	32.7							269
8H-2, 117–127	32.99	972,969	2,259	15.5	13.5			5,214	71	2,382	431

Notes: * = pure gas hydrate sample (minimal contamination from sediment). C_1 = methane, C_2 = ethane, C_3 = propane, *i*-C_4 = isobutane, *n*-C_4 = normal butane, *i*-C_5 = iso-pentane, H_2S = hydrogen sulfide, CO_2 = carbon dioxide, O_2 = oxygen, N_2 = nitrogen.

Table T9. Composition of gas samples from PCS experiments, Holes 1249C and 1249F. (See table note. Continued on next page.)

Sample	Volume (mL)	C_1 (ppm)	C_2 (ppm)	C_3 (ppm)	*i*-C_4 (ppm)	*n*-C_4 (ppm)	*i*-C_5 (ppm)	*n*-C_5 (ppm)	O_2 (ppm)	N_2 (ppm)	CO_2 (ppm)	C_1/C_2
204-1249C-6P (33.5 mbsf)												
G1	50	12							163,955	753,440	252	624
G2	250	533,029	772.7	27.1	3.3				78,293	370,026	698	
G3	640	904,610	1,401.4	58.5	7.1	5.3			14,366	67,557	667	
G4	610	947,587	1,462.3	72.1	8.0	6.1			5,165	30,777	663	
G5	610	936,083	1,431.5	73.4	8.1	6.1			8,056	41,279	780	
G6	650	717,037	1,219.3	67.0	7.8	6.2			2,873	12,883	922	
G7	570	863,454	1,402.8	70.1	8.1	6.4			4,491	20,500	1,083	
G8	700	895,132	1,438.1	71.5	8.6	6.6			3,688	17,765	1,204	
G9	730	864,439	1,357.4	74.1	8.8	7.2			2,796	15,634	1,464	
G10	700	845,353	1,566.0	75.2	9.6	7.3			4,504	25,059	1,790	
G11	750	838,399	1,300.6	74.7	9.6	7.4			3,165	18,315	2,380	
G12	750	850,214	1,290.6	74.6	13.3	7.1			2,388	14,521	2,587	
G13	740	840,256	1,287.6	76.1	10.0	7.7			3,407	17,689	2,924	
G14	770	816,762	1,254.6	192.3	12.2	7.1			6,647	36,618	3,141	
G15	790	814,593	1,322.3	77.6	10.1	7.6			7,840	44,175	3,555	
G16	810	854,357	1,335.8	78.3	10.6	8.1			11,737	69,775	3,527	
G17	890	828,584	1,303.3	79.1	11.1	8.7	3.9		17,898	110,532	4,000	
G18	850	877,045	1,392.7	93.1	13.6	10.9	4.7		12,860	79,242	5,767	
G19	510	852,658	1,391.2	95.8	14.4	12.4	5.5		16,523	102,101	7,307	
G20	80	864,653	1,440.2	102.3	16.1	13.6	6.2		14,530	90,359	8,658	
G21	70	808,647	1,356.0	86.4	13.0	11.8	6.1		26,795	153,275	5,843	
G22	130	770,930	1,338.0	83.5	12.3	11.6	5.6		33,365	190,455	4,086	
204-1249F-4P (13.5 mbsf)												
G1	120	674,103	1,015.6	22.5	5.6				55,782	264,287	413	867
G2	500	967,087	942.9	67.0	15.9	8.5	10.1		679	1,334	495	
G3	90	969,724	964.4	66.1	15.3	8.0	9.4		583	1,031	408	
G4	350	969,483	963.8	58.4	13.1	6.5	7.0			774	446	
G5	510	960,618	919.0	58.3	13.1	6.4			3,210	6,891	444	
G6	440	966,405	1,016.5	58.4	13.5	6.5			1,890	1,605	424	
G7	780	973,997	885.8	62.5	15.4	7.5	8.3			693	369	
G8	770	973,551	739.3	68.5	18.0	8.6	10.0		164	1,024	335	
G9	780	975,031	699.5	70.1	19.2	8.8	11.0			783	408	
G10	800	970,961	775.8	51.4	16.5	7.5	9.0		1,292	1,411	383	
G11	920	973,806	990.0	48.2	15.5	7.4	10.2		24	766	646	
G12	780	966,434	1,192.2	42.7	12.3	5.9	8.2		1,845	1,458	510	
G13	650	969,085	1,286.6	42.2	12.1	6.0	8.0		479	861	464	
G14	1,050	960,736	1,222.0	35.5	10.7		6.8		5,437	12,244	556	
G15	1,015	971,873	1,305.7	38.0	11.1		7.8		2,461	3,519	526	
G16	900	961,404	1,179.2	38.1	10.8		7.2		5,987	14,818	610	
G17	1,000	976,189	1,158.9	35.3	10.0				1,691	1,068	688	
G18	1,050	975,959	1,246.0	36.4	9.1				2,143	1,028	696	
G20	960	970,948	1,378.0	29.6	6.8		14.2		157	955	753	
G22	890	984,445	1,428.6	32.0	6.3				360	633	873	
G23	1,060	980,651	1,428.4	28.8	5.2					586	1,132	
G24	980	974,535	1,445.4	25.9					62	467	1,130	
G25	950	969,079	1,309.7	24.0					3,451	4,007	1,055	
G26	1,080	974,456	1,272.2	24.5					2,003	1,420	1,080	
G27	1,140	975,439	1,245.0	24.7					2,012	1,464	1,190	
G28	1,000	982,595	1,317.5	27.3						452	1,314	
G30	1,100	968,524	1,398.3	28.9					5,921	11,056	1,323	
G31	1,020	982,113	1,467.8	28.6					274	4,821	1,396	
G32	1,000	983,456	1,528.9	30.8					281	5,870	1,535	
G33	980	981,268	1,525.5	29.0					240	5,036	1,536	
G34	1,040	980,264	1,525.0	29.5					199	4,899	1,494	
G35	990	979,426	1,478.1	30.0					122	3,524	1,374	
G36	1,120	980,618	1,530.4	31.2					75	3,357	1,435	
G37	1,020	982,383	1,539.9	30.4					67	3,003	1,483	
G38	940	964,085	1,520.1	25.5					637	18,583	1,391	
G39	890	970,799	1,520.4	25.6					362	10,968	1,364	
G40	1,140	968,481	1,415.5	31.9					300	8,467	1,299	
G41	950	969,626	1,413.8	28.9					244	7,825	1,398	
G42	1,040	979,611	1,474.1	30.9					147	3,980	1,416	
G43	1,020	981,932	1,485.2	28.1					129	3,764	1,419	
G44	1,070	976,353	1,482.2	30.4					101	3,589	1,478	
G45	1,080	952,942	1,426.0	28.2					9,207	13,375	1,558	
G46	1,015	980,993	1,477.5	29.6					30	491	1,432	
G47	1,050	967,732	1,432.1	29.5					5,650	5,518	1,421	

Table T9 (continued).

Sample	Volume (mL)	C_1 (ppm)	C_2 (ppm)	C_3 (ppm)	*i*-C_4 (ppm)	*n*-C_4 (ppm)	*i*-C_5 (ppm)	*n*-C_5 (ppm)	O_2 (ppm)	N_2 (ppm)	CO_2 (ppm)	C_1/C_2
G48	1,015	969,009	1,421.0	29.4					4,688	3,363	1,272	
G49	960	977,859	1,441.0	30.6					561	935	1,179	
G50	1,040	974,570	1,430.4	32.2					549	792	1,005	
G51	1,000	973,383	1,425.9	30.9					2,030	1,124	894	
G52	980	976,559	1,438.8	26.5					95	716	994	
G53	1,050	966,475	1,413.5	30.5					375	842	1,282	
G54	1,050	972,114	1,414.8	29.7					1,035	1,042	1,126	
G55	1,025	967,374	1,412.8	27.1					2,653	1,312	1,306	
G56	1,100	976,366	1,432.4	31.3					15	778	1,422	
G57	960	967,446	1,422.2	30.7					1,541	1,138	960	
G58	1,020	946,926	1,413.2	28.9					9,619	14,130	1,213	
G59	950	973,525	1,452.1	29.1					920	1,155	984	
G60	1,110	977,622	1,432.6	29.2						690	1,174	
G61	980	964,626	1,383.9	29.4					5,022	4,707	1,046	
G62	810	966,424	1,443.6	29.0					895	916	1,345	
G63	1,040	961,636	1,454.3	26.6					1,009	1,330	1,018	
G64	950	891,965	1,272.9	23.6					1,149	1,259	943	
G65	1,150	854,803	1,264.0	21.6					746	1,156	1,555	
G66	820	946,112	1,491.4	24.1					1,216	1,262	1,277	
G67	820	951,352	1,465.3	24.1					839	1,146	1,128	
G68	1,110	971,530	1,340.5	25.1					139	821	1,340	
G69	1,020	971,823	1,480.7	28.5						467	1,896	
G70	1,080	960,228	1,457.3	26.1					4,125	2,108	1,741	
G71	1,080	960,016	1,452.9	27.3					4,784	3,426	1,603	
G72	1,050	968,828	1,469.6	28.2					1,247	1,209	1,513	
G73	1,000	965,355	1,459.7	29.1					538	744	1,579	
G74	1,050	967,890	1,469.5	25.8					454	860	1,405	
G75	1,060	959,143	1,446.4	24.5					2,274	1,446	1,424	
G76	1,180	950,718	1,453.6	25.2					6,184	6,360	1,430	
G77	1,040	969,094	1,475.3	25.0					321	768	1,419	
G79	1,000	970,081	1,483.6	25.7						595	1,431	
G80	970	973,401	1,557.8	26.5					350	691	1,570	
G81	1,040	960,249	1,575.2	25.8					699	996	1,607	
G82	1,010	949,730	1,535.2	24.5					7,711	9,887	1,455	
G83	1,040	954,262	1,556.1	26.2					5,295	5,928	1,491	
G84	1,020	939,457	1,520.1	25.7					10,348	17,532	1,611	
G85	1,020	950,320	1,575.0	24.5					2,913	5,875	1,734	
G86	1,000	935,388	1,551.3	23.1					7,605	11,005	1,972	
G87	1,020	953,020	1,563.0	24.6					1,734	1,319	2,021	
G88	1,000	958,809	1,600.9	21.6					204	973	2,116	
G89	1,090	946,200	1,577.9	31.9					29	863	2,462	
G90	1,070	958,550	1,588.0	29.2						792	2,891	
G91	1,030	944,980	1,577.9	29.7					4,222	3,930	3,343	
G92	1,020	958,599	1,618.8	31.7					83	963	3,674	
G93	1,020	937,548	1,579.3	31.2					7,657	10,481	3,988	
G94	1,020	927,697	1,581.7	32.0					11,797	19,253	4,427	
G95	1,050	939,687	1,645.2	34.6					5,002	7,813	5,281	
G96	1,000	955,300	1,719.8	33.7						591	6,888	
G97	1,030	945,787	1,785.5	30.9					3,434	2,236	8,126	
G98	1,050	944,389	1,862.8	41.3					112	703	10,239	
G99	390	946,748	2,062.6	40.6					310	981	13,176	
G100	270	936,214	2,075.5	44.5					755	1,039	14,447	
204-1249F-14P (71.4 mbsf)												
G1	60	487,986	117.3		6.2	30.0			78,969	357,684	437	4,286
G2	220	946,846	263.1	13.6		23.4			708	28,057	545	
G3	590	968,388	314.5			6.0			147	8,794	620	
G4	760	964,851	286.9	13.6		5.1			195	12,781	1,010	
G5	510	949,063	248.2	22.5		6.3			452	25,940	991	
G6	410	942,551	221.4	16.3		8.4			432	31,275	1,352	
G7	670	922,347	170.3	27.6	14.2	18.8			965	60,080	828	
G9	550	893,293	156.2	28.3	4.7	22.8			762	79,558	2,784	
G10	320	856,641	181.8	31.8	36.9				285	62,801	285	
G11	150	883,895	175.8	32.6	31.6				254	59,059	4,536	
G12	140	900,630	177.2	11.8	38.0	34.4			281	67,326	4,477	

Notes: C_1 = methane, C_2 = ethane, C_3 = propane, *i*-C_4 = iso-butane, *n*-C_4 = normal butane, *i*-C_5 = iso-pentane, *n*-C_5 = normal pentane, O_2 = oxygen, N_2 = nitrogen, CO_2 = carbon dioxide. C_1/C_2 ratio reported corresponds to the integrated value for the entire pressure core.

Table T10. Intervals sampled for microbiology, Hole 1249F.

Core, section, interval (cm)	Depth (mbsf)
204-1249F-	
1H-1, 20–61	0.20
1H-2, 40–84	1.40
6X-1, 0–13	16.50
6X-1, 17–118	16.67
8H-1, 0–142	30.40
10H-4, 35–150	53.65
12H-4, 35–150	65.20
15H-5, 40–135	78.62
16H-4, 65–135	87.80

Table T11. Core quality indicators in intervals sampled for microbiology, Hole 1249F.

Core, section, interval (cm)	Depth (mbsf)	PFT per sample (ag)		Microspheres per gram	
		Inside core	Outer edge	Inside core	Outer edge
204-1249F-					
1H-2, 40–84	1.40	NS	NS	UD	UD
6X-1, 80–90	17.30	NS	NS	BDL	1890
8H-1, 130–142	31.70	NS	NS	1120	2370
10H-4, 140–150	54.70	0.26	13	BDL	906
12H-4, 140–150	66.25	0.031	BDL	UD	UD
15H-5, 125–135	79.47	0.0022	0.11	UD	UD
16H-4, 125–135	88.40	0.18	36	UD	UD

Notes: Core quality indicators are not completely applicable at this site (see **"Core Quality Assessment,"** p. 16, in "Microbiology"). PFT = perfluorocarbon tracer. ag = attograms. NS = not sampled. BDL = below detection limit. UD = unsuccessful deployment.

Table T12. Presence of gas hydrate based on infrared images of cores in liners, Hole 1249F.

Core, section	ΔT (°C)	Gas hydrate texture*	Depth interval (mbsf)† Top	Depth interval (mbsf)† Bottom	Anomaly designation‡	Sampled interval Top (cm)	Sampled interval Bottom (cm)	Sampled interval Depth (mbsf)
204-1249F-								
1H-1						0	20	0
1H-CC						0	10	1.84
3H	–6.0	Disrupted; presumably massive	9.00	9.10	IR295			
3H	–4.0	Disrupted; liner not full; variable ΔT	9.11	9.55	IR296			
3H	–5.0	Nodular	9.65	10.25	IR297			
3H-CC	–2.0	Nodular	10.40	10.95	IR298	8	10	11.03
5H-1	–5.0	Nodular variable ΔT	15.50	15.80	IR299	64	70	16.14
6X-1						13	17	16.63
6X-CC						5	10	17.73
7H	–6.5	Nodular	20.90	21.09	IR300			
7H	–1.7	Disseminated; nodular	22.60	22.80	IR301			
7H	–2.1	Nodular; disrupted	22.90	23.55	IR302			
7H	–6.1	Nodular; massive	23.57	24.48	IR303			
7H	–4.1	Nodular	25.10	25.45	IR304			
7H	–4.9	Nodular disrupted	26.05	26.23	IR305			
7H	–4.0	Nodular	28.00	28.20	IR306			
7H	–2.5	Nodular	28.40	29.60	IR307			
7H-CC	–5.1	Nodular; massive	30.05	30.75	IR308	0	2	24.22
8H-2	–8.0	Massive; nodular	30.60	33.10	IR309	0	42	31.82
2						42	52	32.24
2						112	117	32.94
2						117	127	32.99
8H	–8.8	Massive; nodular	34.70	35.40	IR310			
8H	–1.0	Nodular	36.90	37.15	IR311			
8H	–3.0	Nodular	38.05	38.85	IR312			
9H	–2.9	Disseminated	39.90	39.96	IR313			
9H	–4.2	Nodular	40.30	40.40	IR314			
9H	–2.9	Nodular	40.60	40.70	IR315			
9H	–4.1	Nodular	41.15	41.25	IR316			
9H	–2.6	Nodular; disseminated	41.40	42.00	IR317			
9H	–2.0	Nodular; disseminated	44.80	45.30	IR318			
9H	–3.8	Nodular	45.80	46.85	IR319			
9H	–1.9	Disseminated	47.40	47.65	IR320			
9H	–2.5	Vein; parallel to bedding	47.70	47.75	IR321			
9H	–1.5	Vein; dipping; disseminated	48.20	48.60	IR322			
9H	–1.5	Disseminated	49.00	49.10	IR323			
9H	–2.0	Nodular	49.50	49.60	IR324			
10H	–1.0	Disseminated	49.40	49.70	IR325			
10H	–2.1	Disseminated; nodular	52.10	52.30	IR326			
10H	–0.9	Disseminated	55.70	55.85	IR327			
10H-5	–6.0	Steeply dipping vein	56.95	57.10	IR328	86	106	55.66
10H	–2.4	Vein; dipping	58.50	58.57	IR329			
10H	–0.8	Disseminated	59.05	59.15	IR330			
12H	–3.8	Disseminated; nodular	60.98	61.10	IR331			
12H	–0.7	Disseminated	61.65	62.00	IR332			
12H	–3.2	Vein; moderate dip	64.75	64.80	IR333			
12H	–1.1	Disseminated	66.60	66.66	IR334			
12H	–3.0	Vein; parallel bedding	67.00	67.10	IR335			
12H	–1.5	Disseminated	69.65	69.90	IR336			
15H	–4.8	Disseminated; nodular	76.05	76.25	IR337			
15H-2	–0.4	Disseminated	76.60	76.70	IR338	67	82	75.07
15H	–0.9	Nodular on saddle-shaped fracture	77.05	77.15	IR339			
16H	–3.8	Disseminated; nodular	83.25	83.60	IR340			
16H	–1.6	Disseminated; poor liner contact	84.15	84.55	IR341			
16H	–1.9	Vein; disseminated	85.55	42.00	IR342			
16H	–1.3	Vein; moderate dip	88.00	88.06	IR343			

Notes: * = from anomaly characteristics and core description, if available. † = from uncut core liner. ‡ = Anomaly designations are used for reference to specific anomalies in text and figures. The difference between these depth intervals and the equivalent curated section depth intervals is typically <1 m.

Table T13. Moisture and density, Hole 1249B.

Core, section, interval (cm)	Depth (mbsf)	Density (g/cm³) Bulk	Density (g/cm³) Grain	Porosity (%)
204-1249B-				
2A-1, 34–36	30.24	1.585	2.723	67.0
2A-2, 39–41	31.09	1.598	2.708	65.9
2A-2, 100–102	31.70	1.609	2.709	65.3
2A-3, 9–11	32.20	1.669	2.739	62.4
2A-3, 54–56	32.65	1.660	2.666	61.3
3A-1, 25–27	34.65	1.652	2.718	62.9
3A-2, 76–78	35.71	1.621	2.694	64.2
4A-1, 36–38	39.26	1.632	2.714	64.0
4A-2, 26–28	39.98	1.770	2.762	57.1
5A-1, 64–66	44.04	1.626	2.684	63.7
6A-1, 49–51	48.39	1.607	2.713	65.5
6A-2, 66–68	49.56	1.675	2.706	61.3
7A-1, 20–22	52.60	1.633	2.707	63.8
8A-1, 74–76	57.64	1.715	2.726	59.4
8A-2, 74–76	59.14	1.750	2.736	57.6
8A-3, 42–44	60.32	1.768	2.690	55.3
9A-1, 39–41	66.29	1.605	2.674	64.8
204-1249C-				
1H-1, 103–105	1.03	1.881	2.710	49.2
2H-1, 40–42	2.40	1.551	2.721	69.0
3H-1, 35–36	5.35	1.581	2.777	68.2
4H-1, 18–20	14.68	1.662	2.742	62.8
4H-3, 42–44	16.47	1.642	2.825	65.7
4H-5, 44–46	17.19	1.651	2.705	62.7
4H-6, 65–66	18.41	1.643	2.714	63.4
5H-1, 16–18	24.16	1.622	2.700	64.3
5H-3, 32–34	26.47	1.606	2.690	65.1
5H-4, 36–38	27.62	1.624	2.692	64.0
5H-5, 9–11	27.84	1.591	2.753	67.2
5H-5, 29–31	28.04	1.649	2.762	64.0
5H-5, 49–51	28.24	1.575	2.734	67.8
5H-5, 69–71	28.44	1.629	2.702	63.9
5H-5, 89–91	28.64	1.599	2.747	66.6
5H-6, 60–62	29.31	1.675	2.690	60.9
7H-1, 58–60	35.58	1.614	2.705	64.9
7H-2, 80–82	36.76	1.631	2.748	64.8
7H-4, 74–76	38.00	1.669	2.679	61.0
7H-5, 44–46	38.57	1.656	2.692	62.1
7H-6, 119–121	40.23	1.654	2.674	61.8
8H-1, 74–76	45.24	1.652	2.689	62.3
8H-2, 30–32	46.30	1.689	2.684	59.9
8H-2, 104–106	47.04	1.700	2.755	61.0
8H-3, 74–76	48.20	1.674	2.678	60.7
8H-4, 88–90	49.82	1.708	2.674	58.5
9H-1, 74–76	54.74	1.708	2.726	59.8
9H-3, 74–76	57.72	1.661	2.669	61.3
9H-4, 74–76	59.07	1.716	2.725	59.3
11H-1, 56–58	65.56	1.740	2.706	57.4
11H-3, 8–10	66.71	1.890	2.718	48.8
11H-3, 76–78	67.39	1.715	2.697	58.7
11H-5, 74–76	70.16	1.697	2.706	60.0
11H-7, 50–52	72.57	1.697	2.709	60.0
12H-1, 54–56	75.04	1.760	2.697	56.0
12H-3, 74–76	78.14	1.744	2.721	57.6
12H-4, 12–14	79.02	1.795	2.711	54.3
13H-1, 74–76	84.74	1.591	2.824	68.5
13H-2, 40–42	85.90	1.695	2.689	59.7
13H-3, 74–76	87.23	1.676	2.689	60.8
13H-4, 46–48	88.40	1.688	2.674	59.7
13H-5, 40–42	89.31	1.703	2.702	59.5
204-1249F-				
3H-1, 45–47	9.45	1.588	2.586	63.9
3H-1, 75–76	9.75	1.552	2.591	66.3
3H-1, 76–77	9.76	1.643	2.598	60.7
3H-2, 18–20	10.18	1.481	2.586	70.7
3H-2, 20–21	10.20	1.461	2.644	73.0
3H-2, 33–34	10.33	1.596	2.551	62.5
7H-3, 22–25	23.73	1.553	2.561	65.6
7H-3, 28–30	23.79	1.573	2.763	68.5
9H-3, 9–11	42.30	1.747	2.788	59.0
9H-3, 19–21	42.40	1.722	2.779	60.2
9H-3, 29–31	42.50	1.626	2.644	62.9
9H-3, 39–41	42.60	1.648	2.742	63.7
9H-3, 49–51	42.70	1.643	2.736	63.8
9H-3, 59–61	42.80	1.649	2.736	63.5
9H-3, 69–71	42.90	1.648	2.791	64.7
9H-3, 79–81	43.00	1.644	2.726	63.6
9H-3, 89–91	43.10	1.678	2.724	61.6
9H-3, 99–101	43.20	1.636	2.701	63.5
9H-3, 109–111	43.30	1.640	2.760	64.5
9H-3, 119–121	43.40	1.622	2.692	64.1
11P-1, 82–84	59.72	1.704	2.675	58.8
14P-1, 30–32	71.70	1.677	2.685	60.7
14P-1, 82–84	72.22	1.704	2.726	60.1

Table T14. Thermal conductivity, Holes 1249C and 1249F.

Core, section, interval (cm)	Depth (mbsf)	Thermal conductivity (W/[m·K])	Individual measurements (W/[m·K])		
204-1249C-					
8H-3, 75	48.21	0.926	0.921	0.931	0.925
9H-3, 75	57.73	0.911	0.905	0.925	0.902
11H-3, 75	67.38	0.939	0.942	0.952	0.922
11H-6, 75	71.67	0.972	0.971	0.959	0.987
12H-3, 75	78.15	0.960	0.963	0.962	0.954
13H-3, 75	87.24	0.814	0.810	0.819	0.814
204-1249F-					
8H-3, 48	33.57	0.862	0.836	0.897	0.853
9H-4, 50	44.21	0.956	0.970	0.947	0.955
10H-1, 30	49.70	0.960	0.969	0.969	0.943
10H-3, 100	53.19	1.018	1.047	1.015	0.993
10H-5, 51	55.31	0.985	0.998	0.970	0.987
12H-1, 70	61.60	1.013	1.047	0.984	1.009
12H-3, 116	64.51	1.071	1.087	1.047	1.079
12H-5, 78	67.13	1.089	1.094	1.089	1.084
15H-3, 35	75.57	0.979	0.973	0.996	0.967
16H-1, 115	84.05	0.971	0.964	0.985	0.963
16H-3, 75	86.40	0.946	0.959	0.940	0.938
16H-5, 75	89.40	0.992	1.019	0.991	0.966

Table T15. Temperature measurements, Site 1249.

Ccore	Depth (mbsf)	Temperature (°C)	Thermal conductivity (W/[m·K])	Tool ID	Revised Temperature (°C)	Revised Thermal conductivity (W/[m·K])
204-1249C-						
1H	00.0	4.31	1.20	12	—	—
14P-BOH	90.0	11.50	—	3	—	—
204-1249F-						
5H	16.5	5.92	0.86	12	—	—
8H	39.9	6.29	0.86	12	6.73	0.50–0.55
10H	58.9	7.64	0.99	12	7.93	0.80
12H	70.4	7.73	1.09	12	8.45	0.80
16H	90.0	8.89	0.99	12	9.42	0.70–0.80
9H–10H	49.4	7.15	—	2	—	—
204-1249G-						
3H	24.0	4.65	0.86	11	5.74	0.45–0.50
204-1249I-						
3H	32.5	5.19	0.86	11	5.46	.060
204-1249L-						
4H	37.5	5.81	0.86	11	6.28	0.70

Notes: Measurements for which two core numbers are given (e.g., 204-1249F-9H–10H) were made with the DVTPP between these two cores. APCT measurements were made at the core catcher of the core listed. For APCT measurements, thermal conductivity represents the average of the nine measurements taken in the adjacent core. The last two columns show results of simultaneous inversion for the best-fit thermal conductivity and in situ temperature. ID = identification.

Table T16. Results from degassing experiments, Holes 1249C and 1249F.

Core	Depth (mbsf) Top	Depth (mbsf) Bottom	Run time (min)	Total volume (mL)*	Volume (mL)† $O_2 + N_2$	Volume (mL)† C_1	Volume (mL)† CO_2	Volume (mL)† C_{2+}	Concentration (%)‡ $O_2 + N_2$	Concentration (%)‡ C_1	Concentration (%)‡ CO_2	Concentration (%)‡ C_{2+}	Core length (m)	Porosity (%)	C_1 (mM)**
204-1249C-															
6P	33.5	34.5	967	12,667	876.6	11,733.6	36.7	20.09	6.9	92.6	0.3	0.159	0.23–1.00	63	524.0–2,278.4
204-1249F-															
4P	13.5	14.5	11,268	95,110	586.2	94,211.3	170.2	142.31	0.6	99.1	0.2	0.150	0.80–1.00	66	4,027.2–5,033.9
14P	71.4	72.4	1,580	4,800	231.2	4,561.1	6.3	1.29	4.8	95.0	0.1	0.027	0.99–1.00	60	215.7–217.9

Note: * = volume of gas released. † = volume of components released. ‡ = concentration of components released. ** = concentration in situ. Core length is reported as measured after the core was degassed and split (i.e., curated length). All cores had a nominal length of 1 m. The difference between the measured length and 1 m may be due to two factors: (1) incomplete recovery and (2) dissociation of gas hydrate during degassing. The lower concentration estimate corresponds to the assumption of 100% recovery; the higher estimate corresponds to the assumption that core length represented the percentage of recovery.

Table T17. HYACINTH pressure coring summary, Holes 1249D, 1249F, 1249G, 1249H, and 1249L.

Core	Deployment number	Date (Aug 2002)	Local time (hr)	Depth Water (mbsl)	Depth Core (mbsf)	BSR (mbsf)	Lithology	Core recovered (cm)	Presssure bar (bar)	Comments
204-1249D-										
2Y	FPC 5	5	0305	777	8	115	Massive hydrate and soft clays near seabed	80 (bagged)	Pressure lost then rose to 20 kbar	Cut good core; could not transfer because of gas expansion; mousse put in bag; hydrate visible
204-1249F-										
2E	HRC 4	5	1130	777	8	115	Massive hydrate and soft clays near seabed	88	Full 80 kbar, then rose briefly to over 250 kbar during disassembly	Hydrate core; 101 liters of gas collected
13Y	FPC 6	6	0230	777	70	115	Unconsolidated silty clay	91	0	Cut good core, full retraction lower valve did not seal
204-1249G-										
2E	HRC 7	28	0230	777	13.5	115	Massive hydrate and soft clays near seabed	75	80	Good core; much hydrate; lost 25 cm from catcher; tilted, frozen, and transferred to line 2
204-1249H-										
2Y	FPC 10	28	1000	777	13.5	115	Massive hydrate and soft clays near seabed	75	80	Hydrate core with free gas
204-1249L-										
5E	HRC 8	29	1925	777	37.5	115	Soft clays and hydrate	30	30 kbar pumped to 90 kbar	Lost pressure briefly on disassembly

Note: BSR = bottom-simulating reflector, FPC = Fugro Pressure Corer, HRC = HYACE Rotary Corer.

Table T18. RAB-8 coring test summary, Hole 1249B.

Core	Hole advance (m)	Recovery (m)	Recovery (%)	Local time (hr)	Coring time (min)
204-1249B-					
1W	29.9				
2A	4.5	3.05	67.78	0305	115
3A	4.5	1.92	42.67	0940	75
4A	4.5	1.15	25.55	1115	25
5A	4.5	0.93	20.67	1240	15
6A	4.5	2.06	45.78	1325	15
7A	4.5	0.57	12.67	1415	15
8A	9.0	3.81	42.33	1530	30
9A	9.0	0.52	5.78	1645	30

Note: RAB = resisitivity-at-the-bit.